Investigation of Viscoelastic Behaviour and Permanent Deformation Modelling for New Zealand Hot Mix Asphalts

by

MILAD Ghorban Ebrahimi

A dissertation submitted in partial fulfilment of the requirements for the Degree of Doctor of Philosophy in Civil Engineering

Department of Civil and Natural Resources Engineering

University of Canterbury
Christchurch, New Zealand

2015

Table of Contents;

Acknowledgement ..... **xiv**

ABSTRACT: ..... **xv**

Co-Authorship Form ..... **xvii**

1 Chapter 1: Introduction **20**

1.1 Problem Statement 20

1.2 Scope and Objectives 21

1.2.1 Research Methodology 22

1.2.2 Data Analysis 23

1.3 Thesis Outline 24

2 Chapter 2: Literature Review **26**

2.1 Introduction 26

2.2 Background 26

2.3 Permanent Deformation Tests 28

2.3.1 Binder Tests 28

2.3.1.1 Dynamic Shear Rheometer 28

2.3.2 Hot Mix Asphalt Tests 31

2.3.2.1 Complex Modulus Test 31

2.3.2.2 Indirect Tensile Test 32

2.3.2.3 Static Creep Test 34

2.3.2.4 Repeated Creep Test 36

2.3.2.5 Loaded Wheel Test....38
2.4 Rutting Prediction Models....39
2.4.1 The Empirical Modeling....39
2.4.2 Limiting Shear Failure Methods....39
2.4.3 Limiting Deflection Methods....40
2.4.4 Mechanistic-Empirical Models....40
2.4.4.1 Subgrade Rutting Models....40
2.4.4.2 Permanent Strain Model....42
2.4.5 Simple Performance Test (SPT)....44
2.4.6 Viscoelastic Design Method....46
2.4.6.1 Theory of Linear Viscoelasticity....46
2.5 Research Methodology....48
2.5.1 Experimental work....48
2.5.2 Analytical part....50
3 Chapter 3: Dynamic Modulus and its Interrelationship with....51
3.1 Introduction....51
3.2 Background....52
3.3 Linear Viscoelastic Solution....54
3.4 Specimen Preparation....57
3.5 Experimental Testing Program....58
3.6 Test Setup....60

3.7 Results and Discussions 61

3.8 Conclusions 67

4 Chapter 4: Hot Mix Asphalts Viscoelastic parameters and the 69

4.1 Introduction 69

4.2 Creep Compliance to Relaxation Modulus Interconversion 70

4.3 Sample Preparation and Testing 71

4.3.1 Materials 71

4.3.2 Experimental Plan 72

4.4 Determining the State of Linearity 72

4.5 Fitting Prony Series to Experimental Data 73

4.5.1 Static Creep Test 76

4.6 Interconversion betwenn LVE Response Function 77

4.6.1 Exact Solution 78

4.6.1.1 Midpoint Method 79

4.6.1.2 Tikhonov Regularization 79

4.6.2 Approximate interconversion techniques 81

4.6.2.1 Power-law-based Interrelationship 81

4.6.2.2 Interrelation by Denby 82

4.6.2.3 Park and Kim Approximate Interconversion Method 82

4.7 Prony Coefficient Selection and Interconversion between $\boldsymbol{D(t)}$ and $\boldsymbol{E(t)}$ 84

4.7.1 Approximate interconversion 84

4.7.2 Exact Solution Approach 86
4.8 Creep Compliance and Complex Modulus Interconversion 90
4.9 Experiment Testing Program 90
4.9.1 Complex modulus Test 90
4.9.2 Static Creep Test 92
4.10 Interconversion Techniques 93
4.10.1 Conversion from Creep Compliance, D(t), to Relaxation Modulus, E(t) ... 93
4.10.2 Conversion from Complex Modulus, E^*, to Relaxation Modulus, E(t) 94
4.11 Combined Error Technique 96
4.12 Conclusions 98
5 Chapter 5: Repeated Creep Test 100
5.1 Introduction 100
5.2 Background 100
5.3 Sample Preparation and Testing 104
5.3.1 Material and Sample Preparation 104
5.3.2 Laboratory Experiment 105
5.4 Results and Analysis 106
5.4.1 Flow Number Model 106
5.4.2 Permanent to Resilient Strain Model 111
5.5 Model Accuracy 115
5.6 Conclusion 119

6 Chapter 6: Loaded Wheel Tracker Test 120

6.1 Introduction 120

6.2 Background 120

6.3 Specimen Preparation 122

6.4 Test Setup and Specification 123

6.4.1 Introducing New Test Setup 123

6.4.2 Experiment Specification 125

6.5 Experimental Results and Analysis 125

6.6 Finite Element Simulation 129

6.6.1 Material Characterisation 129

6.6.2 Model Geometry 132

6.6.3 Loading Method 134

6.6.4 Modelling and Results 136

6.6.5 Comparison to Burger's Model 140

6.7 Conclusion 143

7 Chapter 7: Conclusions and Recommendations 145

8 References; 149

Appendix A: Mix Design and Material Properties 158

Appendix B: Data accuracy check for complex modulus test 166

Appendix C: Statistical Analysis 174

1. Australian Method 174

2. AAHTO Method.....176

Appendix D: Interconversions for the various asphalt mixtures 181

List of Figures;

Figure 1.2-1 Research methodology 23

Figure 2.3-1 Component of complex modulus G^* 28

Figure 2.3-2 Basic of dynamic shear rheometer [21] 29

Figure 2.3-3 Haversine loading pattern or stress pulse for the dynamic modulus test 30

Figure 2.3-4 Indirect tensile test 33

Figure 2.3-5 typical stress-strain response for asphalt mixture in creep-recovery test [25] 34

Figure 2.3-6 Static creep test zones 35

Figure 2.3-7 Plot of the rate of change in permanent strain versus loading time on a log–log scale for a repeated creep test 36

Figure 2.3-8 Rut depth vs. number of wheel passes 37

Figure 2.4-1 Measured stress versus pseudo strain 47

Figure 3.5-1 Sinusoidal loading pattern for the uniaxial compression test 58

Figure 3.6-1Test setups; (a) Uniaxial Compression, (b) IDT-Australian Method, ... 60

Figure 3.7-1 Dynamic modulus master curve; binder 60/70 (a) VTM = 4.0%, (b) VTM =5.0% 62

Figure 3.7-2Dynamic modulus master curve; binder 80/100 (a) VTM = 4.0%, ... 62

Figure 3.7-3Change in Poisson's ratio as a function of temperature and frequency 63

Figure 4.4-1 Linearity check; (a) Proportionality, (b) Superposition – with standard deviation 72

Figure 4.6-1 Prony series fit to experimental data 77

Figure 4.6-2 Schematic view of $\boldsymbol{L-curve}$ 80

Figure 4.7-1 effect of $\boldsymbol{n}$ on interrelation approach.....83

Figure 4.7-2 Relaxation modulus curve for Prony coefficients.....84

Figure 4.7-3 log-log graph of time versus creep compliance 84

Figure 4.7-4 Interconversion with various, $\boldsymbol{n}$ 85

Figure 4.7-5 (a) regularization parameter for (b) regularized versus approximate.....86

Figure 4.7-6 Post-Processed data versus approximate solution.....87

Figure 4.7-7 (a) λ for pre-processing technique (b) approximate method versus "Pre".....88

Figure 4.7-8 Logarithmic deviation of the approximate methods from the exact solution 88

Figure 4.9-1 Axial compression/static Figure 4.9-2 Fitting experimental data.....91

Figure 4.9-3 Prony series fit to experiment data.....92

Figure 4.10-1 Converted relaxation modulus from experimental creep test 92

Figure 4.10-2 Prony series fitted to complex.....94

Figure 4.10-3 Interconverted relaxation modulus from.....94

Figure 4.11-1 Interconverted relaxation modulus form.....97

Figure 4.11-2 Complex modulus data versus Prony fit 97

Figure 5.2-1 Repeated creep test result.....100

Figure 5.2-2 Plot of the rate of change in permanent strain versus loading time on a log–log scale for a repeated creep test 100

Figure 5.2-3 Typical repeated creep test and its strain rate 101

Figure 5.3-1The repeated creep test setup 104

Figure 5.4-1 Half-normal probability plot, AC 20.....108

Figure 5.4-2 Half-normal plot - Permanent to Resilient Strain, AC 20.....111

Figure 5.4-3 Three-way interaction, “Binder-Temperature-VTM”, AC20 112

Figure 5.4-4 Three-way interaction, “Binder-Temperature-Pressure”, AC20.....112

Figure 5.5-1 Normal probability plot of the residual, AC14 115

Figure 5.5-2 Normal probability plot of the residual, AC20 115

Figure 5.5-3 Normal probability plot of the residual, AC14 & 20 combined 116

Figure 5.5-4 Plot of residual versus run order, AC14.....117

Figure 5.5-5 Plot of residual versus run order, AC20.....117

Figure 5.5-6 Plot of residual versus run order, AC 14 & 20.....117

Figure 5.5-7 Model verification.....118

Figure 6.2-1 Current wheel tracker test mould 120

Figure 6.3-1 Roller compactor for slab preparation.....121

Figure 6.4-1 Wheel Tracker, Binder 80/100 - VTM =6.0% - before cutting 123

Figure 6.4-2 Wheel Tracker, Binder 80/100 - VTM =6.0% - after cutting 123

Figure 6.4-3 Wheel Tracker, Binder 60/70 - VTM =4.3% - before cutting 123

Figure 6.4-4 Wheel Tracker, Binder 60/70 - VTM =4.3% - after cutting 123

Figure 6.4-5 Proposed test setup.....124

Figure 6.5-1 Permanent deformation versus cycle number – AC20[1]-60/70[2]-7.0[3]-50[4] 125

Figure 6.5-2 Permanent deformation versus cycle number – AC20[1]-60/70[2]-5.5[3]-50[4] 125

Figure 6.5-3 Permanent deformation versus cycle number - AC14[1]-60/70[2]-3.5[3]-60[4] 125

Figure 6.5-4 Permanent deformation versus cycle number - AC14[1]-60/70[2]-5.5[3]-50[4] 126

Figure 6.5-5 Permanent deformation versus cycle number - AC14[1]-60/70[2]-7.0[3]-50[4] 126

Figure 6.5-6 Permanent deformation versus cycle number - AC14[1]-80/100[2]-5.5[3]-50[4] 126

Figure 6.6-1 Correct loading time 131

Figure 6.6-2 Boundary condition and loading for cylindrical specimen 132

Figure 6.6-3 Boundary condition and loading for slab 132

Figure 6.6-4 Wheel tracker rubber tire footprint 133

Figure 6.6-5 Wheel tracker loading pattern 133

Figure 6.6-6 Load distribution used in simulation step 134

Figure 6.6-7 C3D20 – finite element mesh for creep compliance test 136

Figure 6.6-8 Experiment versus simulation 137

Figure 6.6-9 Mesh density effect on prediction/computational effort 137

Figure 6.6-10 Mesh used in finite element simulation 138

Figure 6.6-11 Measured deformation versus prediction AC 14 – 60/70 139

Figure 6.6-12 Measured deformation versus prediction AC 14 – 80/100 139

Figure 6.6-13 Measured deformation versus prediction AC 20 – 60/70 139

Figure 6.6-14 Experiment versus simulation – Burger's model 141

List of Tables;

Table 2.3-1Target stress value for permanent deformation 29

Table 2.4-1Rutting parameters for various agencies 40

Table 2.4-2 General element of performance-based test methods.....44

Table 2.5-1Variables for repeated creep test 48

Table 2.5-2 Variables for complex/IDT tests 48

Table 3.3-1Coefficients for Poisson's ratio and dynamic modulus 56

Table 3.4-1AC 20 Mix aggregate gradation 57

Table 3.7-1 Comparison of various testing protocol 61

Table 3.7-2 Average Dynamic Modulus for Axial and IDT Tests 63

Table 3.7-3 *P* Values for Dynamic Modulus from Uniaxial and IDT-Australian Tests.....64

Table 3.7-4 *P* Values for Dynamic Modulus from Uniaxial and IDT-AASHTO Tests 64

Table 4.3-1 Aggregate gradation 70

Table 4.3-2 Properties of asphalt mixes.....71

Table 4.5-1 Prony series coefficients.....75

Table 4.5-2 Sign controlled Prony series coefficients for the static creep test 76

Table 4.9-1Prony series coefficients.....91

Table 4.10-1 Prony Series Coefficients-.....94

Table 4.11-1 Prony Series Coefficients-.....97

Table 5.2-1Example for flow number determination – AC20 with 80/100 binder 103

Table 5.3-1 Detail of repeated creep test 105

Table 5.4-1 Flow number results for AC 20 106

Table 5.4-2 Analysis of variance for AC 20 107

Table 5.4-3 New set of flow number, AC 20 110

Table 5.4-4 Flow Number results for AC 14 113

Table 6.4-1 Wheel Tracker test result - existing test setup 122

Table 6.4-2 Detail of wheel tracker test 124

Table 6.5-1 Vertical and Horizontal flow number 127

Table 6.6-1 Moving load versus static load simulation results 135

Table 6.6-2 Asphalt mix – material parameters 136

Table 6.6-3 Material properties used in simulation 138

Table 6.6-4 Burge's model parameters 141

Acknowledgement

I would like to thank my supervisory panel, Associate Professor Mofreh Saleh and Dr. Miguel Gonzalez for their insights, support and guidance throughout this study.

My appreciation goes to John Kooloos, the technician of the Transportation Laboratory, University of Canterbury University. Conducting the experimental phase of this research would be considerably more difficult without his help.

Besides, a number of friends have always been around to support me and I should thank them for it.

I owe quit a lot to my family as they have supported me all along in my academic years. I would like to dedicate this study to them as an indication of having their support in my life.

ABSTRACT: Permanent deformation is considered as one of the major modes of failures of flexible pavements in New Zealand. Currently based on the Australian mechanistic-empirical pavement design procedure, rutting is modelled solely based on the subgrade compressive strain criterion. However, the assumptions and the rationale behind the subgrade compressive strain criterion are questionable. Therefore, the main objective of this study is to characterize the permanent deformation behaviour of Hot Mix Asphalt (HMA) based on the extensive laboratory tests to find more accurate correlation with filed performance of flexible pavement.

In this study, asphalt mixes were tested by Simple Performance Test (SPT) method which includes Dynamic Modulus and Repeated Creep tests. The effect of deviator stress, temperature, air void content, mix gradation and binder type were thoroughly investigated through a factorial analysis. It was found that the temperature has leading effect on mix behaviour followed by pressure, air void and binder type. Permanent to resilient strain model was proposed for the New Zealand asphalt mixes. The study proved that, models proposed elsewhere could not be directly adopted in New Zealand due to significant differences in mix design and material properties.

Indirect Tensile test (IDT) was also considered in this research to study bituminous mixture modulus based on New Zealand and Australian design procedure. It was shown that, under accurate conversion backed up by viscoelastic principles, the dynamic modulus of the material could be predicted from the Indirect Tensile Modulus (IDT) counterpart. As a result, it would be feasible for the New Zealand industry to adopt Mechanistic-Empirical Pavement Design method by simply using the current IDT test setup. Resilient modulus then could be converted to the dynamic modulus equivalent.

Finally, Wheel Tracking (WT) test was conducted to evaluate the validity of the SPT results regarding the permanent deformation. A total of 200 cylindrical and 30 slab specimens were fabricated over the course of this research. A modified test setup was proposed for the current wheel tracker test. More realistic responses under the new test setup were recorded as a result. In addition, the material behaviour was simulated through finite element modelling by using ABAQUS program. In order to do so, the Static Creep Test was performed for a selected number of specimens. It was found that the “Creep Model” could closely simulate the mix performance.

Deputy Vice-Chancellor's Office
Postgraduate Office

UNIVERSITY OF CANTERBURY
Te Whare Wānanga o Waitaha
CHRISTCHURCH NEW ZEALAND

Co-Authorship Form

This form is to accompany the submission of any thesis that contains research reported in co-authored work that has been published, accepted for publication, or submitted for publication. A copy of this form should be included for each co-authored work that is included in the thesis. Completed forms should be included at the front (after the thesis abstract) of each copy of the thesis submitted for examination and library deposit.

Please indicate the chapter/section/pages of this thesis that are extracted from co-authored work and provide details of the publication or submission from the extract comes:

Chapter 3:

Ebrahimi, M., Saleh, M., & Gonzalez, M, *Dynamic modulus determination from Australian IDT test.* Road and Transport Research Journal, 2014. **23**(4).

Ebrahimi, M., Saleh, M., and Gonzalez, M, *The Interrelationship between Indirect Resilient Modulus and Dynamic Modulus for Dense Graded Hot Mix Asphalt.* International Journal of Pavement Research and Technology, 2013. **6**(5).

Ebrahimi, M., Saleh, M., and Gonzalez, M, *The Utilization of vertical and horizontal measurements in the determination of the indirect resilient modulus and the effect on the accuracy of the interconversion to dynamic modulus*, in *Transportation Research Board 93rd Annual Meeting* 2014, TRB: Washington DC, USA.

Ebrahimi, M., Saleh, M., and Gonzalez, M. . *The Interrelationship between Indirect Resilient Modulus and Dynamic Modulus for Dense Graded Hot Mix Asphalt*.

in *8th International Conference on Road and Airfield Pavement Technology (8th ICPT)* 2013. Taipei-Taiwan.

Chapter 4:

Ebrahimi, M., Saleh, M., and Gonzalez, M, *Interconversion between Viscoelastic Functions using Tikhonov Regularization Method and its Comparison with Approximate Techniques.* Road Materials and Pavement Design, 2014. **15**(4).

Ebrahimi, M., Saleh, M., & Gonzalez, M, *Investigating the Applicability of Complex Modulus and Creep Compliance Interconversion in Asphalt Concrete.* Advances in Civil Engineering Materials, 2014. 3(1): p. 106-121.

Chapter 5:

Ebrahimi, M., Saleh, M., and Gonzalez, M, *Mechanistic-Empirical Permanent Deformation Modelling for New Zealand Asphalt Mixtures.* To be submitted to TRB 95th Annual Meeting, 2016.

Chapter 6:

Ebrahimi, M., Saleh, M., and Gonzalez, M, Introducing a *Modified Loaded Wheel Test Method.* In Peer Review. Canadian Journal of Civil Engineering, 2015.

Please detail the nature and extent (%) of contribution by the candidate:

The candidate did all the work (100%) under the panel supervision.

Certification by Co-authors:

If there is more than one co-author then a single co-author can sign on behalf of all

The undersigned certifies that:

- The above statement correctly reflects the nature and extent of the PhD candidate's contribution to this co-authored work

- In cases where the candidate was the lead author of the co-authored work he or she wrote the text

Name: *Miguel Moyers Gonzalez* Signature: *Miguel Moyers Gonzalez*

Date: *27/03/2015*

Chapter 1: Introduction

1.1 Problem Statement

Flexible pavements encounter various types of distresses such as permanent deformation, fatigue and thermal cracking during their service life. Among all these distresses rutting or permanent deformation is classified as a primary criterion in structural deterioration [1, 2]. Rutting is generally defined as developing longitudinal deformation (depression) under the action of repeated loads [3]. It is called permanent since it shows accumulation of small amounts of unrecoverable depression (deformation and/or strain) which occurs under the repeated load of vehicles in the wheel path [4]. While rutting is a major structural failure, it is also a serious safety issue. Hydroplaning is a direct consequence of rutting and this occurs when water is left at the surface [5].

Currently based on the Australian mechanistic-empirical design procedure, rutting is modelled solely based on the subgrade criterion as a determinant factor for pavement deformation;

> "The pavement is designed to limit the vertical compressive strain at the top of the subgrade to a tolerable level through the life of the pavement" [6].

According to Austroads, the strain induced by traffic on pavement is predominantly elastic deformation which is mainly recoverable. However, small plastic or unrecoverable strain may be left in the pavement. The permanent deformation major effect will be on subgrade with much lesser extent through the rest of the pavement layers. The logic behind this argument can be explained as follows;

> "In pavement materials the magnitude of the plastic strain is directly proportional to the magnitude of the (vertical) elastic strain. In a pavement system the elastic strain increases from the subgrade to the surface. Accordingly, by setting the elastic strain at the subgrade surface at a specific value, the elastic strain in the components above this plane are controlled as the values for the

> associated plastic strain. Integration of the plastic strains over the pavement section provides a measure of the permanent deformation (rut depth) which will occur at the pavement surface". [7]

However, additional studies have shown that rutting takes place in all the pavement layers and it can't be eliminated just by controlling the subgrade strain. Moreover, a number of studies revealed that higher severity level of permanent deformation would occur as a result of shear deformation instead of simple densification [8, 9].

Rutting is a result of a complex combination of densification (volume change) and shear deformation (zero volume change) from the repetitive application of traffic loads. In general, rutting is divided into three main categories; first, one dimensional densification which is due to vertical compression. This type of rutting takes place because of excessive amount of air voids or inadequate compaction of the Hot Mix Asphalt (HMA) layer or underlying layers. Second, lateral flow or plastic deformation which occurs in the mixtures with inadequate shear strength or with insufficient amount of total air voids in the HMA layer.

Finally, mechanical deformation that is the third type of rutting known as consolidation of the unbound material such as base, sub-base and/or subgrade layers. This category is classified as the least common type of permanent deformation [10]. Based on the past studies it has been specified that the primary mechanism of rutting which causes moderate to high severe level of deformation is due to shear deformation that happens within the HMA layer and is limited to the upper 100 mm of flexible pavements [8, 10, 11].

Hence, there is a need for further investigation on flexible pavements in New Zealand in order to find enhanced design models that would be able to address permanent deformation in a more accurate and more reliable approach.

1.2 Scope and Objectives

The aim of this study is to characterize and evaluate New Zealand Hot Mix Asphalt performance and its behaviour toward permanent deformation through Simple Performance Test (SPT) procedure. This study examines HMA characteristics in performance based test methodology in order to introduce a new model to accurately predict permanent deformation.

In addition, the viscoelastic nature of asphaltic materials will be investigated through finite element modelling.

It must be noted that research outcomes conducted elsewhere cannot be simply implemented into New Zealand practice. Significant differences in mix property and specimen preparation are observed in New Zealand based mixtures. First of all, binder specification in New Zealand is based on penetration grade system. Moreover, mixing, pre-conditioning and compaction are conducted at the temperature of 150 °C with conditioning time duration of 60 ± 10 min. Finally, for the compaction phase, the gyration angle equals to 3 ± 1° with ram pressure of 240 ± 10 kPa.

1.2.1 Research Methodology

In order to have a profound understanding of HMA characteristics for the purpose of new design procedure for NZ mixes, the following objectives will be covered;

1. Conducting SPT test procedures in order to investigate asphalt mixtures parameters. In this regard, several factors will be investigated in a comprehensive full factorial design of experiment. The effect of *mix gradation*, *binder type*, *percentage of air voids in the compacted mix* and *deviatoric stress* will be investigated for the following performance indicators;

    - Dynamic Modulus $\left|E^*\right|$, determined from the complex modulus test,
    - Flow Time F_T, determined from the static creep test, and
    - Flow Number F_N, determined from the repeated creep test.

2. Since in the New Zealand and Australian pavement design guidelines (AS/NZS 2891.13.1) the asphalt modulus is determined in indirect mode therefore, indirect tensile test will also be considered as a complementary factor along with uniaxial compression test. The relationship between dynamic modulus and indirect resilient modulus will be investigated. Master curves of both dynamic modulus and resilient modulus will be studied for further investigation,
3. Wheel Tracking test will also be carried out on different combinations of *binder type*, *gradation*, *air void* and *temperature* to check the validity of SPT test results, and

4. About 200 cylindrical and 30 slab specimens will be fabricated over the course of this research for analysis part.

1.2.2 Data Analysis

In this part, data obtained from the laboratory step are used for the following objectives;

5. Interconversion is a common procedure to obtain unknown viscoelastic responses from other available ones. This approach is commonly taken into consideration because of, test difficulty, time consuming issue and lack of laboratory equipment. Over the course of this study, interconversion techniques will be checked with experimental data for their level of accuracy.

6. Dynamic modulus will be calculated from the Indirect Tensile Test through the theory of linear viscoelasticity. Therefore, the interrelationship between dynamic modulus resulted from the IDT test and that from complex modulus test will be studied.

7. Two types of permanent deformation modelling will be introduced as a result of this study;

    a) By using SPT test results as a performance-based approach, a Rut Depth (RD) design formula will be obtained as a function of *mix gradation*, *binder type*, *percentage of air voids in the compacted mix*, *deviatoric stress* and *confining pressure* and,

    b) Viscoelastic parameters and creep data will be incorporated into the Finite Element Models (FEM) to predict the permanent deformation.

The following graph summarises the research methodology;

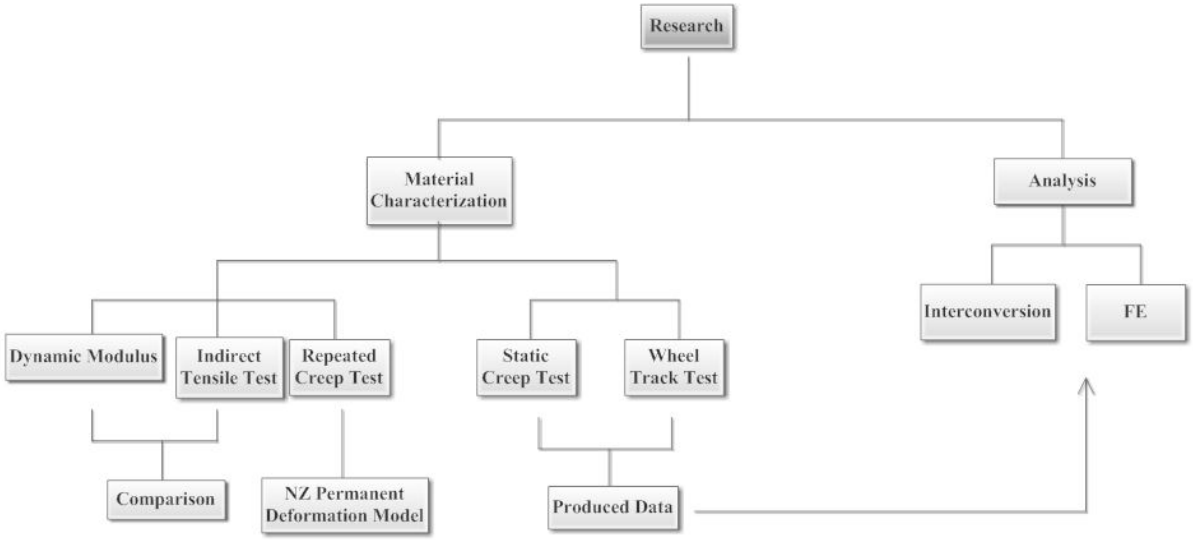

Figure 1.2-1 Research methodology

1.3 Thesis Outline

This thesis is divided into 7 chapters. Chapter 1 provides an introduction while Chapter 2 provides the literature review relevant to this study. It includes the background as well as the methodology used in this research. Chapters 3 to 5 cover a number of significant material properties in asphaltic materials.

In Chapter 3, the Dynamic and Indirect Tensile Modulus are taken into consideration. A simple method of extracting dynamic modulus from, well-stablished, indirect tensile test result is discussed in this chapter.

Chapters 4 will investigate two major material properties, known as Creep and Relaxation Modulus to define mix behaviour. These three; i.e. creep, relaxation with dynamic modulus, form the main material properties when asphalt mixtures are of concerns. Various interconversion techniques are reviewed in these chapters. As a result, asphalt mix material behaviour can be fully studied even if, solely, one of these responses is known to researchers.

Chapter 5 examines the mechanistic-empirical design approach resulted from the repeated creep test. The significant parameters, ones which statistically affect the final outcome, are identified through full factorial design; 2^k design of experiment.

Chapter 6 provides the wheel tracker test data. Finite element simulation is also undertaken in this chapter. Modification applied to the current wheel tracker test is discussed and its

advantages are reviewed in chapter 6. Finally, Chapter 7 includes a summary plus the main conclusions and recommendations of this thesis.

Chapter 2: Literature Review

2.1 Introduction

This chapter provides a literature review and synthesis on permanent deformation of Hot Mix Asphalt (HMA). It examines tests and theories behind modelling the rutting phenomenon and provides a summary of gaps in the existing literature.

2.2 Background

Rutting or Permanent Deformation is a primary mode of deformation in the structural performance of flexible pavements [1]. Rutting is generally defined as developing longitudinal deformation under the action of repeated load [3, 8]. The accumulation of small amounts of unrecoverable depression under the load repetition forms permanent deformation that is not only a structural failure but also a serious safety issue [4, 5]. Rutting is caused by inelastic or plastic deformation and can take place in any or all of the pavement layers and subgrade. These deformations are due to first, densification known as one dimensional compression and consolidation and/or second, lateral movements or plastic flow of materials such as Hot Mix Asphalt (HMA), aggregate base and subgrade soils. The latter most often occurs in HMA with air voids of %3.0 or less. Deformations caused by plastic flow/loss of shear strength are much more severe than the one occurred by one dimensional consolidation. Rutting can be classified into three distinct categories [10]:

1. One dimensional densification or vertical compression. This type of rutting takes place because of excessive amount of air voids or inadequate compaction of the HMA mat or underlying layers results in a low to moderate severity level. It is a depression near the centre of wheel path without any associated humps on either side.

2. Lateral flow or plastic movement. Similar to the previous class of rutting, lateral flow also happens near the centre of wheel path with the difference of accompanying humps on either side. Lateral flow occurs in the mixtures with inadequate shear strength or an insufficient amount of total voids in the HMA layer. HMA layers with air voids in the range of three percent or less right after construction are subjected to this kind of rutting because bitumen will act as a lubricant rather than a binder

during hot weather. Lateral flow causes rutting with moderate to high severity. This type of rutting is the most difficult to predict and measure in the laboratory.

3. Mechanical deformation. The third type of rutting is known as consolidation and/or lateral movement of the unbound material which is less common type of rutting. Mechanical deformation is usually accompanied by a longitudinal cracking pattern in the centre and along the outside edges of the ruts at the pavements surface with high elastic modulus HMA surface.

Permanent Deformation Characterization: As it was mentioned earlier, rutting is caused by inelastic or plastic deformation under the applied load. Asphalt and other pavement layers deform when the load is applied and by unloading not all these occurred deformations will be recovered i.e. pavement layers go through elastic deformation followed by inelastic/plastic deformation as the load increases. This plastic deformation results in residual amount of unrecoverable deformation in different layers.

The Strategic Highway Research Program (SHRP) began developing a new system for asphalt material characterisation in the lab to simulate field condition in a more accurate way in the 1980's. The final product of the SHRP was a new system called Superpave, short for Superior Performing Asphalt Pavements [12]. The Superpave design method for HMA mixtures consists of three phases:

- Materials selection for the asphalt binder and aggregate.
- Aggregate blending, and
- Volumetric analysis on specimens compacted using the Superpave gyratory compactor (SGC).

Many Departments of Transportation (DOTs) in the United States and elsewhere have adopted different parts of the Superpave method, including the Performance Grade (PG) binder specification. Since Superpave was based solely on volumetric proportioning of the asphalt mixtures not on the direct measurement of mechanical properties, needs for simple performance test arose. Some studies have addressed the issue that using Superpave volumetric mix design alone as a criterion is insufficient and there should be complementary tests for more reliable design procedure [13-15].

To overcome this obstacle, the National Cooperative Highway Research Program (NCHRP) conducted a comprehensive research program under Project 9-19. The aim of the study was

to recommend a Simple Performance Test (SPT) to complement the Superpave volumetric design procedure. The NCHRP Project 9-19 recommended three tests as promising simple performance tests for permanent deformation. (1) dynamic modulus, $|E^*|$, determined by the complex modulus test; (2) the flow number, F_N, determined from the repeated creep load test; and (3) the flow time, F_T, determined from the static creep test. Among these responses dynamic modulus is more critical since it was selected for the HMA materials characterization input in the Mechanistic – Empirical (M-E) Guide for Design of New and Rehabilitated Pavement Structure [2].

2.3 Permanent Deformation Tests

Permanent deformation is a phenomenon which is deeply correlated with asphalt binder, aggregate and combination of these two. Therefore, tests to address this issue are divided into two main categories: binder tests and mix tests.

2.3.1 Binder Tests

2.3.1.1 Dynamic Shear Rheometer

The dynamic shear rheometer (DSR) is used to characterize the viscous and elastic behaviour of asphalt binders at high and intermediate service temperature. The DSR measures two important factors of asphalt binder; complex shear modulus $(G^*)$and phase angle (δ).

The (G^*) is known to be as the total resistance of the binder to deformation, when it is repeatedly sheared [16]. The complex modulus comprises of two components, storage modulus (G') and loss modulus (G''). The former illustrates the elastic or recoverable part while the latter is a characteristic for viscous or non-recoverable behaviour of asphalt binder. Phase angle in asphalt binder is defined as the time lag between applied shear stress and respond shear strain [17].

Although (G^*) is a proper parameter for binder characterization, it is not a sufficient measure on its own. Figure 2.3.1 shows two different binders with identical complex shear modulus but different phase angles (i.e. $|G^*|$ of Binder A is equal to that of Binder B).

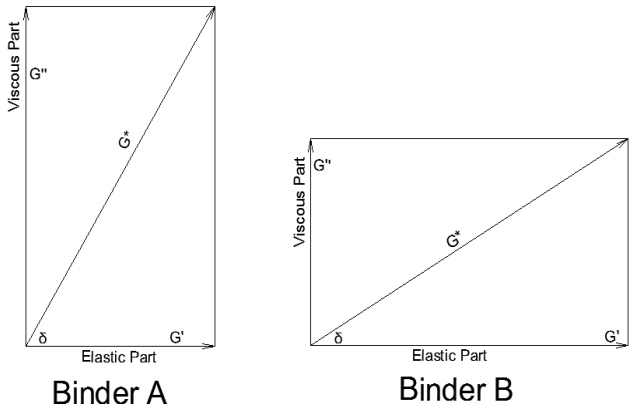

Figure 2.3-1 Component of complex modulus G^*

As can be seen, Binder B has a larger elastic component compare to Binder A. It means, under the load pressure Binder B will display more elastic or recoverable deformation, while the opposite response is seen in Binder A. This example demonstrates clearly that complex modulus, solely, will not be able to rank asphalt binders.

High complex modulus value and low phase angle are both needed for a better rutting resistance. The higher the (G^*) value the stiffer and thus the more rut resistant the binder will be. Also, by having lower (δ) binder will show higher elastic behaviour. Phase angle with $\delta = 0$ shows the binder behaving as complete elastic material while binder with $\delta = 90$ illustrates pure viscous behaviour. It is noteworthy to remember that a real viscoelastic material does have a significant amount of delayed elastic response which will be recovered completely after removing the load. Both storage and loss moduli contain a portion of this delayed elastic response, that's why the storage and loss moduli cannot be considered purely elastic or viscous, respectively [18].

As for flexible pavements, each loading cycle has its share of deformation work. Some part of this work is recovered by elastic rebound while some is dissipated in the form of permanent deformation and heat. Mathematically the dissipated work per loading cycle as a constant stress is calculated by Equation 2.3-1.

$$W_c = \pi \sigma_0^2 \left[\frac{1}{\frac{G^*}{\sin \delta}} \right] \qquad 2.3\text{-}1$$

As can be seen from Equation 2.3.1, the amount of dissipated work has an inverse proportion to $G^*/\sin\delta$. In this regard, $G^*/\sin\delta$ is defined as Superpave asphalt binder parameter for rutting specification or rutting factor. Obviously, higher G^* and lower δ both result in better binder performance regarding permanent deformation [19].

The DSR test is completed in accordance with ASTM D 7175 "*Standard Test Method for Determining the Rheological Properties of Asphalt Binder Using a Dynamic Shear Rheometer*". Asphalt binder is placed between a fixed and oscillating plate. By the applied torque from the spindle, the oscillating plate starts from A and moves to B. Then, it goes back to point C passing the point A and finally returns back to the first point – A. A complete movement is one cycle of oscillation as it is shown in Figure 2.3.2. One hertz (Hz) is defined as one cycle per second. The loading frequencies can range from 1 to 160 rad/s. Specification testing is performed at a test frequency of 10 rad/s which is equivalent to 1.59 Hz [20].

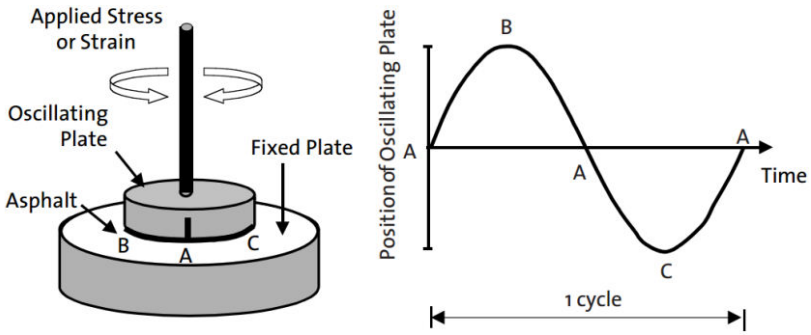

Figure 2.3-2 Basic of dynamic shear rheometer [21]

The thickness of the binder sample sandwiched between two plates and spindle diameter depends on temperature at which the test is carried out. For high temperature (46 ℃ or greater) small gap of 1000 microns (1 mm) with large spindle (25 mm) are used where the opposite is true for lower temperature [21].

As mentioned, the higher the rutting factor the better the rutting resistance of asphalt binder. In this regard, there is a minimum value specified by Superpave to secure asphalt binder behaviour which can be seen in Table 2.3.1.

Table 2.3-1Target stress value for permanent deformation

Material	kPa	Target Value	Stress Range - kPa
Original Binder	1	0.12	0.090 to 0.150
RTFO Residue	2.2	0.22	0.180 to 0.260

2.3.2 Hot Mix Asphalt Tests

2.3.2.1 Complex Modulus Test

Among compression tests, dynamic modulus is the oldest and the best documented test [2]. It was standardized in 1979 as ASTM D3497, "Standard Test Method for Dynamic Modulus of Asphalt Concrete Mixtures". The test consists of applying a uniaxial sinusoidal compressive stress to an unconfined or confined HMA cylindrical test specimen with 100 mm diameter by 150 mm height, as shown in Figure 2.3.3.

For linear viscoelastic material such as HMA, complex dynamic modulus E^* is equal to the ratio of the amplitude of the sinusoidal stress (at any given time, *t*, and angular load frequency, ω), to the amplitude of the sinusoidal strain at the same time and frequency.

$$E^* = \frac{\sigma}{\varepsilon} = \frac{\sigma_0 e^{i\omega t}}{\varepsilon_0 e^{i(\omega t - \Phi)}} = \frac{\sigma_0 \sin(\omega t)}{\varepsilon_0 \sin(\omega t - \Phi)} \qquad 2.3\text{-}2$$

where,

σ_0 = Peak (maximum) stress,
ε_0 = Peak (maximum) strain,
Φ = Phase angle,
ω = Angular velocity, and
t = Time, seconds

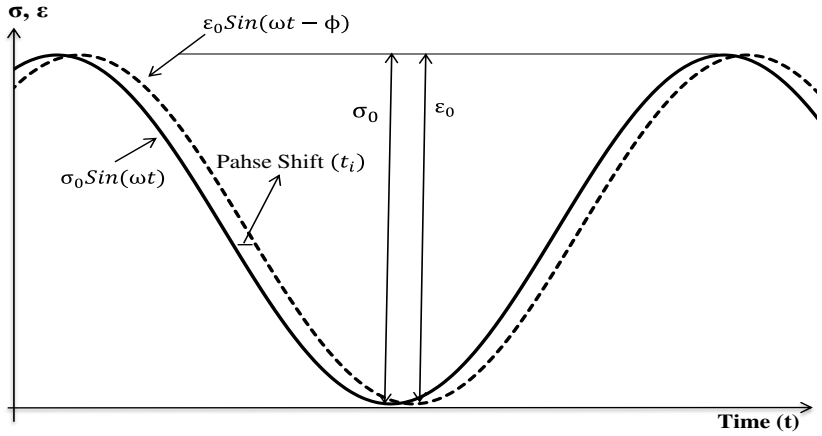

Figure 2.3-3 Haversine loading pattern or stress pulse for the dynamic modulus test

The dynamic modulus is then defined as the absolute value of complex modulus $|E^*|$. The dynamic modulus is equal the peak stress (σ_0) divided by peak recoverable axial strain (ε_0):

$$\left|E^*\right| = \frac{\sigma_0}{\varepsilon_0} \qquad 2.3\text{-}3$$

where,

σ_0 and ε_0 as defined before.

In general, the complex modulus, $\left|E^*\right|$, is divided into two parts. The so called real part E', which is referred to the storage or elastic modulus component. And the imaginary part E'', which is the loss or viscous part of complex modulus as can be seen in the following equation:

$$E^* = E' + iE'' \qquad 2.3\text{-}4$$

In the equation above, $i = \sqrt{-1}$.

The phase angle Φ is the lag between applying stress and responding strain. It is an indicator of the viscous properties of the material being evaluated. Mathematically, this is expressed as;

$$E^* = \left|E^*\right|\cos\Phi + i\left|E^*\right|\sin\Phi \qquad 2.3\text{-}5$$

$$\Phi = \frac{t_i}{t_p} * 360 \qquad 2.3\text{-}6$$

where,

t_i = Time lag between a cycle of stress and strain (s),
t_p = Time for a stress cycle (s), and
$i = \sqrt{-1}$

$\Phi = 0$ indicates a pure elastic material in which complex is equal to the absolute value. On the other hand, $\Phi = 90°$ shows the material acts pure plastic [22].

2.3.2.2 Indirect Tensile Test

An alternative method in determining modulus of asphalt concrete is to carry out an indirect resilient modulus test. Due to its simplicity and applicability to test field cores as compared to dynamic complex modulus test, the indirect modulus is a popular test with many laboratories. Currently dynamic modulus is tested in accordance with ASTM D3497 which requires a specimen with the dimension of 150 by 100 mm. It is often difficult to obtain this size specimen from actual pavements, considering that a typical asphalt layer thickness is less than 150 mm and coring is the most effective method of obtaining specimen from actual pavements.

Indirect tension (IDT) test can be conducted on 101 ± 3.8 mm or 152 ± 9 mm diameter specimen that are 38.1 mm to 63.5 mm in thickness. The method is very similar to the dynamic complex modulus test with the following differences [19]:

- Inelastic as well as elastic deformations are measured in the complex modulus test unlike the indirect resilient modulus test.
- Sinusoidal wave loading pattern is used in the dynamic complex modulus whereas a haversine wave loading is considered for indirect modulus.

IDT test is completed based on ASTM D 7369, a repeated vertical compressive force is applied acting parallel to and along the vertical diametrical plane and the horizontal displacement are measured mid height through the horizontal diameter [23] as it is shown schematically in Figure 2.3.4. The resilient modulus is calculated using Equation 2.3.7;

$$M_R = \frac{P}{\delta_h t}(\mu + 0.273) \qquad 2.3\text{-}7$$

where,

M_R = Instantaneous or total resilient modulus of elasticity, MPa,
μ = Poisson's ratio,
t = Thickness of the specimen, mm,
δ_h = Recovered horizontal deformation, mm, and
P = Maximum applied load, N

Unlike those of the uniaxial test procedure, IDT test has biaxial distribution of stress-strain relationship. This biaxial state can cause errors in determining material properties with IDT test if it is not considered properly. Differences between dynamic modulus resulted from axial compression and IDT test could be that significant so criteria and design methods based

on axial compression test cannot be implemented in forensic studies where the asphalt layer is not thick enough to yield 150 mm tall specimen. More information is provided in Chapter 3; Dynamic Modulus and its Interrelationship with Indirect Resilient Modulus.

Figure 2.3-4 Indirect tensile test

2.3.2.3 Static Creep Test

In a static creep test, under constant stress condition the total strain versus time relationship for a mixture is obtained in laboratory. Even though modulus is a common term to specify the relation between stress and strain, it is recommended to use "compliance" or $D(t)$ in creep test:

$$D(t) = \frac{\varepsilon_t}{\sigma} \qquad 2.3\text{-}8$$

The main advantage of using compliance in viscoelasticity/viscoplasticity is that it allows for the separation of the strain time components [24]. The test is conducted under confined or unconfined condition. The creep test, using either one load-unload cycle or incremental load-unload cycles, provides sufficient information to determine the instantaneous elastic (recoverable) and plastic (unrecoverable) components (i.e. time independent), and the viscoelastic and viscoplastic components (i.e. time dependent) of the material's response. Figure 2.3.5 illustrates these components. The total strain is a combination of all components.

$$\varepsilon_T = \varepsilon_e + \varepsilon_p + \varepsilon_{ve} + \varepsilon_{vp} \qquad 2.3\text{-}9$$

where,

ε_T = Total strain,

ε_e = The elastic strain, recoverable and time-independent,

ε_p = The plastic strain, irrecoverable and time-independent,

ε_{ve} = The visco-elastic strain, recoverable and time-dependent, and

ε_{vp} = The visco-plastic strain, irrecoverable and time-dependent

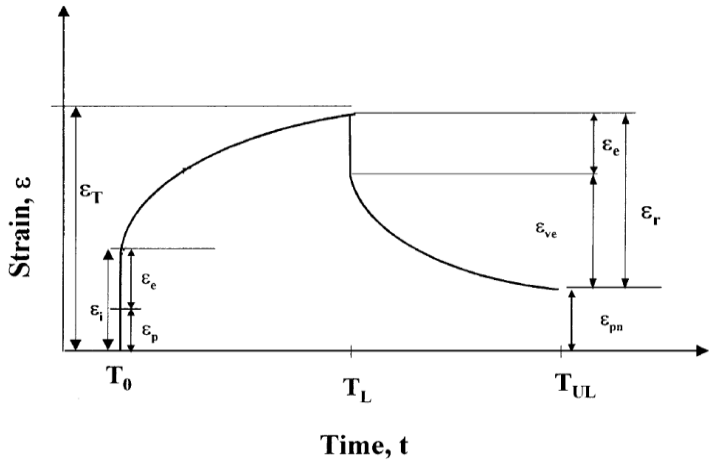

Figure 2.3-5 typical stress-strain response for asphalt mixture in creep-recovery test [25]

The creep compliance curve obtained from the static creep test is principally divided into three major zones; Primary, Secondary and Tertiary zones.

In the primary phase, creep compliance begins with the decreased rate of permanent strain accumulation and continues until it reaches a constant rate in the secondary phase.

The rate of permanent strain starts to increase sharply again at the beginning of tertiary zone. The onset of the tertiary deformation is defined as flow time which is a shear deformation under constant volume. Ideally the large increase in compliance generally occurs at this point. The flow point is believed to be strongly correlated with permanent deformation as can be seen in Figure 2.3.6.

In general, power-law model is used to fit the static creep test data in its secondary (i.e. linear) phase;

$$D' = D(t) - D_0 = at^m \qquad 2.3\text{-}10$$

where,

D' = Viscoelastic compliance component at any time, $1/MPa$

$D(t)$ = Total compliance component at any time, $1/MPa$

D_0 = Instantaneous compliance, $1/MPa$

t = Loading time, seconds and

a, m = Materials regression coefficients.

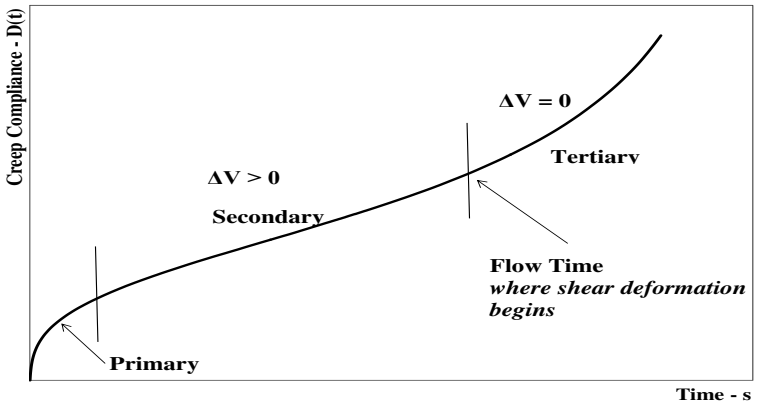

Figure 2.3-6 Static creep test zones

2.3.2.4 Repeated Creep Test

Another approach for measuring the permanent deformation characteristic of HMA material is to run a repeated dynamic load test. The test is employed for approximately 10,000 cycles and records the cumulative permanent deformation as a function of the number of cycles (repetitions) over the testing period. A load cycle of 0.1s haversine pulse load and a 0.9s dwell (i.e., rest) time is applied for the test duration (typically about 3 h). Similar to the static creep test, the cumulative permanent strain curve is also defined by three major zones; primary, secondary, and tertiary zone. The curve increases at a decreasing rate in the primary zone and reaches a constant rate of change in the secondary zone. At the onset of tertiary zone the permanent strain rate increases rapidly. The starting point, or cycle number, at which tertiary flow occurs is the flow number. It should be mentioned that, as discussed in the static creep test, all permanent deformation parameters in dynamic creep test are also obtained from the secondary (linear) zone only. These parameters include the intercept (*a*) and slope (*b*) parameters. The power-law model is typically used to analyse the test results as shown in Equation 2.3.13:

$$\varepsilon_p = aN^b \qquad 2.3\text{-}11$$

The intercept a represents the permanent strain at $N = 1$ whereas the slope b represents the rate of change of the permanent strain as a function of the change in loading cycles in log – log graph.

An alternative form of the mathematical model for characterizing permanent deformation can be achieved by applying permanent strain per load repetition [26] as brought in Equation 2.3.14;

$$\frac{\delta\varepsilon_p}{\delta N} = \varepsilon_{pn} = \frac{\delta\left(aN^b\right)}{\delta N} \text{ or, } \varepsilon_{pn} = abN^{b-1} \qquad 2.3\text{-}12$$

Figure 2.3.7 shows rate of change of permanent strain versus loading cycle on a log–log scale. As can be seen the flow number is specified as a point where minimum rate of change takes place.

Advantages and Disadvantages of Tertiary Flow Parameters: The static and repeated creep load permanent deformation tests each have their pros and cons [27]. The following can be mentioned amongst the advantages of the static creep test;

- Test uses simple equipment with static load capacity,
- Inexpensive to implement, and
- Exhibits the best correlation to the experimental sites for confined condition

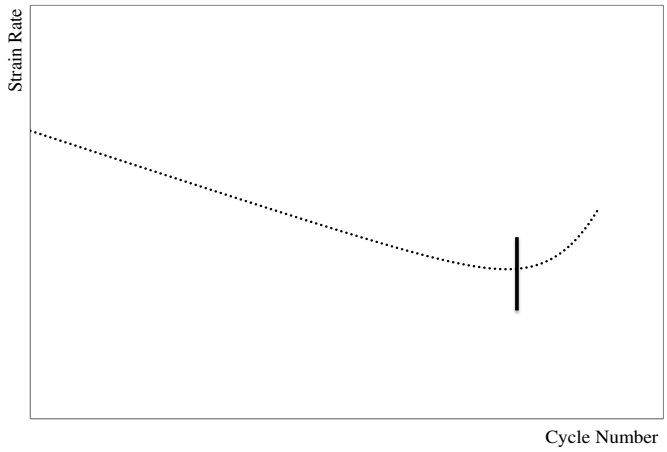

Figure 2.3-7 Plot of the rate of change in permanent strain versus loading time on a log–log scale for a repeated creep test

However, disadvantages include the complexity in developing the design criteria guideline, and secondly the creep test in its essence does not simulate the field dynamic loading phenomenon.

On the other hand, for the repeated permanent deformation test these advantages can be mentioned;

- Unlike the static creep test, repeated load test simulates field loading conditions, and
- Test parameters are provided for multiple applications. These parameters cover material behaviours from elastic to plastic properties.

And the disadvantages are; the complexity in developing the final gain criteria, and the confinement measures that may be required.

2.3.2.5 Loaded Wheel Test

One of the most common types of rutting test is the Loaded Wheel Tester (LWT). Numerous types of LWT equipment are available, such as the Georgia Loaded Wheel Tester, the Asphalt Pavement Analyzer (APA), the Superfos Construction Rut Tester, the Hamburg Wheel Tracking Device, and the French Laboratoire Central des Ponts et Chaussées (LCPC) Wheel Tracker. For a better characterization of asphalt mixtures, many agencies have begun implementing LWT as a supplement to their design procedure [28]. In the Australian design procedure, wheel tracking test is used in level three mix design which is intended for very heavy loading to indicate the resistance of the asphalt mix to permanent deformation [23].

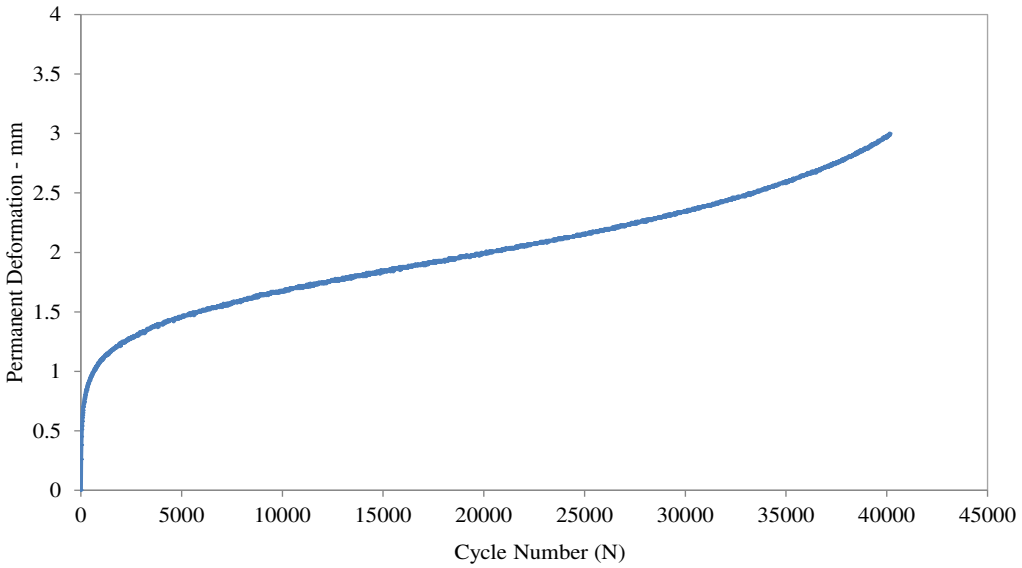

Figure 2.3-8 Rut depth vs. number of wheel passes

After preparing the specimen, it is placed in the test frame and conditioned at the desired temperature. Initial reading is taken at beginning and the rut depth is recorded after the test has begun. The tracking rate can be calculated as the change in rut depth with cycle number. The test is an indication of cumulative deformation as it is brought in Figure 2.3.8.

2.4 Rutting Prediction Models

During the last 50 years, researchers in pavement engineering have focused on permanent deformation. In spite of all the efforts, reports of permanent deformation have increased in especially in hot climate zones and in heavily trafficked regions. Increase in traffic volume and truck tyre pressures have been a major attributing factor to this problem. Even though these factors have a direct effect on permanent deformation, encountering more severe level of rutting also indicates that existing design procedure are inadequate of supporting today's traffic load demand. The most common permanent deformation models used in design procedures are covered herein.

2.4.1 The Empirical Modeling

The empirical models are the group of models developed based on observation and their accuracy depends on the number of field tests [29].

In 1929, the California Highway Department of Transportation used strength in a designing procedure for the first time by relating pavement thickness to the California Bearing Ratio (CBR). CBR was defined as the penetration resistance of a subgrade soil relative to standard crushed rock [25]. This method is still used by many agencies today in pavement design.

The empirical models have serious limitations including deficiencies when accommodating heavier vehicle loads, new material properties, climatic effects, and the inability to handle long-life pavement designs since they are derived from limited sets of materials and environmental conditions. That makes these results not transferable to other conditions. In general, past studies have revealed that there is poor correlation between these models and the observed field performance.

2.4.2 Limiting Shear Failure Methods

Limiting shear failure method was used by Barber in 1946 as a new design procedure [30]. Barber applied Terzaghi's bearing capacity formula to determine pavement thickness based on the shear failure by using major subgrade components, cohesion and angle of internal friction. His work was later further improved on by Mcleod in 1953. Yoder reviewed this method in his book, *Principal of Pavement Design*, in 1959 but it was excluded in the second

edition [31], as the pavement was designed for riding comfort and not to prevent shear failure.

2.4.3 Limiting Deflection Methods

This method is used to determine the pavement thickness by constraining vertical deflection and preventing it from exceeding the allowable limit. Boussinesq used an elastic half space theory in 1885 and obtained stress, strain and deflection due to circular loaded area. This theory can be used for the subgrade if the unity (or close to unity) ratio exists between the pavement and subgrade moduli. A thin asphalt surface and/or a thin granular base are examples of where this situation occurs. Burmister improved the linear elastic model in 1943 based on the fact that, flexible pavements are layered system with better materials on top and cannot be represented by a homogenous mass. At first he developed a two-layer system and then extended it to a three-layer system. Now, with the advent of computers, the theory can be easily applied to a multilayer system.

The Kansas State Highway commission modified Bossinesq's equation in 1947 and limited the subgrade deflection to 2.54 mm. The U.S Navy also used the deflection method by applying Burmister's two-layer theory in 1953. They limited the surface deflection to 6.35 mm. The use of deflection as a design procedure has an apparent advantage; it is easy to measure in the field. But since pavement failure is caused by excessive stresses and strains instead of deflections the limiting deflection method could not be satisfactory [32].

2.4.4 Mechanistic-Empirical Models

In the Mechanistic-empirical models, approaches to rutting prediction have been done by using mechanistic computations of pavement stresses and strains and then substituting these responses in the empirical prediction models. These models must be calibrated based on observed field performance data [33].

2.4.4.1 Subgrade Rutting Models

It was at the first International Conference on the Structural Design of Asphalt Pavements in 1962 that Shell Oil Company presented the first pavement design model in which fatigue and rutting were explicitly considered as mechanism of distresses. In this procedure rutting was controlled by limiting the vertical compressive strain on the top of the subgrade. This can be

achieved by ensuring sufficient structural layer above the subgrade to minimize the plastic deformation in the subgrade. Hence the assumption is that the permanent deformations at all layers above the subgrade are insignificant. In 1976 symposium on rutting in asphalt pavements, several studies emphasized on rut depth prediction [34]. But it was in 1977 that the earliest mechanistic-empirical was introduced. At that time only the strain on the top of the subgrade was considered as factor of rutting distress. Chen and his colleagues and Pidwerbesky *et.al* provide brief summaries of the evaluation of early model to predict the number of load cycle results in permanent (N_d) deformation as function of vertical compressive strain (ε_c)at the top of the subgrade [35, 36];

$$N_d = f_4 \varepsilon_c^{-f_s} \qquad 2.4\text{-}1$$

In which f_4 and f_5 are model calibration parameters and they have different values depending on the soil properties and local conditions.

Table 2.4-1Rutting parameters for various agencies

Agency	f_4	f_5	Allowable Rut Depth, mm (in)
Asphalt Institute (1982)	1.365×10^{-9}	4.477	13 (0.5)
Shell (1978)			
50% reliability	6.15×10^{-7}	4	13 (0.5)
85% reliability	1.94×10^{-7}	4	
95% reliability	1.05×10^{-7}	4	
TRRL (Powell et al. 1984), 85% reliability	6.18×10^{-8}	3.95	10 (0.4)
Belgian (Verstraeten et al.1982)	3.05×10^{-9}	4.35	10 (0.4)

Table 2.4.1 has a summary of f_4 and f_5. It also should be noted that the implicit permanent deformation limits is different for these agencies. For example, total rut depth for Asphalt institute at pavement surface is 133 mm (0.5in), whereas for TTRL procedure it is 10 mm (0.4) in at the reliability of 85%.

The Corps of Engineers (COE) also developed a subgrade model for different soil which was used by Quintus and his colleagues [37] to modify the relationship between vertical

compressive strain and the number of wheel loads for various subgrade moduli with the allowable rut depth of 13mm (0.5in);

$$N_d = 0.09174 M_R^{0.9555} \varepsilon_\upsilon^{-4.082} \qquad 2.4\text{-}2$$

2.4.4.2 Permanent Strain Model

The mechanistic-empirical models in this part relate the permanent compressive strain, ε_p, at the mid-thickness of an asphalt sublayer to the temperature T and number of cycle [38];

$$\Delta\varepsilon_p(N) = \varepsilon\mu N^{-\alpha} \qquad 2.4\text{-}3$$

In which $\Delta\varepsilon_p(N)$ is the incremental strain caused by the N^{th} load cycle. ε is the mathematically computed peak total strain, and μ and α are material properties which are functions of temperature, mixture type and the stress rate.

Asphalt Institute developed a permanent strain model in which considers the effect of mixture variables on rutting [39];

$$\begin{aligned}\log \varepsilon_p = {} & -14.97 + 0.408\log(N) + 6.865\log(T) + 1.107\log(\sigma_d) - 0.117\log(\eta) \\ & + 1.908 V_{beff} + 0.971(V_a)\end{aligned} \qquad 2.4\text{-}4$$

in which,

ε_p = Permanent strain,
T = Temperature, $^\circ F$,
N = Number of load cycles,
σ_d = Mechanistically determined deviator stress (psi) in the asphalt layer,
η = The binder viscosity at $70^\circ F$, 10^6 poise,
V_{beff} = Effective asphalt volume, %, and
V_a = Volume of air voids, %.

In the year 2002 Deacon *et.al* used Westrack field experiment for permanent deformation based on permanent shear strain [40];

$$\lambda_p = a e^{b\tau} \gamma_e N^C \qquad 2.4\text{-}5$$

In which, λ_p is the permanent shear strain at a depth of 2 inches below the surface of the asphalt layer. τ and γ_e are elastic shear stress and strain at the same location which need to be calculated mechanistically. Constants a, b and c are material properties determined from Superpave Shear Tester (SST).

To find the rut depth time hardening principle was also used. In this approach

$$RD_{HMA} = K_r \gamma_{p,t} \qquad 2.4\text{-}6$$

In which K_r is a coefficient relating rut depth to permanent strain and is a function of the thickness of asphalt layer. $\gamma_{p,t}$ is the permanent shear strain for the t^{th} hour of loading which is equal to

$$\gamma_{p,t} = a_t \left[\left(\frac{\gamma_{p,t-1}}{a_t} \right)^{1/c} + \Delta N_t \right]^c \qquad 2.4\text{-}7$$

$$a_t = a e^{b\tau} \gamma_{e,t} \qquad 2.4\text{-}8$$

$\gamma_{e,t}$ is the elastic shear strain for the t^{th} hour of loading and ΔN_t is the number of load application during the t^{th} hour.

2.1.1.1 Permanent Strain to Resilient Strain Ratio Models

Temperature and stress level are the two most significant factors affecting permanent deformation and need to be explicitly considered. Resilient elastic strain is also influenced by these two factors the same as permanent strain. NCHRP Project 1-37A uses the same concept in its mechanistic-empirical design methodology [41]. The model is developed as a results of extensive laboratory study carried out by Leahy in 1989 on the repeated load permanent deformation of more than 250 asphalt concrete specimens consists of two aggregate, two binder types, three binder contents, three stress levels and three temperatures. The developed model is shown in Equation 2.4.9;

$$\log\left(\frac{\varepsilon_p}{\varepsilon_r}\right) = -6.631 + 0.435\log(N) + 2.767\log(T) + 0.110\log(\sigma_d) + 0.118\log(\eta) + 0.930\log(V_{beff}) + 0.501\log(V_a) \quad R^2 = 0.76 \qquad 2.4\text{-}9$$

In which ε_r is the resilient "elastic" strain and the other terms are as defined for Asphalt Institute Model (Equation 2.4.4). Later Kaloush, in his PhD dissertation improved the robustness of the model by experimenting very large number of repeated load permanent deformation results in NCHRP Project 9-19 [42]:

$$\log\left(\frac{\varepsilon_p}{\varepsilon_r}\right) = -3.1555 + 0.39 + 94\log(N) + 1.7340\log(T) \quad R^2 = 0.64 \qquad 2.4\text{-}10$$

The much broader and more diverse data set resulted in lower R^2 for this model.

Many mechanistic-empirical rutting models have been developed over the past decades, but one of the main disadvantages is that they have not been any systematic comparisons of the predictions from these models for a common set of data. In addition, most of these models have been calibrated with very limited set of laboratory or field data. Among these entire models, NCHRP 1-37A is arguably the leading model for HMA rutting since it has a robust calibration of about 400 field test sections. The model also has an option of regional calibration [33].

2.4.5 Simple Performance Test (SPT)

Simple performance test was one of the objectives of the NCHRP project 9-19 to complement Superpave mixture design procedure. Since Superpave was based solely on volumetric proportioning of the asphalt mixtures and not on the direct measurement of rutting, needs for simple performance test arose.

Asphalt mixture laboratory tests can be divided into three general categories. First, empirical tests (such as Marshall Stability) which are often of limited usefulness since the measured properties are not related directly to the asphalt performance. Second, performance related tests in which the engineering properties are measured such as compressive strength. Although they are more accurate than the empirical tests, they still are considered as insufficient for wide varieties of mixture types. Finally, the performance based tests which are known as the best candidates for a simple performance test. The performance based test

methods measure material properties that can be used in modelling to predict mixture response [43]. They are categorized based on test, load application and load pulse type as shown in Table 2.4.2.

Table 2.4-2 General element of performance-based test methods

Types of Test or Test Geometry	Type of Load Application	Type of Load Pulse
• Uniaxial or Triaxial Compressive • Direct Tension • Simple Shear • Direct Shear • Hydrostatic • Torsional or Rotational	• Static or Creep • Constant Deformation Rate • Repeated Load or Cyclic • Dynamic Loading	• None • Square • Haversine • Sinusoidal • Triangular

Regarding the accuracy of relations between laboratories measured strain and pavement deformation in the field, it is important to conduct laboratory tests conditions (stress and environment) similar to the actual field. Three important factors need to be considered in this regard:

- Climatic conditions (e.g., pavement temperature) at the given geographic site,
- Traffic level (i.e., number of repetitions) expected during the pavement service life, including the rate of loading, and
- Stress levels expected within the asphalt layer for a given pavement structure.

Different tests were evaluated by NCHRP project 9-19 and in between dynamic modulus test, repeated load permanent deformation test and the static creep permanent deformation test were identified as the most useful among the others. Details of test candidates can be found elsewhere [2].

Kaloush contributed an initial conceptual framework to find a relationship between flow number and rut depth [42]. Additional development was carried out by Qayoum to incorporate temperature and traffic level effects on rut depth [44]. The primary step was the relation between reduced flow number F_{Nr} to rut depth (RD) by power law relationship;

$$RD = \alpha(F_{Nr})^{b} \qquad 2.4\text{-}11$$

where, a and b are functions of mixture properties and traffic. Reduced flow number F_{Nr} which is analogous to reduced time or reduced frequency in dynamic modulus testing can be calculated from flow number F_N by a temperature shift factor $a(T)$;

$$F_{Nr} = \frac{F_N}{a(T)} \quad \text{2.4-12}$$

Findings by Qayoum suggests that $a(T)$ values obtained from dynamic modulus testing are adequate for shifting the flow number [44];

$$a = mN^{-n} \quad \text{2.4-13}$$

$$b = k\log(N)^{-l} \quad \text{2.4-14}$$

where, m, n, k and l are constants and N is traffic level in EASL. So, the final equation can be showed as;

$$RD = mN^{-n}\left(F_{Nr}\right)^{k\log(N)-l} \quad \text{2.4-15}$$

2.4.6 Viscoelastic Design Method

This design category is characterized by the consideration of advanced material constitutive models. As Sousa and his co-workers mentioned in their study on permanent deformation, there are two major factors in the mechanical analysis of asphalt mixtures; the material characterization method and its accuracy, and the accuracy of mechanistic models to predict pavement response [34]. Although the viscoelastic concept is not considered new, its pavement design application has not been dominant to date. The earliest application in this regard might go back to early 1960s, when Sector and Monismith applied viscoelastic principles by using triaxial test data to predict the behaviour of asphalt concrete pavement [45].

2.4.6.1 Theory of Linear Viscoelasticity

Conventionally, asphalt materials are designed as an elastic material even though they behave viscoelastically in their nature. Unlike the elastic materials, the behaviour of viscoelastic material varies significantly at different temperatures and loading frequencies. Dependency

on loading frequency implies the fact that materials response is a function of the current situation as well as their loading history [46].

The word “viscoelastic” means concurrent existence of viscous and elastic properties in a material [47]. These materials act as elastic solids at low temperature and high loading frequency whereas their behaviour tends to pure viscous by either increasing temperature or decreasing loading frequency. In between, the situation which covers significant part of flexible pavement service life, these materials exhibit a major level of elastic solid stiffness, while flow and dissipate energy by fractional loss as a viscous fluid [48].

The viscoelastic materials (e.g. asphalt mixtures) seemingly lose their stiffness under the repeated load test. However, what actually happens in the viscoelastic type of materials is that, a part of this energy is used to overcome the viscous resistance of the material and does not contribute to the damage in material. Therefore, it is necessary to provide a proper estimation of the amount of this energy in order to have a correct relation between the apparent and real relaxation moduli of the viscoelastic materials.

Pseudostrain energy has been introduced for this reason and it is defined as the amount of energy available to damage the material. In order to check the linearity of the material behaviour, a graph of linear viscoelastic stress σ_{LVE} versus applied stress is plotted. If the graph forms a straight line, it means the material is behaving as a linear viscoelastic material. On the other hand, if a closed curve figure as shown in Figure 2.4.1appears as a result, then the material is behaving as nonlinear viscoelastic material.

The pseudostreain energy is the difference between the energy that has been lost in loading and unloading the material and the energy that has been lost in overcoming the viscous resistance of the material. Therefore, it denotes the energy available to damage the material. However, if the closed loop does not change size after repetitive loading, it indicates that the material is not changing and it is no longer being damaged.

Damage to the material is indicated by a change in the shape and area of the dissipated pseudostrain energy loop [49].

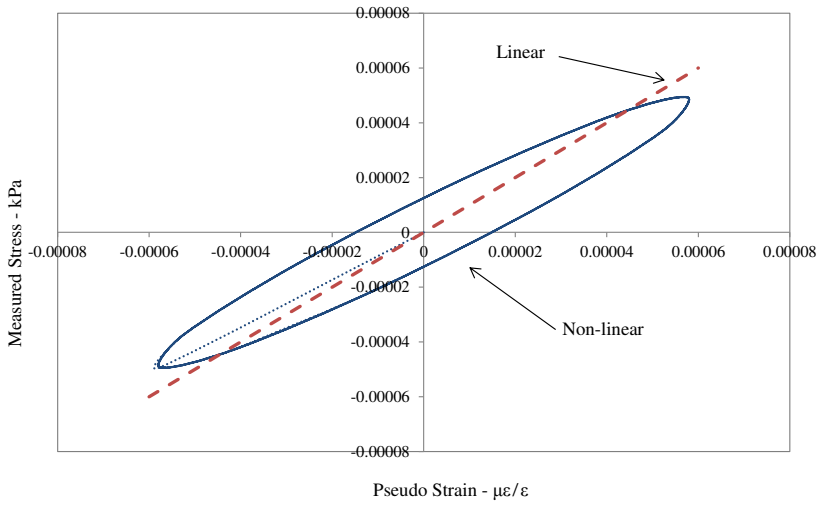

Figure 2.4-1 Measured stress versus pseudo strain

2.5 Research Methodology

As discussed earlier, the aim of this research is to introduce a new permanent deformation model which is more suitable to New Zealand hot mix asphalts. Unlike the current models developed elsewhere, the permanent deformation model introduced in this study will be, specifically, compatible with the New Zealand mixtures and their characteristics. In addition, the research work will investigate utilising test setup for the current wheel tracker test to better characterise and understand the permanent deformation behaviour of the hot mix asphalts.

This study also aims to undertake a finite element simulation of the asphaltic material behaviour. Successful simulation will be another step on the path to a pure mechanistic design procedure.

As a result, in order to accomplish the objectives above, the research methodology could be summarized into two main categories namely; experimental work and analytical part.

2.5.1 Experimental work

The outcome of this research recommends a set of laboratory experiments know as Simple Performance Test (SPT) that includes the followings;

(1) Complex Modulus test,

(2) Repeated and static creep tests.

Table 2.5-1Variables for repeated creep test

Binder 60/70, 80/100							
AC 14, AC 20							
$V_a = 3.0\%$				$V_a = 5.0\%$			
Temp.1 = 40 °C		Temp.2 = 50 °C		Temp.1 = 40 °C		Temp.2 = 50 °C	
$\sigma_1 = 240$ kPa	$\sigma_1 = 600$ kPa	$\sigma_1 = 240$ kPa	$\sigma_1 = 600$ kPa	$\sigma_1 = 240$ kPa	$\sigma_1 = 600$ kPa	$\sigma_1 = 240$ kPa	$\sigma_1 = 600$ kPa

As a result in this study, the SPT test will be performed on the cylindrical specimens. Table 2.5.1 highlights variables considered over the course of this research for the repeated creep load test. 2 test replicates are produced for each test combinations. About 200 cylindrical specimens will be prepared for this purpose.

The complex modulus test will also be taken into consideration at 5 different temperatures; -10, 4.4, 20, 37.8, and 54.4 ºC and 6 frequencies; 0.1, 0.5, 1.0, 5, 10, and 15 Hz for the development of master curves so the material modulus can be determined at any temperature/frequency combination. 3 replicates are considered for each test combinations. The test variables is shown in Table 2.5.2

Table 2.5-2 Variables for complex/IDT tests

Binder 60/70, 80/100			
AC 14		AC 20	
$V_a = 3.0\%$	$V_a = 5.0\%$	$V_a = 3.0\%$	$V_a = 5.0\%$

As a requirement for New Zealand and Australian standard design method, Indirect Tensile test (IDT) will be carried out in this study. Similar to the complex modulus test, the IDT test will be carried out at 5 different temperatures; -10, 4.4, 20, 37.8, and 54.4 ºC and 6 frequencies; 0.1, 0.5, 1.0, 5, 10, and 15 Hz. Table 2.5.2 covers the test variables for the IDT tests. Similar to dynamic modulus test, 3 replicates is produced for the IDT tests.

In addition to the experiments mentioned above, the Wheel Tracker test will also be carried out for this thesis. *Loaded Wheel Tester (LWT)* is the most common type of standardized laboratory test to predict HMA rutting potential that is fairly popular within New Zealand industry. In this study asphalt samples will be tested in a full factorial analysis;

- 2 binder types; 60/70 & 80/100,

- 2 gradations; AC 14 and AC 20, and
- 2 percentages of air void; 3.5% and 5.5%.
- 2 temperatures; 50 and 60 °C.

2 replicates are produced for the wheel tracker test.

2.5.2 Analytical part

The analytical stage is divided into two categories; first, a mechanistic-empirical formula is proposed based on the simple performance test which is explained in details in Chapter 6. Moreover, the finite element modelling will be taken into consideration by using ABAQUS program. The computer simulation modelling by Abaqus is used to simulate the material behaviour under repetitive traffic loading. Hence, the data can be studied for the permanent deformation modelling based on the advanced constitutive parameters, detail of which is covered in Chapter 7.

Chapter 3: Dynamic Modulus and its Interrelationship with Indirect Resilient Modulus

3.1 Introduction

As discussed in the literature review, the Superpave mix design and analysis method was developed more than a decade ago under the United States Strategic Highway Research Program [50] in order to overcome the shortcomings of then available test procedures. The Superpave method was a significant step forward in Hot Mix Asphalt (HMA) design procedure due its robust material selection, aggregate blending and volumetric analysis of compacted mix prepared by Superpave Gyratory Compactor (SGC) [51].

In spite of these meticulous mix preparations, there was not any general strength or mechanical test to complement volumetric procedure as it was in Marshall and Hveem design methods. In this regard, there were number of researchers who had questioned Superpave for relying solely on volumetric data and addressed the need for complementary design methods [13-15].

In response to this requirement, National Cooperative Highway Research Program (NCHRP) conducted a comprehensive research study under the Project 9-19. The aim of this study was to recommend a Simple Performance Test (SPT) in order to complement the Superpave volumetric design procedure. This effort resulted in recommending three sets of testing procedure known as, dynamic modulus, repeated and static creep test among which the dynamic modulus is considered as the primary input parameter. Dynamic modulus is directly implemented in the Mechanistic-Empirical (M-E) Guide for Design of New and Rehabilitated Pavement Structure. The dynamic modulus master curve represents the temperature-frequency (or temperature-time) dependent stiffness characteristic of asphalt material [2, 52]. It should be mentioned that, the SPT, and as a result the dynamic modulus test as part of it, was introduced to perform on the laboratory compacted specimens with the test results being used as input data in design process. However, it is rather a common practice to use cores from pavement sections for quality control purposes and forensic investigations.

In order to find the dynamic modulus, the current protocol calls for axial compression testing of 100 mm -diameter- by 150 mm -height- specimen cut and cored from gyratory compacted

mixtures [53]. It is necessary to recognize that, flexible pavements in areas such as New Zealand are primarily designed with relatively thick unbound granular base layer and thin asphalt surface commonly less than 150 mm. In other situations, the asphalt layer is 50 mm or less and mainly treated as a layer which provides proper riding comfort and is not considered as a structural layer with loading capability. That results in surface thickness varying typically from 50 to maximum 150 mm. Therefore, considering the fact that the actual pavement thickness is often less than 150 mm and that coring is the most effective approach for data procurement from actual pavements, the indirect tensile (IDT) test appears to be more desirable for existing pavement evaluation due to its privilege of testing on thin cored size specimens.

In addition, the dynamic modulus as mentioned above, is used in the structural pavement design. On the other hand, IDT is the predominant laboratory test for asphalt mixture stiffness characteristic due to its simplicity and practicality. One of the objectives of this chapter of the thesis is to provide a smooth transition between these two approaches. Data from the IDT test, then, can be easily converted to dynamic modulus. Therefore, the mechanistic empirical design procedure can still be undertaken even if performing complex modulus test is not feasible for any practical reasons.

However, there are some concerns regarding the interchangeability of dynamic modulus values obtained from compression and indirect tests. First, axial compression test deals with uniaxial state of stress, whereas in indirect test the state of stress is biaxial. Moreover, in the uniaxial test, the applied stress and measured strain are in the same direction as compaction while in indirect testing the directions are perpendicular. Therefore, researchers generally believe that the effect of anisotropy will likely to be a factor and affects this difference [54].

3.2 Background

Kim and his colleagues extended the elastic solution for IDT developed by Hondros [54, 55] and applied it to the theory of linear viscoelasticity. Unlike the uniaxial compression test, the state of stress and strain distribution in the IDT test is biaxial. The difference between axial and biaxial form of loading can be well understood by considering Hooke's generalized law.

In uniaxial cases (i.e. the dynamic modulus test) one can simply obtain the Young's modulus (E) by dividing the axial stress σ_y by the axial strain ε_y as follows:

$$\sigma_y = E * \varepsilon_y \qquad 3.2\text{-}1$$

Whereas in the biaxial cases (i.e. IDT test), the modulus cannot be considered as an outcome of the horizontal stress σ_x to the horizontal strain ε_x division. Instead, in here, the biaxial stress ($\sigma_x - \nu\sigma_y$) is what needed to be considered in modulus calculation:

$$\varepsilon_x = \frac{1}{E}\left(\sigma_x - \nu\sigma_y\right) \qquad 3.2\text{-}2$$

where, ν is Poisson's ratio.

Inaccurate material properties determination can be a result of an incorrect solution. This could cause enough difference between the dynamic modulus determined from the IDT test and that from axial compression test so that these two methods cannot be used interchangeably in forensic studies. Therefore, having an accurate analytical method which could yield results similar to those of the axial compression test but use a smaller size specimen is highly required in countries such as New Zealand.

In order to obtain stresses along the horizontal and vertical diametral axis, Hondros developed a closed form solution due to a strip loading. Stresses along the principal diameters are given by the following equations;

Horizontal axis;

$$\sigma_x(x) = \frac{2P}{\pi ad}\left[\frac{\left(1 - x^2/R^2\right)\sin 2\alpha}{1 + \left(2x^2/R^2\right)\cos 2\alpha + x^4/R^4} - \tan^{-1}\left(\frac{1 - x^2/R^2}{1 + x^2/R^2}\tan\alpha\right)\right] = \frac{2P}{\pi ad}\left[f(x) - g(x)\right] \quad 3.2\text{-}3$$

$$\sigma_y(x) = -\frac{2P}{\pi ad}\left[\frac{\left(1 - x^2/R^2\right)\sin 2\alpha}{1 + \left(2x^2/R^2\right)\cos 2\alpha + x^4/R^4} + \tan^{-1}\left(\frac{1 - x^2/R^2}{1 + x^2/R^2}\tan\alpha\right)\right] = -\frac{2P}{\pi ad}\left[f(x) + g(x)\right]$$

……..3.2-4

Vertical axis;

$$\sigma_x(y) = \frac{2P}{\pi ad}\left[\frac{\left(1 - y^2/R^2\right)\sin 2\alpha}{1 - \left(2y^2/R^2\right)\cos 2\alpha + y^4/R^4} - \tan^{-1}\left(\frac{1 + y^2/R^2}{1 - y^2/R^2}\tan\alpha\right)\right] = \frac{2P}{\pi ad}\left[f(y) - g(y)\right]$$

……..3.2-5

$$\sigma_y(y) = -\frac{2P}{\pi ad}\left[\frac{\left(1 - y^2/R^2\right)\sin 2\alpha}{1 - \left(2y^2/R^2\right)\cos 2\alpha + y^4/R^4} + \tan^{-1}\left(\frac{1 + y^2/R^2}{1 - y^2/R^2}\tan\alpha\right)\right] = -\frac{2P}{\pi ad}\left[f(y) + g(y)\right]$$

……..3.2-6

where,

P = applied load, N;
a = loading strip width, m;
d = thickness of specimen, m;
R = specimen radios, m;
x = horizontal distance from specimen centre;
y = vertical distance from specimen centre; and
α = radial angle.

3.3 Linear Viscoelastic Solution

By assuming the plane stress state, Equation 3.2.2 can be rewritten for viscoelastic materials subjected to sinusoidal loading. The only difference will be having complex modulus in the denominator instead of Young's modulus.

$$\varepsilon_x = \frac{1}{E^*}\left(\sigma_x - \nu\sigma_y\right) \qquad 3.3\text{-}1$$

$$E^* = \left|E^*\right|.e^{i\varphi} \qquad 3.3\text{-}2$$

where,

E^* = Complex modulus,

$\left|E^*\right|$ = Dynamic modulus,

$i = \sqrt{-1}$, and

φ = Phase angle.

Since the test is performed in a *linear* state, the response to the sinusoidal load will be the imaginary part of the response to the complex load, P:

$$P = P_0 e^{i\omega t} = P_0\left[\cos(\omega t) + i\sin(\omega t)\right] \qquad 3.3\text{-}3$$

where,

P_0 =Amplitude of the sinusoidal load,
ω = Angular frequency, and
t = Time.

So, the strain in the viscoelastic state can be calculated by substituting Equations 3.2.3, 3.2.4, 3.3.2, 3.3.3 into Equation 3.3.1:

$$\varepsilon_x(x,t) = \frac{2P_0}{\left|E^*\right|\pi ad} e^{i(\omega t-\varphi)}\left[(1+\nu)f(x) + (\nu-1)g(x)\right] \quad 3.3\text{-}4$$

To find the horizontal displacement $U(t)$, Equation 3.3.4 is integrated over the gauge length (l is considered as half of the gauge length):

$$U(t) = \int_{-l}^{+l} \varepsilon_x(x,t)dx = \frac{2P_0}{\left|E^*\right|\pi ad} e^{i(\omega t-\varphi)}\left[(1+\nu)\int_{-l}^{+l} f(x)dx + (\nu-1)\int_{-l}^{+l} g(x)dx\right] \quad 3.3\text{-}5$$

Finally, the dynamic modulus from the horizontal displacement can be determined from the imaginary part of the total response.

$$\left|E^*\right| = \frac{2P_0\sin(\omega t-\varphi)}{\pi ad.U(t)} A \quad 3.3\text{-}6$$

where,

$$A = \left[(1+\nu)\int_{-l}^{+l} f(x)dx + (\nu-1)\int_{-l}^{+l} g(x)dx\right] \quad 3.3\text{-}7$$

with,

$$f(x) = \frac{\left(1-x^2/R^2\right)\sin 2\alpha}{1+\left(2x^2/R^2\right)\cos 2\alpha + x^4/R^4} \quad 3.3\text{-}8$$

and,

$$g(x) = \tan^{-1}\left(\frac{1-x^2/R^2}{1+x^2/R^2}\tan\alpha\right) \quad 3.3\text{-}9$$

Following the same argument for vertical displacement $V(t)$ results in analogous expression for the dynamic modulus;

$$\left|E^*\right| = \frac{2P_0\sin(\omega t-\varphi)}{\pi ad.V(t)} B \quad 3.3\text{-}10$$

where,

$$B = \left[(\nu-1)\int_{-l}^{+l} g(y)dy - (1+\nu)\int_{-l}^{+l} f(y)dy\right] \quad 3.3\text{-}11$$

where,

$$f(y) = \frac{\left(1 - y^2/R^2\right)\sin 2\alpha}{1 - \left(2y^2/R^2\right)\cos 2\alpha + y^4/R^4} \quad 3.3\text{-}12$$

$$g(y) = \tan^{-1}\left(\frac{1 + y^2/R^2}{1 - y^2/R^2}\tan\alpha\right) \quad 3.3\text{-}13$$

A unique form of dynamic modulus can be determined by combining Equations 3.3.6 and 3.3.10;

$$\left|E^*\right| = \frac{P_0 \sin(\omega t - \varphi)AV(t) + P_0 \sin(\omega t - \varphi)BU(t)}{\pi ad.U(t).V(t)} \quad 3.3\text{-}14$$

After substituting Equations 3.3.7 and 3.3.11 into Equation 3.3.14 one can find the following expression;

$$\left|E^*\right| = \frac{4P(\beta_1\gamma_1 + \beta_2\gamma_2)\sin(\omega t - \varphi)}{\pi ad(U(t)(\beta_1 - \beta_2) - V(t)(\gamma_1 + \gamma_2))} \quad 3.3\text{-}15$$

where,

$$\gamma_1 = \int_{-l}^{+l} f(x)d(x) \quad 3.3\text{-}16$$

$$\gamma_2 = \int_{-l}^{+l} g(x)d(x) \quad 3.3\text{-}17$$

$$\beta_1 = \int_{-l}^{+l} g(y)d(y) \quad 3.3\text{-}18$$

$$\beta_2 = \int_{-l}^{+l} f(y)d(y) \quad 3.3\text{-}19$$

$$V(t) = V_0 \sin(\omega t - \varphi) \quad 3.3\text{-}20$$

$$U(t) = U_0 \sin(\omega t - \varphi) \quad 3.3\text{-}21$$

Therefore, the final form of dynamic modulus resulted from IDT test will be as follows;

$$\left|E^*\right| = \frac{4P(\beta_1\gamma_1 + \beta_2\gamma_2)}{\pi ad(U_0(\beta_1 - \beta_2) - V_0(\gamma_1 + \gamma_2))} \quad 3.3\text{-}22$$

where, U_0 and V_0 are the constant amplitudes of horizontal and vertical displacements, respectively.

Poisson's ratio can be calculated by equating Equations 3.3.6 and 3.3.10;

$$\nu = \frac{U_0(\beta_1 + \beta_2) + V_0(\gamma_1 - \gamma_2)}{U_0(\beta_1 - \beta_2) - V_0(\gamma_1 + \gamma_2)} \qquad 3.3\text{-}23$$

The coefficients γ_1, γ_2, β_1 and β_2 for different specimen diameters and various gauge lengths are brought in Table 3.3.1.

Table 3.3-1Coefficients for Poisson's ratio and dynamic modulus

Specimen Diameter - mm	Gauge Length - mm	Loading Strip - mm	γ_1	γ_2	β_1	β_2
100	25	12.7	0.0059	0.003	0.0033	0.0064
100	38	12.7	0.0083	0.0044	0.0053	0.01
100	50	12.7	0.01	0.0054	0.0075	0.0136
150	25	19	0.0063	0.0032	0.0032	0.0065
150	38	19	0.0092	0.0048	0.0052	0.01
150	50	19	0.0116	0.0061	0.007	0.0134

3.4 Specimen Preparation

In this study, AC 20 mix is used. AC 20 is a heavy duty dense graded hot mix asphalt that is commonly used in New Zealand; it has 20 mm maximum nominal aggregate size. Table 3.4.1 shows the AC 20 aggregate gradation used in this study. Two types of asphalt binders were used in this research; 60/70 and 80/100 penetration grades. The aggregates, binders and job mix formula of the mix were taken from a local contractor in Christchurch**.** Details for mix design and aggregate properties are provided in Appendix A. More than thirty asphalt mixture specimens were mixed and compacted in the University of Canterbury Transportation laboratory. Asphalt mixtures were tested at two different air percentages (VTM = 4.0 & 5.0%).

Specimens were prepared in accordance with the Australian standard AS 2891.2.1 "Methods of Sampling and Testing Asphalt" [56]. Accordingly, the asphalt cements were mixed and compacted at 150 °C. All mixtures were also aged at 150 °C for one hour before compaction.

For the axial compression test, the cylindrical specimen has a 100 mm -diameter- by 150 mm -height- were cut and cored from 150 mm -diameter- by 180 mm -height- gyratory compacted specimens. For IDT test, 100 mm -diameter- by 150 -height- gyratory compacted specimen

specimens were sawn into three specimens each has 100 mm diameter and 40 mm height. Three replicates of each combination were prepared for axial compression as well as the indirect tensile test.

Table 3.4-1AC 20 Mix aggregate gradation

	% Passing	
Sieve Size (mm)	Blend Result	AC 20 Specification
19	100	100
13.2	91	83 - 95
9.5	78	70 - 90
6.7	70	60 - 79
4.75	66	52 - 70
2.36	44	40 - 55
1.18	32	29 - 43
0.6	24	20 - 32
0.3	17	13 - 23
0.15	9	8 - 16
0.075	5	4 - 10

3.5 Experimental Testing Program

The uniaxial compression test consists of applying a uniaxial sinusoidal compressive stress to an unconfined or confined hot mix asphalt cylindrical test specimen. Measured stresses and strains are used to calculate the resulting dynamic modulus and phase angle. Figure 3.5.1 represents a schematic of typical data from the dynamic modulus test. The dynamic modulus and phase angle are defined by Equations 3.5.1 and 3.5.2, respectively.

Dynamic modulus samples were tested at 5 different temperatures (4.4, 15, 21.1, 30 and 40 °C) and frequencies (10, 5, 1, 0.1, and 0.01 Hz) in order to plot the Master Curve. The test is considered as a non-destructive test which means, single specimen can be used for the entire range of temperatures and frequencies.

In order to minimize any damage or changes of the volumetric properties of the test specimens, testing program began with the lowest temperature and proceeded to the highest. At any given temperature, the test began with the highest frequency of loading and progressed to the lowest. This sequence is intuitive because asphalt concrete becomes stiffer at low temperatures and high frequencies. Therefore, that helps to minimize the chance of damaging the specimen.

In the uniaxial test, to keep the stress state in the linear viscoelastic region, the loading patterns were applied in a way that the generated strains were in the target range of 50 to 150 με to maintain linearity.

In order to check the quality of the test data, the complex plane and black space are also plotted. In complex plane, the storage modulus, E_1, is plotted against the loss modulus, E_2. The plot should form a unit curve which would signify the independence state of complex modulus from frequency and temperature. In Black space, the complex modulus and phase angle are plotted in logarithmic scale. This method is believed to result in higher accuracy assessment at high temperatures. Similar to complex plane, the Black space also shows the frequency/temperature independent relationship of the complex modulus and phase angle. The graphs plus the master curve table of parameters and shift factors for mixtures used in this study are provided in Appendix B [43, 57].

The IDT tests were conducted at 5 different temperatures (4.4, 15, 21.1, 30, 40 °C) and frequencies (2, 1, 0.6, 0.2 and 0.1 Hz). Due to software limitations, the authors were not able to run the tests at the exact same frequencies and without rest period similar to the uniaxial test. The tests were run based on the same concept of linearity to prevent possible damages. According to the Australian Standard AS 2897.13.1 "Determination of the Resilient Modulus of Asphalt – Indirect Tensile Method" [58], the applied load level was adjusted so that the recoverable horizontal strain would be in the range of 50 ± 20 με.

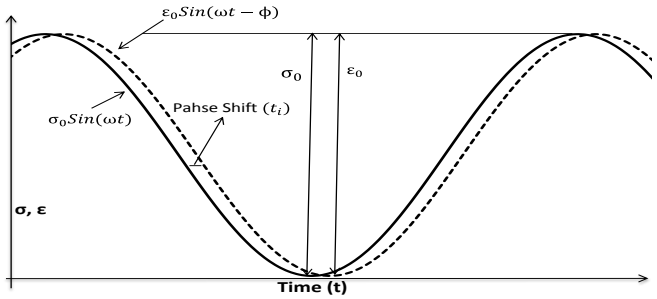

Figure 3.5-1 Sinusoidal loading pattern for the uniaxial compression test

$$\left|E^*\right| = \frac{\sigma_0}{\varepsilon_0} \qquad 3.5\text{-}1$$

$$\varphi = \frac{t_i}{t_p} * 360 \qquad 3.5\text{-}2$$

where,

$|E^*|$ = Dynamic modulus,
σ_0 = Peak (maximum) stress,
ε_0 = Peak (minimum) strain,
φ = Phase angle, degrees,
t_i = Time lag between a cycle of stress and strain (s),
t_p = Time for stress cycle (s).

In plotting the dynamic modulus master curve, the abovementioned temperature-frequency combinations are selected, so the data will have proper overlap for an accurate and smooth curve. However, this requirement was not necessarily met for all the frequency-temperature combinations in the case of the indirect tensile test. This could be noticed among the data bridging results from 4.4 to 15.0 °C although the data were close enough that the accuracy of final curve was not alternated. Additionally, as the high frequency test (i.e. 1000 Hz) could not be performed for the IDT, it was not possible to compare the dynamic modulus from the compression test with that from indirect tensile test.

3.6 Test Setup

Considering the uniaxial compression test, three on specimen vertical Linear Variable Displacement Transformers (LVDTs) with a gauge length of 100 mm were mounted on the specimen at 120° from one another. Figure 3.6.1(a) shows the setup for the uniaxial compression test. To maintain a uniform stress distribution and reduce the friction between the load platens and the specimen, two layers of friction reducers were used in this study. One layer was under the bottom face of the specimen and the other one at the top of the specimen under the top load platen.

Two different test setups were considered for the IDT test. The conventional method was conducted based on the Australian Standard AS 2897.13.1 [58]. According to this procedure, two horizontal LVDTs were placed on the sides of the specimen to measure the horizontal deformation as it can be seen in Figure 3.6.1(b).

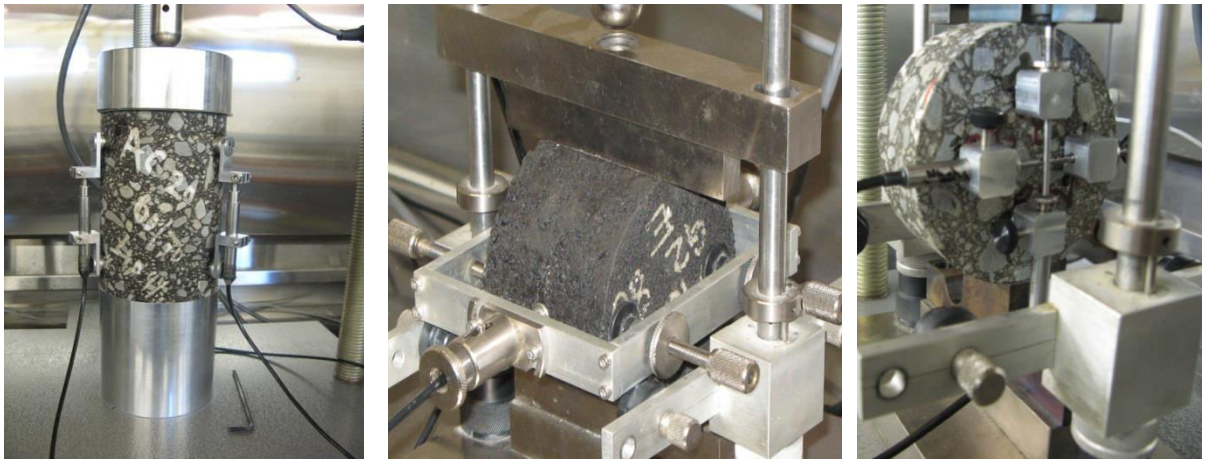

(a) (b) (c)

Figure 3.6-1Test setups; (a) Uniaxial Compression, (b) IDT-Australian Method, (c) IDT-AASHTO Setup

Consequently, gauge length for the Australian method will be equal to specimen diameter (i.e. 100.0 mm). In the Australian method, Poisson ratio needs to be assumed and usually it is assumed in a range of 0.35 to 0.40. For the second type of IDT test set up recommended by AASHTO T 322, deformation measurement LVDTs were mounted on the specimen surface so that both horizontal and vertical deformations can be recorded. In this setup, Poisson ratio can be determined from the horizontal and vertical deformations. The gauge length for this method was fixed at 50.0 mm for both vertical and horizontal LVDTs. Figure 3.6.1(c) illustrates the AASHTO test setup for IDT test.

To control the temperature during the experiment, a temperature chamber with a temperature range from "-5 to 60 °C" and accuracy of "± 0.1 °C" was used. Dummy specimens with the temperature sensor mounted at the centre were used in order to monitor the actual specimen temperature during testing process.

3.7 Results and Discussions

The dynamic modulus master curve is constructed based on the concept of the time-temperature superposition principle. This principle is applied to *thermorheologically simple (TRS)* materials. For this class of materials, the same modulus value can be obtained either at the low test temperatures and long loading times or at high test temperatures but short loading times. In other words, the material exhibits similar behaviour either at high temperature and fast loading rate or at low temperature and slow loading rate [59].

In the original AASHTO test protocol, in order to plot the master curve, the dynamic modulus test was required to be conducted at five temperatures (-10, 4.4, 21.1, 37.8 and 54.4 °C) and six frequencies (25, 10, 5, 1, 0.5 and 0.1 Hz). However, through the course of time, it was felt that the testing protocol requires some modifications in order to reduce both the time and the cost of testing procedure. After a number of robust testing [59, 60] it was found that the test can be successfully run at three temperatures (4, 21 and 40 ºC) and four frequencies (10, 1, 0.1 and 0.01). With this modified regime, considerable time saving could be effected for the dynamic modulus test. Number of test replicates depends chiefly on the estimated standard error of the mean. However, recommended number of specimens generally varies between 2 and 3 [2].

Table 3.7-1 Comparison of various testing protocol

Test Protocol	No. of Temperatures	Testing Temperatures (°C)	No. of Frequencies	Testing Frequencies (Hz)
AASHTO – TP62	5	-10, 4, 21, 38, 54	6	25, 10, 5, 1, 0.5, 0.1
Modified – Witczak (2003)	3	-10, 21, 54	4	33, 2.22, 0.15, 0.01
Modified – Bonaquist 2008	3	4, 21, 40	4	10, 1, 0.1, 0.01
Modified – Current study	5	4, 15, 21, 30, 40	5	10, 5, 1, 0.1, 0.01

In this study, in order to thoroughly have the required overlap on the obtained data for a feasible master curve, it was decided to perform the tests at 5 different temperatures and frequencies as brought in Table 3.7.1

Results of the axial compression test were analysed according to the NCHRP 1-37A protocol. As for the IDT test, the modulus was calculated by applying the biaxial linear viscoelastic solution as discussed earlier. Two separate approaches were implemented in this study to investigate the pros and cons of each method. First, the dynamic modulus was calculated based on the Australian test set up method (i.e. by recording only horizontal deformation [61]. Hence, Poisson's ratio was considered constant in data analysis equal to 0.40 following the Australian standard procedure [6].

For the next stage of testing, both horizontal and vertical deformations were considered in modulus calculation in accordance to the AASHTO test setup. The Arrhenius equation was considered for this study in order to find the required shift functions to plot the dynamic

modulus master curves. The final curves are plotted in the Figures 3.7.1and 3.7.2. The data presented in these figures are the average results of three replications.

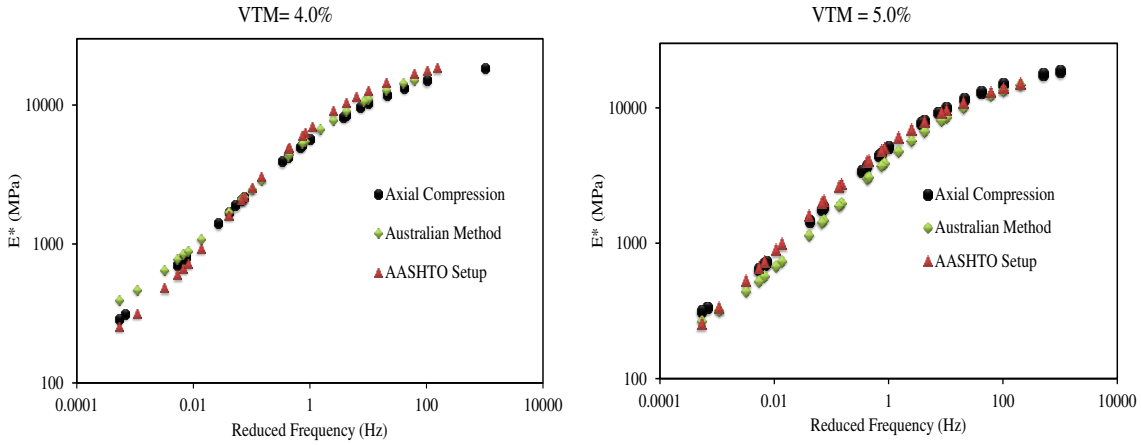

(a) (b)

Figure 3.7-1 Dynamic modulus master curve; binder 60/70 (a) VTM = 4.0%, (b) VTM =5.0%

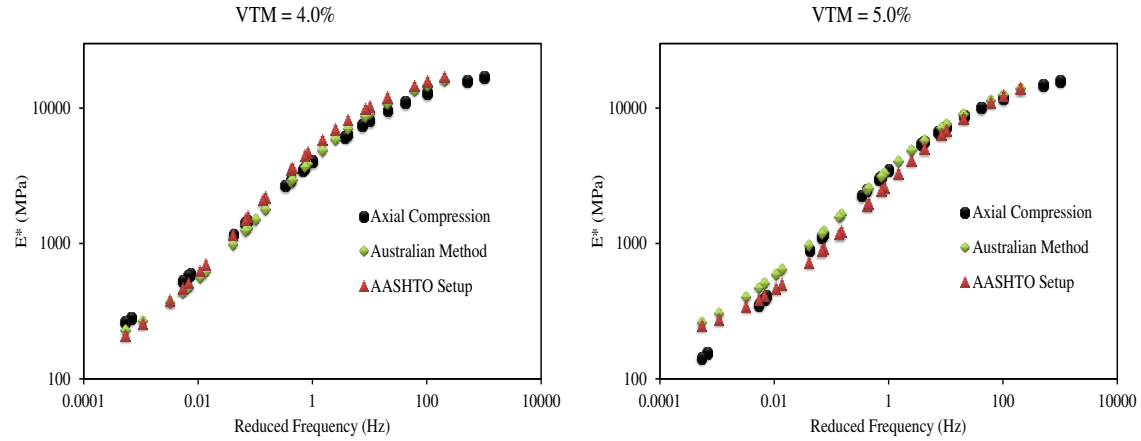

(a) (b)

Figure 3.7-2Dynamic modulus master curve; binder 80/100 (a) VTM = 4.0%, (b) VTM =5.0%

Obtaining reasonable values of Poisson's ratio verifies the quality of the recorded data. This could be an indication of a sound complex modulus value and proves the validity of the available data. As long as the Poisson's ratio is less than 0.5, the experiment is considered to be performed in a linear phase. Exceeding the linear elastic limit of 0.5 would be the sign of damage in specimen. Figure 3.7.3 presents the Poisson's ratio calculated from the IDT test for different asphalt mixtures. As can be seen from Figure 3.7.3, Poisson's ratio in this study is mainly less than 0.5. It is also evident that the Poisson's ratio is slightly frequency dependent.

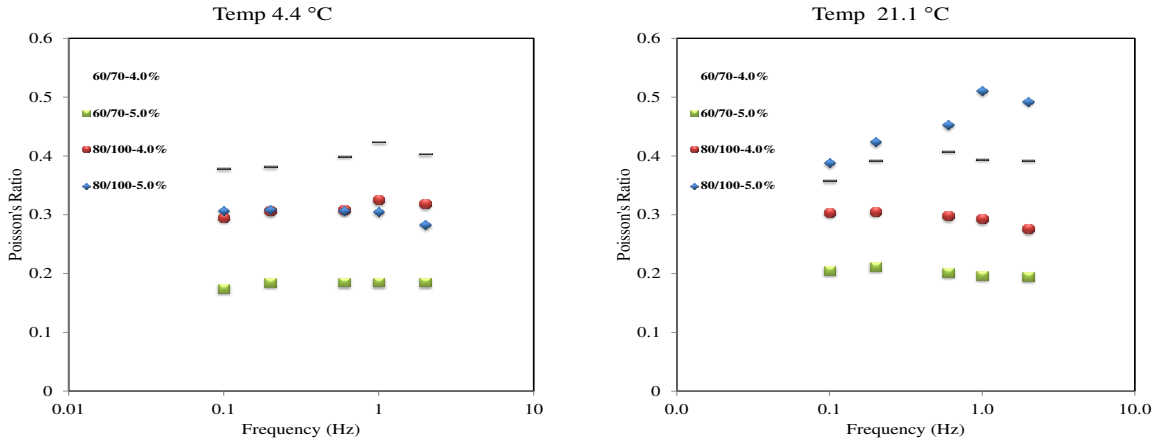

(a) (b)

Figure 3.7-3Change in Poisson's ratio as a function of temperature and frequency

In order to have a closer look at the analysed data, the table below summarizes the dynamic modulus calculated from the axial and IDT tests. Due to having large amount of data collected in this experiment, only selected groups of these data are presented for the purpose of comparison. Two sets of mix are presented in Table 3.7.2. The sets chosen were; the mix AC 20 with "binder 60/70, 4.0% air voids" and with "binder 80/100, 5.0% air voids".

Table 3.7-2 Average Dynamic Modulus for Axial and IDT Tests

	AC 20 - Binder 60/70 -VTM = 4.0%			AC 20 - Binder 80/100 -VTM = 5.0%		
Frequency	Dynamic modulus (MPa)			Dynamic modulus (MPa)		
(Hz)	Uniaxial	IDT		Uniaxial	IDT	
		Australian Setup	AASHTO		Australian Setup	AASHTO
100	15023	15210	15790	11854	12595	12095
10	10350	12550	10460	7547	7281	7077
0.7	5152	5324	5610	3143	3108	2890
0.07	2167	2178	2230	1239	1162	1173
0.0005	290	395	340	261	143	277

As can be seen from the presented data, the visual observation suggests rather promising link between IDT and uniaxial compression test data. The data are closely matched in a wide range of frequency. But recognizing the existence of sample to sample variation, a statistical analysis was considered with the unequal variance t-test. The t-test assesses whether the means of two groups are *statistically* different from each other [62]. The null hypothesis in here is that the dynamic modulus obtained from either of the IDT tests is equal to that from the axial compression test. The level of significance, α which is probability of type 1 error for

the test is considered equal to 0.05. In order to reject or accept the hypothesis the P-value was calculated and compared with α. P-value indicates the probability of getting a mean difference between the groups as high as what is observed by chance. The lower the P-value is, the more significant the difference between the groups will be. Therefore, in this study a P-value greater than 0.05 indicates the statistical similarity between IDT and axial compression test results.

Tables 3.7.3 and 3.7.4cover the t-test result between "conventional IDT and uniaxial test" and also between "IDT with new setup and uniaxial test", respectively. More information on the statistical data analysis is covered in Appendix C.

Table 3.7-3 *P* Values for Dynamic Modulus from Uniaxial and IDT-Australian Tests

	AC 20			
	Binder 60-70		Binder 80-100	
	VTM		VTM	
	4.00%	5.00%	4.00%	5.00%
P Value				
Less than 0.05	5%	15%	5%	5%
Greater than 0.05	95%	85%	95%	95%

Table 3.7-4 *P* Values for Dynamic Modulus from Uniaxial and IDT-AASHTO Tests

	AC 20			
	Binder 60-70		Binder 80-100	
	VTM		VTM	
	4.00%	5.00%	4.00%	5.00%
P Value				
Less than 0.05	10%	5%	5%	5%
Greater than 0.05	90%	95%	95%	95%

Results of statistical analysis for 28 tests (4 mixtures by 7 frequencies) are presented separately for each of the IDT test methods. Based on the statistical analysis, more than 90.0% of the test data indicate no statistical difference between dynamic modulus resulted from uniaxial test than that from IDT tests. Hence, the statistical analyses advice that the dynamic modulus determined from the IDT tests with the linear viscoelastic solution *could be* the same as the one measured from the axial compression test. The finding is in agreement with the recent National Cooperative Highway Research Program (NCHRP), Project 9-22B,

which concluded that it was possible to use the dynamic modulus calculated from IDT test mode as an input for pavement performance software program[63].

Theoretically speaking, the data above proved the applicability of the theory of linear viscoelasticity, within its acceptable range, to the asphaltic materials. Converting data from either of the two IDT test setups showed quite promising results. The outcome was further validated through the statistical analysis. As a result of this research, the highway agencies could, confidently, run their forensic studies even for the thin layer pavements evaluation. In addition, the researchers would also be able to test IDT-size specimen in laboratories, a size that is more convenient and consume noticeably less material in the preparation stage.

Examining the IDT test setups reveals that either of these two setup methods has its own privilege over the other. Considering the Australian method with horizontal LVDTs on the side shows that, calculated graphs are not equally compatible for the entire test range. Given that the Poisson's value changes with the change of temperature and frequency, therefore, assuming constant Poisson's ratio could contribute to the part of the existing differences observed between the dynamic modulus from the Australian IDT and uniaxial compression tests. This could be solved by introducing vertical LVDT. By running the test under the AASHTO T322, change in Poisson' ratio will be considered in the modulus calculation. However, the AASHTO test setup will have its particular deficiencies. Literature suggests that, vertical measurement is predominantly more sensitive to local perturbation in comparison to horizontal measurement. Mirza and his colleagues [64] concluded in their study that, any local discontinuity in the test specimen would have greater influence on the vertical displacement than the horizontal displacement. They showed that around 85 percent of the total deformation in the horizontal direction is within the central strain region, whereas it drops to merely 30 percent considering the vertical displacement. Therefore, conducting vertical measurement would be only beneficial where the nominated specimen is highly uniform with no big aggregate sizes within the gauge length. Otherwise, the vertical measurement will simply increase the risk of incorrect modulus calculation. In addition, having two LVDTs mounted on the specimen needs great attention of keeping them perpendicular to each other.

In addition, the effect of anisotropy is another expected factor. In the uniaxial test the loading is in the same direction as the compaction of the specimen, but in the IDT test the loading is

perpendicular to the compaction of the specimen. The effect of anisotropic is intrinsic due to the compaction direction and aggregate orientation.

3.8 Conclusions

This chapter examined the current approaches to testing asphalt specimen in New Zealand (i.e. IDT) and tried to utilise the data from this test to determine dynamic modulus and also compare the difference in dynamic modulus measured utilising two different setups of the IDT test and the axial compression test. The IDT test is reasonably well known by the industry in New Zealand due its simplicity and practicality. In New Zealand, thin asphalt pavements are the most predominant type of pavements, therefore, it is difficult to core 150 mm height specimen from the actual pavement for the current axial compression test method. Thus, this study tried to apply an analytical method derived from the theory of linear viscoelasticity to calculate dynamic modulus of asphalt mixtures from the IDT test procedures. Dynamic modulus was calculated based on the theory of linear viscoelasticity from two different IDT configurations - horizontal versus horizontal and vertical displacement reading. The advantages and disadvantages of each of these methods were discussed in this section.

The calculated data were analysed by the statistical approach to check the significance of the observed differences amongst these methods. More than 90% of the test data showed no statistical differences between the dynamic modulus determined from IDT and axial compression tests. According to the statistical analysis, the dynamic modulus determined from the IDT test with the linear viscoelastic solution *is likely to be the* same as the one measured from the axial compression test.

The following can be derived as a result of this study;

a) Given the popularity of the Indirect Tensile test with the industry and based on the data extracted, the IDT test can be utilised to determine the dynamic modulus of the mix.
b) By running the IDT test, less material and time is required in the preparation phase which makes it economically superior to the current axial compression test protocol,

c) Comparing the Australian method with the AASHTO test protocol reveals the compatibility between these two methods. As a result of that, the Australian approach can be selected by the industry.

d) The Australian test method has an advantage of being, unlike the AASHTO, simpler (no need to glue any gauge points on the specimen) and less complicated in set up preparation by just having two horizontal LVDTs on the sides compare to the AASHTO method.

Chapter 4: Hot Mix Asphalts Viscoelastic parameters and the Interconversion amongst Viscoelastic Functions

4.1 Introduction

Creep Compliance and Relaxation Modulus tests are two of the main laboratory experiments when it comes to viscoelastic characterization of asphaltic materials. These tests results are directly used in some of the finite element programs such as ABAQUS for the simulation purposes. As a result, material properties resulted from the above tests will be studied in this chapter in order to provide the necessary data required for the analytical stage.

Asphalt concrete is a composite material comprising aggregate and bituminous mastic which possesses viscoelastic characteristic. It behaves as a linear viscoelastic material (LVE) under the low level of the applied loads [65-68]. The asphaltic material maintains linearity as long as the loading conditions do not contribute to damage in the material. This linear viscoelastic response could be expressed by the following convolution integral [69]:

$$R = \int_0^t R_H(t-\tau)\frac{dI}{d\tau}d\tau \qquad 4.1\text{-}1$$

where,

R_H = Unite response function,
I = Input,
t = Time of interest, and
τ = Integration variable.

The convolution integral above reveals a significant characteristic in viscoelastic type materials such as asphaltic concrete mix. It exhibits the time-temperature rate of loading dependence material response, with the response being not only a function of the current input, but also of the current and past input history.

The linear theory of viscoelasticity yields a mathematically tractable solution for stress-strain-time relations of the linear viscoelastic materials. Several functions are available to describe the viscoelastic characteristic of asphalt concrete mixes. These functions are either in time domain, such as relaxation modulus $E(t)$ and creep compliance $D(t)$ or in frequency domain, such as complex modulus E^*. Any of these methods can be used to characterize the

viscoelastic material properties. The permanent deformation phenomenon and fatigue are evaluated conducting the creep and relaxation tests [70, 71].

It is well-known that all these viscoelastic functions are mathematically interrelated and each function contains essentially the same information on relaxation and creep properties [43, 72, 73]. Therefore, by having one of these responses and applying proper interconversion technique all the other responses could be predicted. Hence, through the appropriate mathematical procedure, a linear viscoelastic material function can be converted into other viscoelastic material functions. The importance of applying interconversion technique exists for different reasons. For instance, it is difficult to undertake a strain-controlled relaxation test on stiff materials; however, stress-controlled creep test is much more convenient for researchers to run. As a result, the relaxation modulus is generally converted from either the static creep or the complex modulus test data.

This chapter is divided into two parts. First, various interconversion techniques will be studied in converting creep compliance to relaxation modulus. It will cover approximate as well as exact conversion approaches. The level of accuracy of the approximate technique will also be validated in this part.

As mentioned, the creep compliance and the relaxation modulus are both time domain functions. However, the complex modulus test is conducted in the frequency domain resulting in a frequency domain output. Contrary to what is mathematically believed, experience has revealed that, the interconverted data from frequency domain do not necessarily match the one resulted from time domain laboratory experiment. Therefore, the second part of this chapter will investigate the true relationship amongst these viscoelastic functions.

4.2 Creep Compliance to Relaxation Modulus Interconversion

Considering the creep compliance and the relaxation modulus interconversion, several approximate techniques can be found in the literatures [74-76]. The first part of this chapter will, briefly, review some of the most prominent approximate techniques and compare their results. In addition, the exact interconversion technique will be covered in details. In this regard, the relaxation modulus will be converted from the static creep test applying the

Tikhonov regularization. As a result, the accuracy of the approximate methods will be checked against the exact solution.

In order to do so, the Prony series coefficients were fitted to experimental data with and without presmoothing technique. The data were resulted from the static creep test for various asphalt mixtures. It was found that, the smoothing technique will not necessarily result in positive Prony coefficients. The data were, afterward, converted to the relaxation modulus through various numerical techniques. This study shows that, the converted relaxation curves could deviate from each other based on the applied technique and the Prony coefficient selection. The reason for this discrepancy was sought and proper solution was recommended. The exact conversion technique was also studied for the creep–relaxation conversions by applying the Tikhonov regularization technique. In general, data resulted from the approximate methods showed around 93% accuracy.

4.3 Sample Preparation and Testing

4.3.1 Materials

In this study, AC 20 and AC 14 were utilized which are commonly used hot mix asphalts in New Zealand highway industry. AC 20/14 mixes have 20 and 14 mm maximum nominal aggregate size, respectively. The aggregates, binders and job mix formula of the mix were taken from a local contractor who designed these mixes for one of the Motorways in Christchurch. Table 4.3.1 covers the aggregate gradation for these mixtures. Details for mix design and aggregate properties are provided in Appendix A.

Table 4.3-1 Aggregate gradation

	Percentage Passing	
Sieve Size (mm)	**AC 20**	**AC 14**
19.0	100	100
13.2	91	100
9.5	78	87
6.75	76	75
4.75	66	69
2.36	44	46
1.18	32	33
0.600	24	25
0.300	17	17

The optimum binder contents were found to be 5.0 and 5.5% for AC 20 and AC 14, respectively. 60/70 and 80/100 penetration grade binders were used in mix preparation. Mixtures above have identical job mix formula to the ones used in Chapter 3. Cylindrical specimens which had a diameter of 100 mm and a height of 150 mm were cut and cored from 150 mm in diameter and 170 mm height gyratory compacted specimens. The asphalt mixture was prepared based on Australian Standard AS 2891.2.1 "Methods of Sampling and Testing Asphalt" [56]. Accordingly, the asphalt samples were mixed and compacted at 150 °C. Based on AS 2891.2.1, all mixtures were aged at 150 °C for one hour before compaction to simulate the short term aging.

4.3.2 Experimental Plan

For the first part of this research, the static creep test was performed in order to record the source function for the interconversion purpose. The test is utilized under the uniaxial loading for 1000 seconds. Asphalt specimens of various properties were tested at different temperatures in order to verify the proposed approach. Table 4.3.2 shows the specimens as well as the test conditions. Three specimen replications were manufactured for each test combination. Air void content and test temperatures for this preliminary set of experiment are selected in order to cover the actual test properties.

Table 4.3-2 Properties of asphalt mixes

	Mix type	Binder	Air void percentage %	Temperature (°C)
1	AC 14	60/70	3.0 ± 0.5	30.0
2	AC 14	80/100	3.0 ± 0.5	25.0
3	AC 20	60/70	3.5 ± 0.5	15.0
4	AC 20	60/70	4.5 ± 0.5	15.0

4.4 Determining the State of Linearity

The creep compliance – relaxation modulus relations are governed as long as the linearity is guaranteed. As a result, the linear limit was determined prior to the experiment stage. The material characteristic is said to satisfy the linearity if it follows the Boltzmann's principles (i.e. proportionality, and superposition). It was found, in a preliminary stage, that 400 microstrains is the maximum strain measured for the static creep test. As a result, the Boltzmann's principles were checked for 450 microstrains in this research.

The proportionality principle states that the specimen strain is directly proportional to the applied stress. As a result, if the input stress is doubled, the response strain doubles as well. Figure 4.4.1-a shows the strain curves resulted from the static creep test for two stress levels; 70 and 35 kPa. As can be seen in the figure, doubling the stress is increased the strain level by twofold. Meanwhile, based on the superposition principle, the strain response from two independent stresses should be the equivalent of the strain response to the sum of these stresses. Figure 4.4.1-b displays the data for three stress levels. Based on the figure, the strain path for the 70 kPa can be found by combining 50 and 20 kPa. In conclusion, Figure 4.4.1 (a and b) show that the mixture under the given strain level clearly satisfies the linear superposition principle. The data presented in these figures are the averages of three replications.

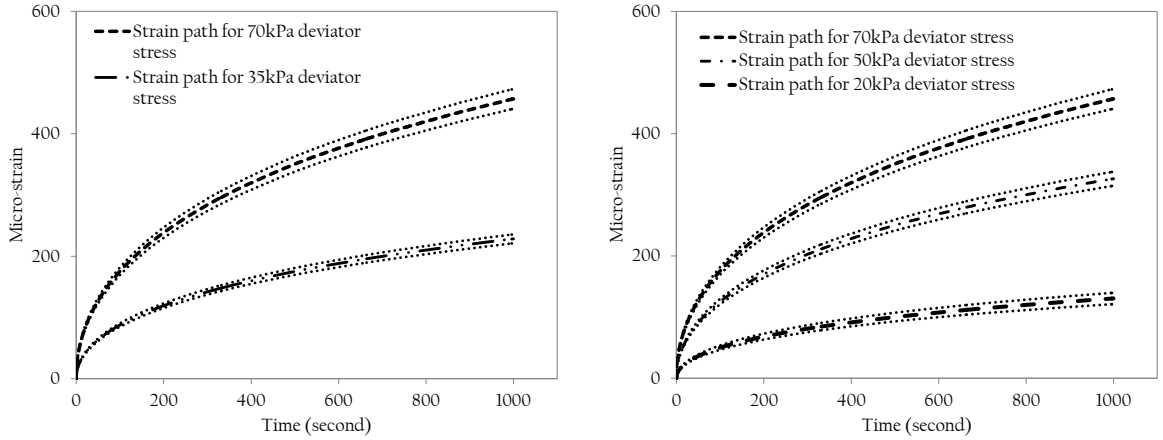

(a) (b)

Figure 4.4-1 Linearity check; (a) Proportionality, (b) Superposition – with standard deviation

4.5 Fitting Prony Series to Experimental Data

In order to have an accurate material characterization, it is required to establish a representative analytical expression of LVE response functions regardless of how these functions are developed. There are two common approaches for representing viscoelastic response; Power-law and Prony series. The latter is widely acceptable among researchers [77, 78] due to its ability of describing a wide range of viscoelastic response. Additionally, the Prony series expression has a relatively simple and rugged computational efficiency regarding its exponential basis functions [79]. It consists of a sequence of decaying exponential terms as shown in Equation 4.1.1. Moreover, compared to the power-law, the

Prony expression has also an advantage of having a physical basis in the theory of mechanical models dealing with linear springs and dashpots.

For creep compliance in a time domain, the response function, in Prony representation, is of the following form which is often referred to as the *generalized Voigt model [80]:*

$$D(t) = D_g + \sum_{j=1}^{N} D_j \left[1 - e^{-t/\tau_j} \right] \qquad 4.5\text{-}1$$

where,

τ_j = Retardation time,
D_j = Regression coefficients and,
D_g = Glassy compliance.

The glassy compliance in Equation 4.1.1 denotes the short term creep behaviour i.e. $D_g = \lim_{t \to 0} D(t)$. The retardation time, considering the mechanical analogous, is defined as the ratio of the viscosity to elastic modulus in the generalized Voigt (Kelvin) model. In other words, it is the time required for the spring and the dashpot to deform to 63.2% of the total creep.

There are several methods available to fit Prony series coefficients to the given experimental data. The collocation method by Schapery is known to be as one of the primary techniques in this regard [77]. Cost and Becker developed the so-called multi data method in Laplace domain based on least squares approach [81] while Park and Schapery and Schapery and Park evaluated and developed new methods of interconversion based on numerical and approximate analytical method [82, 83]. Recently, Silva and his colleagues and Sousa *et.al* established a computer program in order to fit the Prony series to experimental data [84, 85].

In fitting the creep compliance using a Prony representation, there are 2N unknowns involved; D_j and τ_j $(j = 1...N)$ and correspondingly there will be $2N$ nonlinear equations. Yet, in order to avoid the complexity resulting from solving nonlinear equations, the retardation times τ_j are usually specified a priory from experience. That leaves D_j as the only unknowns to be solved through linear system of equations. To solve these linear algebraic equations, the collocation method is used when the number of equation is equal to the number of unknowns. In case of having greater number of equations than unknowns, the

least square method will be applied [82]. Typically, one decade interval is considered adequate for τ_j and the glassy compliance D_g could be obtained by extending the experimental curve asymptotically to time $t = 0$.

As for allocating the retardation times, apart from assigning them by experience, Feng and Hallquist in their research came up with an expedient suggestion [86]. They argue that, the retardation time value should be the inverse of the largest time in the experiment. For example, if the largest value of time is 10^4 seconds, then τ_j should be considered as 0.0001. As for the number of terms, they believe they should be equal to the number of decades of time covered by the experiment. For instance, for the experiment with the time span from 10^{-2} to 10^4 seconds, N should be assigned as six.

As it was mentioned, it is quite desirable to implement Prony series as a material function due to its simplicity and amenability to mathematical operations. However, one concern regarding the Prony application is that it often yields in negative values, a physically unrealistic case. It is believed that a wide scatter and unsmoothed set of experimental data most likely leads to this problem. Several attempts have been done to overcome the problem of negative coefficients. One of the latest approaches was introduced by Park and Kim [87]. In their research they recommended using modified power-law series to presmooth the large scattered data before fitting Prony coefficients to the experimental data.

Power-law series is an accepted method used to represent the viscoelastic response [79]. The main draw back with power-law representation is its mathematical deficiency which makes it analytically undesirable for material function development from computational point of view. For example, considering the Laplace transform of a material function, it is typically required for viscoelastic materials to eliminate the time factor in equation. Unlike the Prony series expression, obtaining the transformed function in power-law series is rather cumbersome task to undertake [87, 88]. But, that does not reject the idea of using power-law expression to presmooth data to which a Prony series will finally be fitted. The only mathematical operation involved is a simple linear regression.

4.5.1 Static Creep Test

As it was mentioned, the static creep test was performed in this study. The test was utilized under uniaxial loading with 70 kPa deviator stress at 15.0 °C for duration of 1000 seconds

(Details for the AC 20 mix with 60/70 binder grade and 4.5 ± 0.5 °C is explained in this section, only. Data for the rest of mixtures are brought in Appendix D).The experimental data were fitted by a 5-term Prony series representation. Initially, data were fitted without smoothing which, as it was expected, resulted in negative coefficients; a physically unrealistic case. In order to account for this problem, the raw data were then smoothed by the pure power-law expression. Prony coefficients were then fitted to the smoothed data. Yet, presmoothing did not help either in this particular case (as shown in Table 4.5.1). The reason, should be that smoothing process is believed to be reasonably effective where the experimental data are widely scattered and unsmoothed such as the case with the complex modulus test data. Whereas, the data recorded in this study as a result of uniaxial static creep test are fairly smooth and noise free. This could be a result of running the test at low temperature (15.0 °C) and under the relatively low stress (i.e. 70 kPa).

Table 4.5-1 Prony series coefficients

	Before Presmoothing		**After Presmoothing**	
j	τ_j sec	D_j 1/MPa	τ_j sec	D_j 1 /MPa
1	1	0.000164	1	0.000172
2	10	0.000656	10	0.000623
3	100	0.001523	100	0.001531
4	1000	0.006970	1000	0.007100
5	10000	*-0.003620*	10000	*-0.003510*
$D_g = 0.0000612 \left(1/MPa\right)$				

Finally to achieve the required positive value, Equation 4.5.1 was formulated for the raw experimental dada to column vectors, $\{A\}$ and $\{C\}$, and matrix $[B]$, as expressed below [89]:

$$\{A\} = [B] * \{C\} \qquad 4.5\text{-}2$$

where,

$$\{A\} = D(t_m) - D_g\,, \qquad [B] = \sum_{j=1}^{N}\left[1 - e^{-t_m/\tau_j}\right],\ m = 1...M\,, \qquad \{C\} = \sum_{j=1}^{N} D_j$$

Using the following rearrangement forces Prony coefficients to be positive while also satisfies Equation 4.5.2:

$$\text{minimize } \left|[B]\{C\} - A\right| \text{ satisfying } \{C\} > 0 \qquad 4.5\text{-}3$$

To solve the linear set of problem in Equation 4.5.3, non-negative least square (NNSL) algorithm was used as a built in function in MATLAB. NNLS algorithm is designed for linear least square problems involving linear inequality constraints. The algorithm minimizes the error while guaranties non-negative solutions, which is the technique required for solving Equation 4.5.3. Details of NNSL algorithm can be found in [90].

Table 4.5.2 covers the sign controlled Prony coefficients resulted from applying Equation 4.5.3 on the raw static creep test data. In order to investigate the effect of Prony terms on the interconversion technique, two sets of coefficients applying the same optimization procedure were fitted to the experiment data in this study.

Table 4.5-2 Sign controlled Prony series coefficients for the static creep test

	Applying Equation 4.5.3			
	Before Presmoothing		**After Presmoothing**	
j	τ_j sec	D_j 1/MPa	τ_j sec	D_j 1 /MPa
1	1	0.000958	1	0.000526
2	10	0.001472	10	0.000167
3	100	0.005181	100	0.001841
4	1000	0.007373	1000	0.005101
5	10000	0.007676	10000	0.007227
$D_g = 0.0000612 \left(1/MPa\right)$				

The graphs in Figure 4.5.1 illustrate the uniaxial static creep test data recorded from laboratory experiments plus the Prony expression fitted to these creep data (the experimental data are average of three test replications). The coefficient of determination for the Prony coefficients was found to be well-above 0.99. The value, which is an indicator of how well the predicted model fits the experimental data, certifies the accuracy of the proposed model (5-term Prony representation).

4.6 Interconversion betwenn LVE Response Function

Linear viscoelastic response functions can be converted into each other by means of various types of interconversion methods. These methods are particularly useful when functions are defined in Prony series form [82]. There are a number of studies that have been conducted to find the true conversion from the complex modulus test [72, 73, 89, 91], while the aim of the

current study is to determine accurate relaxation modulus form the creep compliance test at a single temperature. Generally, creep compliance can be converted from the relaxation modulus through the approximate or the exact solution. These two approaches are further investigated in the following section.

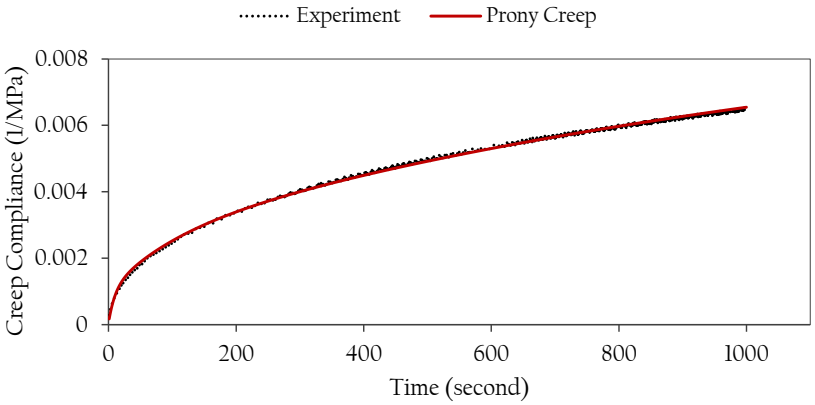

Figure 4.6-1 Prony series fit to experimental data

4.6.1 Exact Solution

Creep compliance $D(t)$ and relaxation modulus $E(t)$, based on the linear viscoelastic constitutive model are related by the Volterra integral equation of the first kind [92]:

$$\int_0^t D(\tau - t)E(t)d\tau = t \qquad 4.6\text{-}1$$

Equation 4.6.1 is considered as an ill-posed problem [93] which means, the solution for this class of equations is either, not unique or, it does not depend continuously on the data. In other word, small perturbation on the input information could cause arbitrary large effect on the output data. Even though this type of integral models have wide range of applications, they are difficult to solve numerically.

The most prominent approach in finding the viscoelastic material function would be a numerical solution of the constitutive integral without using any prior assumption [94]. For Volterra's equation of the first kind, it has been shown that the midpoint method produces a numerically stable algorithm [95]. A regularization technique needs also to be applied since for the ill-posed problems, the midpoint method by itself cannot be considered satisfactory [96].

4.6.1.1 Midpoint Method

To solve the problem by the help of midpoint method, first, the relaxation modulus is approximated on the time interval $[0,T]$. Then, the Volterra integral will be rewritten by considering the homogeneous partition, $0 = t_0 \langle t_1 \langle t_2 ... \langle t_n = T$ with a constant time step, $\Delta t = t_{k+1} - t_k$ for any k between 0 and $N-1$.

$$t_n = \sum \Delta t D(t_n - t_{i-1/2}) E(t_{i-1/2}) \qquad \text{for} \qquad n = 1,2,...,N \qquad \text{4.6-2}$$

Equation 4.6.2 constitutes of a linear system of equations of the following form:

$$Ax = b, \qquad A \in \Re^{N \times N}, \qquad x, b \in \Re^N \qquad \text{4.6-3}$$

where,

$$A_{ij} = \begin{cases} \Delta t D\left(t_i - t_{j-\frac{1}{2}}\right) & if\ j \le i, \\ 0 & if\ i > \text{j}, \end{cases}$$

$$x_i = E\left(t_{i-\frac{1}{2}}\right), \qquad b_i = t_i.$$

4.6.1.2 Tikhonov Regularization

As stated earlier, the problem is mathematically ill-conditioned and therefore the system of equations shown by Equation 4.6.3 cannot be inverted directly and a regularization technique has to be applied.

Tikhonov regularization is one of the most common and recognized form of regularization methods. The technique has been successfully applied in the estimation of viscoelastic material parameter [97, 98]. The Tikhonov's regularization solution is in the following form [99]:

$$x_\lambda = \arg\min \left\{ \|Ax - b\|^2 + \lambda^2 \|Lx\|^2 \right\} \qquad \text{4.6-4}$$

or equivalently

$$x_\lambda = \left(\lambda L^T L + A^T A\right)^{-1} A^T b \qquad \text{4.6-5}$$

where, λ is the regularization parameter and L is the first order difference $(N-1)\times N$ matrix:

$$L=\begin{pmatrix} -1 & 1 & & & \\ & \ddots & \ddots & & \\ & & \ddots & \ddots & \\ & & & -1 & 1 \end{pmatrix} \in \Re^{(N-1)\times N} \qquad 4.6\text{-}6$$

Large λ , in Equation 4.6.4, favours small norm of the solution to the cost of a large residual. On the other hand, a very small λ would result in a good fit but the solution will be dominated by data errors and the problem becomes "more" ill-conditioned. Thus, the regularization parameter controls the sensitivity of x_λ to perturbations in A and b and minimizes big variations in the solution.

One way to calculate the optimal λ is by means of $L-curve$ method [100]. In this method the constraint (i.e. $\| Lx_\lambda \|_2$) is plotted against the residual norm (i.e. $\|Ax_\lambda - b\|_2$) for different values of λ in a log-log scale. The resulting curve is usually L-shaped. The regularization parameter is then chosen to be near the curve's corner. In other words, the point with maximum curvature is computed when the constraint is plotted against the residual norm in log-log scale (Figure 4.6.1).The regularization parameter can be defined as the "corner" of the $L-curve$ graph. More detailed analysis of the $L-curve$ method can be found in the literature [99, 101].

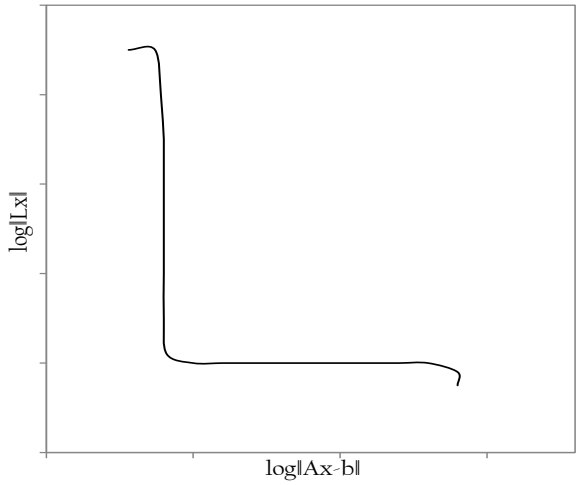

Figure 4.6-2 Schematic view of $\boldsymbol{L-curve}$

4.6.2 Approximate interconversion techniques

Approximate methods in creep compliance/relaxation modulus co nversion are mostly based on elastic-like, reciprocal relationship. Several approximate methods can be found in the literature. Some of these techniques are reviewed here in order to check their accuracies.

4.6.2.1 Power-law-based Interrelationship

Relaxation modulus $E(t)$ and creep compliance $D(t)$ can be approximately modelled by the pure power-law presentation in their transition zones as shown by Equations 4.6.7 & 4.6.8

$$E(t) = E_1 t^{-n} \qquad 4.6\text{-}7$$

$$D(t) = D_1 t^{n} \qquad 4.6\text{-}8$$

where, E_1, D_1 and n are all positive constants.

The following can be found taking the Laplace transform from Equations 4.6.1 and 4.6.7 respectively;

$$E(s)D(s) = \frac{1}{s^2} \qquad 4.6\text{-}9$$

$$E(s) = \frac{E_1 \Gamma(1-n)}{s^{(1-n)}} \qquad 4.6\text{-}10$$

where, $f(s) \equiv \int_0^\infty f(t)e^{-st}dt$ is as the Laplace transform of $f(t)$ with s, the transform parameter. $\Gamma(n) = \int_0^\infty x^{n-1}e^{-n}dx$ denotes as gamma function.

From Equations 4.6.9 & 4.6.10 we will have;

$$D(s) = \frac{1}{E_1 \Gamma(1-n)s^{1+n}} \qquad 4.6\text{-}11$$

And finally, by taking the Laplace inversion of Equation 4.6.11 and having $\Gamma(n)\Gamma(1-n) = \pi/\sin n\pi$ and $\Gamma(n+1) = n\Gamma(n)$, the power-law-based equation will be formed as the following;

$$E(t)D(t) = \frac{\sin n\pi}{n\pi} \qquad 4.6\text{-}12$$

The power-law interconversion is quite accurate in a region where $E(t)$ and $D(t)$ are represented by straight line on a log-log scale. In this case, n, the local log-log slope, is calculated by applying Equation 4.6.13;

$$n = \left| \frac{d \log F(\tau)}{d \log \tau} \right|_{at\tau=t} \qquad 4.6\text{-}13$$

where, $F(\tau)$ is either $E(\tau)$ or $D(\tau)$.

4.6.2.2 Interrelation by Denby

Another approach in creep-relaxation interconversion was proposed by Denby based on an approximation of the convolution integral [75];

$$E(t)D(t) = \frac{1}{1 + \frac{n^2\pi^2}{6}} \qquad 4.6\text{-}14$$

where, n is as defined in Equation 4.6.13.

4.6.2.3 Park and Kim Approximate Interconversion Method

Based on the same premise of power-law interconversion, Park and Kim developed new approximate interconversion method [102]. It is well-known that the power-law-based method could result in an accurate interconversion when $E(t)$ and $D(t)$ are presented by pure power-law expression. In addition, it has been argued that Equation 4.6.12 still results in a good approximation even when those functions are not exactly described by power-law but they have a smooth logarithm of the source function.

Therefore, Park and Kim tried to derive an approximate interconversion method that could result in rather accurate interconversion even for general relaxation modulus and creep compliance (i.e. non-power-law material representation).

The power-law-based interrelationship indicates that the target function is given by appropriate adjustment of the reciprocal of the source function. Therefore, by rewriting Equations 4.6.7 & 4.6.12 one may obtain the following expression.

$$D(t) = \frac{\sin n\pi}{n\pi E_1} t^n \qquad 4.6\text{-}15$$

Now, by considering $D(t)E(t^*) = 1$, where $t^* = \left(\frac{\sin n\pi}{n\pi}\right)^{1/n} t$, and setting $t^* \equiv \alpha t$, the final form of this interconversion will be as follows;

$$D(t) = \frac{1}{E(\alpha t)} \qquad 4.6\text{-}16$$

or,

$$E(t) = \frac{1}{D(t/\alpha)} \qquad 4.6\text{-}17$$

where,

$$\alpha = \left(\frac{\sin n\pi}{n\pi}\right)^{1/n} \qquad 4.6\text{-}18$$

Once again, n is the local slope of the source function on log-log scale as defined by Equation 4.6.13.

4.7 Prony Coefficient Selection and Interconversion between $D(t)$ and $E(t)$

Mathematically speaking, due to the nature of viscoelasticity, there is an infinite set of coefficients that will potentially reproduce good fit to the measured creep data. However, not all of them would be acceptable when one considers the physics of the deformation mechanism. First of all, the coefficients should be positive to be acceptable since negative coefficients result in unrealistic stress and strain. Moreover, researchers try to select the monotonically increasing set of coefficients which simulates the gradual change according to the Equation 4.5.1. Based on the discussion above and in order to evaluate the effect of Prony series coefficients on converted response function, two set of coefficients were selected to be used in the interconversion techniques. It has found that the selection of Prony series coefficients itself, could also alter the final converted function which means that the final relaxation modulus might be related to the selected Prony coefficients.

4.7.1 Approximate interconversion

The performance of power-law and Denby conversion techniques depend on the local slope of the source function; n as shown in Figure 4.7.1. It can be seen that their level of agreement changes as the magnitude of n varies. As it is illustrated in the figure, as n grows larger, correspondingly, the difference also becomes greater between Denby and the power-Law. The percentage difference varies from 0% (full compatibility) for very small value of n (« 1) to more than 200.00% for higher n values.

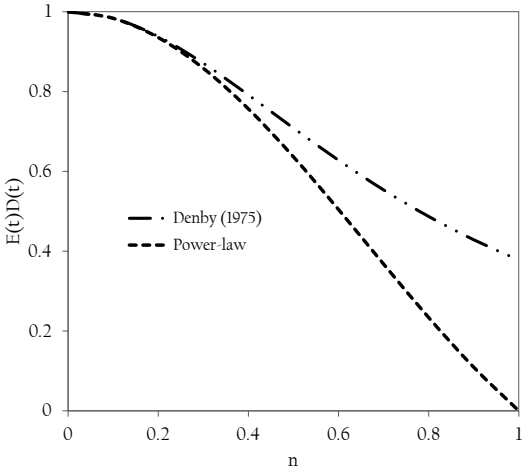

Figure 4.7-1 effect of $\boldsymbol{n}$ on interrelation approach

As it was mentioned in the Prony coefficients selection (i.e. Table 4.5.2), both sets of selected terms are shown to be in complete agreement with the creep compliance curve. As a result, one expects to observe the similar behaviour in the converted relaxation modulus curves.

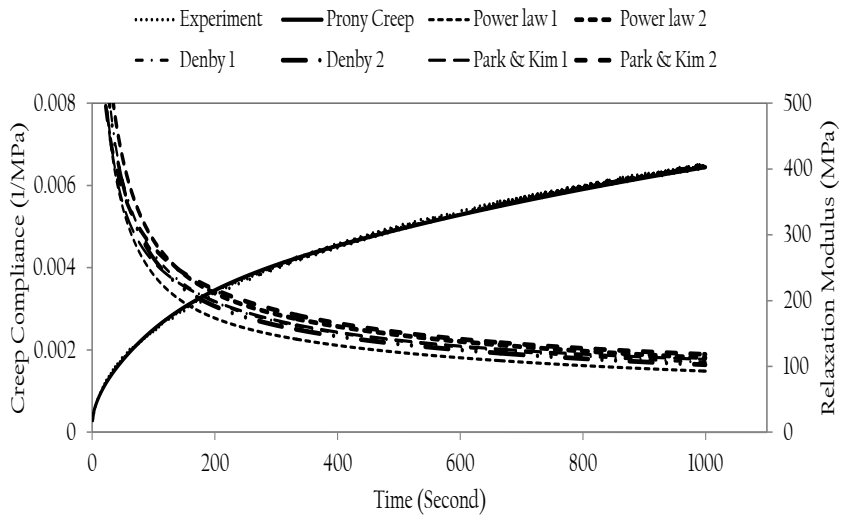

Figure 4.7-2 Relaxation modulus curve for Prony coefficients

Nevertheless, the converted graphs in Figure 4.7.2 illustrate the effect of Prony coefficients on the output data. The percentage difference between each two of conversion methods changes from 5.0 to 20.0%.

The log-log slope of the source function is defined where the plotted graph forms a straight line. Even though the graph is considered to be linear, it can be shown that the linearity is not always perfect as it is illustrated in the Figure 4.7.3.

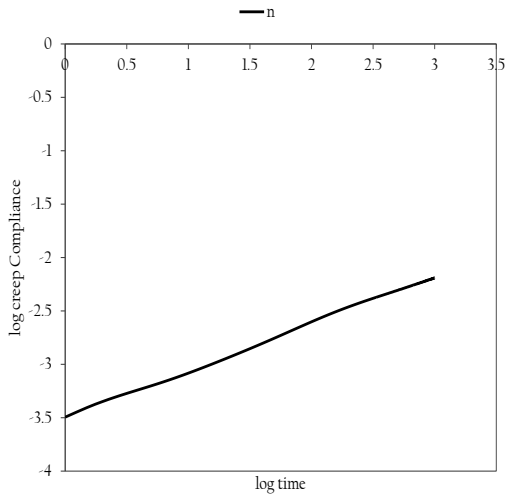

Figure 4.7-3 log-log graph of time versus creep compliance

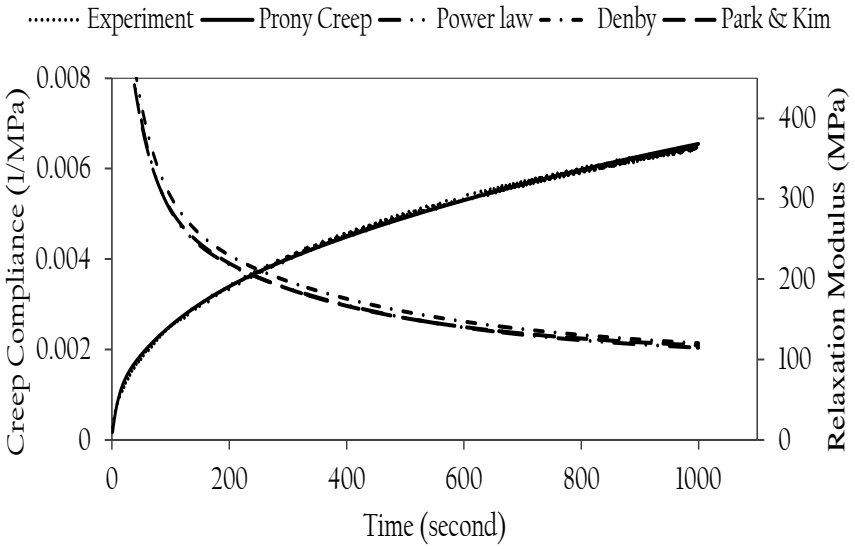

Figure 4.7-4 Interconversion with various, $\boldsymbol{n}$

As can be seen in Figure 4.7.3, the graph is not an absolute straight line, meaning that using a constant value of n, will not be satisfactory over the entire range of time. As a result, in order to minimise the discrepancy observed among various conversion approaches, instead of

allocating a single, n, for the entire range of the log-log graph, a series of, n, were considered for the interconversion purpose.

It is found that, by considering a range of n, all three different interconversion methods will be comparable with each other, regardless of the Prony coefficients selection. The percentage difference, now, varies from 0.6% to 2.3% as illustrated in Figure 4.7.4.

4.7.2 Exact Solution Approach

MATLAB toolbox "Regularization Tools" developed by Hansen [96] was used in this study in order to solve Equation 4.6.1 directly.

Initially, unsmoothed raw experimental data were considered for the first phase of exact interconversion. The regularization parameter, λ, by the help of $L-curve$ method was determined as it was explained in section 4.6.1.2. For this study, λ was found to be equal to 0.043 as can be seen in Figure 4.7.5 (a).

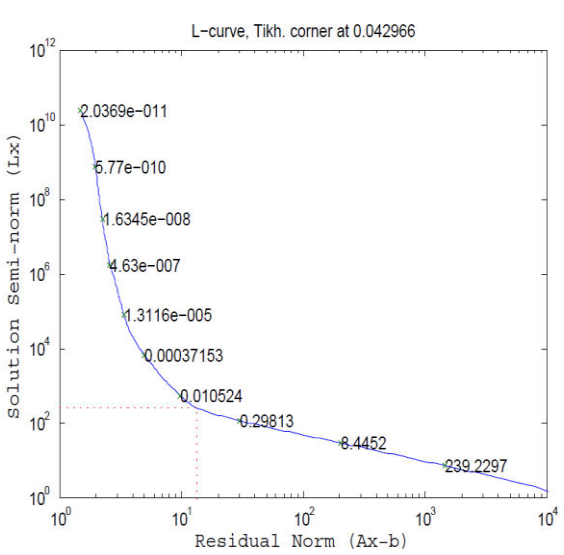

(a)

Figure 4.7-5 (a) regularization parameter for raw creep test

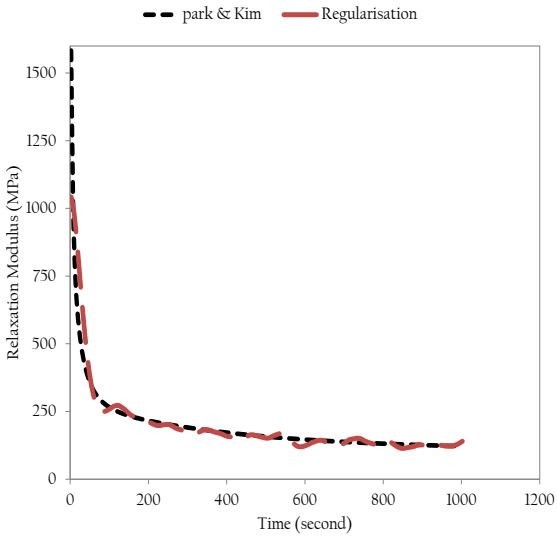

(b)

(b) regularized versus approximate method

By determining the regularization parameter, the relaxation modulus can be converted from the creep compliance data by applying Tikhonov technique. Figure 4.7.5 (b) shows the converted modulus and compares it to the "Park & Kim" approximate method.

As can be seen, the converted relaxation modulus graph is rather noisy with some fluctuations. In order to remove the oscillations from the graph, the converted data were then

post-processed with Prony series expression. The resulted graph is illustrated in Figure 4.7.6. The approximate solution showed to be just above 7.0% off when it compares to the exact solution.

For the next phase, the raw experimental data were first smoothed by Prony series and then converted to relaxation modulus. Pre-processing approach removes the oscillations in the solution by removing the experimental noise.

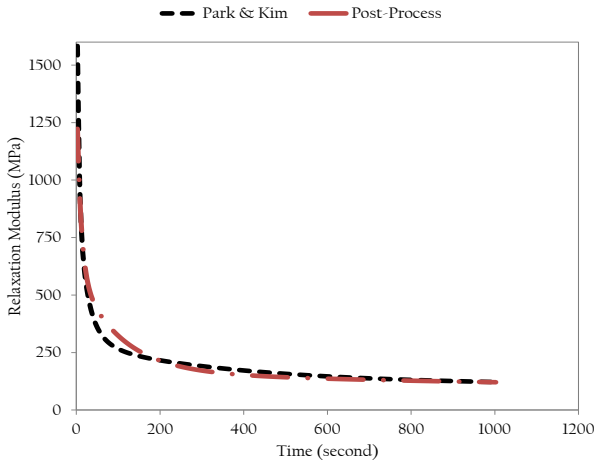

Figure 4.7-6 Post-Processed data versus approximate solution

The regularization parameter, λ , was found to be equal 0.109 considering the pre-processing technique. Comparison against the approximate solution showed the maximum error of 5.6%. The results substantiate that there is not a significant difference between using the "pre" or "post" process approach in exact interconversion technique. Figure 4.7.7 shows the regularization parameter along with the converted relaxation modulus resulted from "pre" and "post" processing.

Considering the converted data, this study recommends utilising the exact method over the approximate approaches. There are two main reasons in this regards. First, the exact interconversion technique is derived from the convolution integral which forms the true relation between the creep compliance and the relaxation modulus. Therefore, the exact solution has preference over the approximate method and is recommended by the authors for the interconversion purposes. Additionally, the required computational effort of the exact solution is not excessive and the ability of the available commercial programs is a great help in solving complex problems with no difficulty.

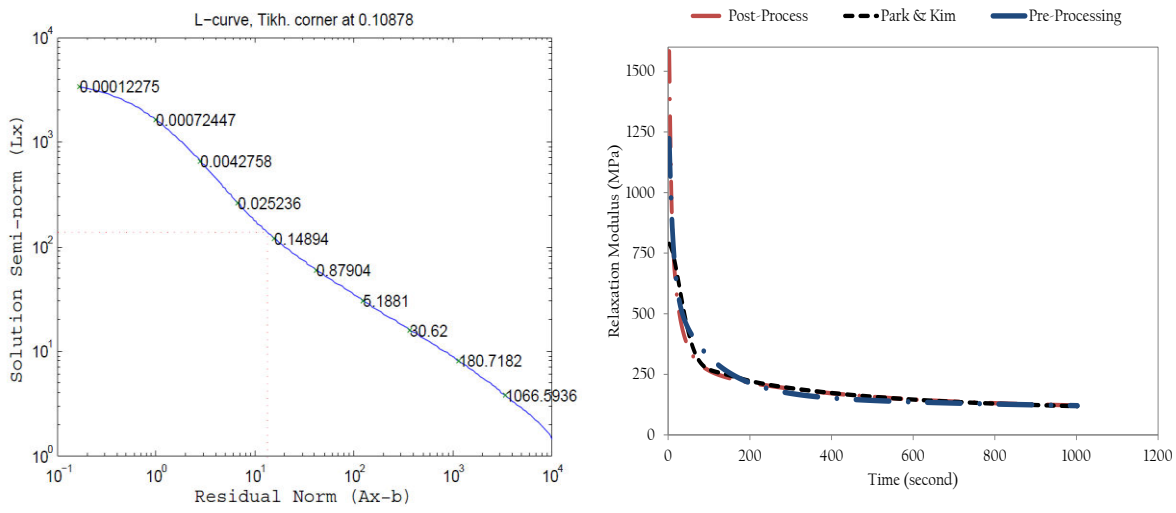

(a) (b)

Figure 4.7-7 (a) λ for pre-processing technique (b) approximate method versus "Pre"

If for any reason, the exact method could not be applied, the "Park & Kim" method would be suggested as an alternative approach. The reason of selecting the "Park & Kim" method over the other techniques can be found in Figure 4.7.8. To enhance the divergences exist among various approaches, the logarithmic deviation (i.e. $\log\left(\frac{E_{approximate}}{E_{exact}}\right)$) of each of these solutions from the exact method is plotted in Figure 4.7.8.

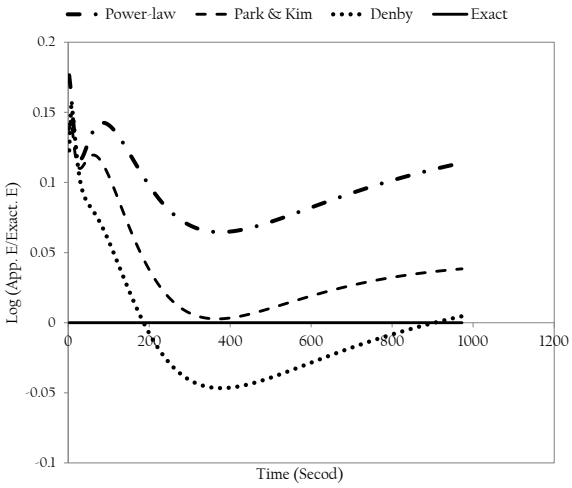

Figure 4.7-8 Logarithmic deviation of the approximate methods from the exact solution

It can be seen that, the "Park & Kim" method has the lowest deviation from the exact solution. As a result, this method is recommended in case that exact solution cannot be applied.

4.8 Creep Compliance and Complex Modulus Interconversion

As mentioned in the introduction, it is believed that all the materials functions are interrelated regardless of their test domain. Yet, the experience has revealed otherwise. Therefore, in the second part of this chapter, to investigate the true relationship among various viscoelastic functions the following will be taken into consideration;

1. The complex modulus (in addition to the static creep tests) will be carried out,
2. The relaxation modulus will be calculated from the creep compliance data by applying available interconversion techniques, and,
3. The dynamic complex modulus will also be converted to the relaxation modulus by utilising the generalized Maxwell model (GMM).

At the end a combined error technique will be introduced to minimize the error from different conversion techniques.

4.9 Experiment Testing Program

For this portion of analysis, the complex modulus test was undertaken in addition to the static creep test. It needs to be mentioned that the tests were performed complying with the linearity principles as argued in this chapter as well as in Chapter 3. A brief explanation of the tests procedure is brought in the following sections. Detailed discussion can be found earlier in this thesis.

4.9.1 Complex modulus Test

Testing cylindrical asphalt specimen under compressive sinusoidal loading pattern is called the complex modulus test. The stress and strain relationship under this continuous sinusoidal loading for linear viscoelastic materials is defined by a complex number called the "complex modulus" (E^*). This complex number relates stress and strain in the frequency domain. It is called complex as it contains both real (elastic) and imaginary (viscous) components of the modulus. The former is known as the material ability to store energy, whereas the latter is considered to be responsible for the energy loss in system. This relationship can be better understood by Equation 4.9.1

$$E^* = E' + iE'' \quad \text{4.9-1}$$

where,

E' = Storage modulus,
E'' = Loss modulus, and,
$i = \sqrt{-1}$.

Due to viscoelastic nature of asphalt mixtures, the resulted stiffness from complex modulus test becomes greatly sensitive to any small change in temperature-frequency combination. By plotting dynamic modulus in a form of master curve, the temperature-frequency (or temperature-time) dependent stiffness characteristic of asphalt material can be studied for a wide range of variables [103].

It is essential to have suitable representative analytical expression for accurate material modelling. Moreover, it is necessary to smooth the data in order to eliminate the noise and waviness of the raw data. For instance, the asphalt modulus can be described by power-law model as a function of frequency for each different temperature level [104]. In addition, polynomial fitting function has shown accurate result in shifting the asphalt mix data. However, a single polynomial model is not capable of solely fitting the whole master curve. The reason is that, the polynomial swing at two extremes (i.e. very low and very high temperatures) causes unreasonable value when extrapolating outside the experimented data. In order to avoid that, this study considers sigmoidal function to smooth the experiment data before conducting the Prony series fitting in the interconversion stage. The sigmoidal function, describes the frequency dependency of the modulus master curve and it is given by Equation 4.9.2 [103]:

$$\log\left|E^*\right| = \delta + \frac{\alpha}{1 + e^{\beta + \gamma(\log f_r)}} \quad \text{4.9-2}$$

where,

$\left|E^*\right|$ = dynamic modulus,
f_r = reduced frequency (Hz),
δ = minimum value of $\left|E^*\right|$,
$\delta + \alpha$ = maximum value of $\left|E^*\right|$, and,
β, λ = parameters describing the shape of the sigmoidal function.

To control the temperature during the test, a temperature cabinet with a temperature range from -5 to 60 °C and accuracy of ± 0.1 °C was used. Dummy specimen with the temperature sensor mounted at the centre was used in order to monitor the test temperature. Figure 4.9.1 & 4.9.2 illustrate the test setup and the sigmoidal master curve, respectively. The data presented in Figure 4.9.2 is the average of three test replications for the mix AC20 with binder 60/70 at 4±0.5% air voids.

Figure 4.9-1 Axial compression/static creep test setup

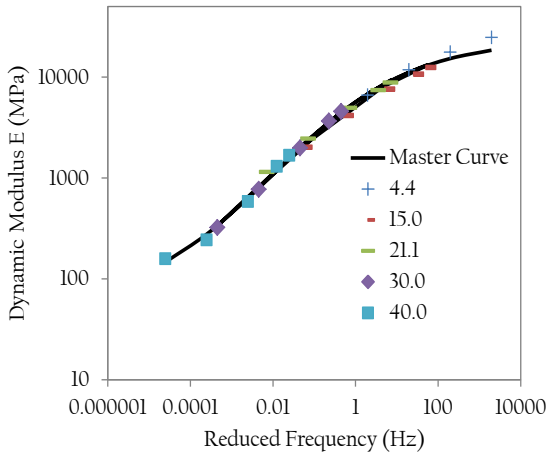

Figure 4.9-2 Fitting experimental data to log sigmoidal function

4.9.2 Static Creep Test

The static creep test procedure is as covered in Section 4.5.1. In this evaluation, a new static creep test was performed at 40 °C and under 240 kPa pressure. The results were fit by an 8-term Prony series coefficients applying the least square method. The test was run up to 1000 seconds so, the long term comparison can be studied between static and cyclic loading.

Table 4.9-1Prony series **c**oefficients

D_j (1/MPa)	1.00E-04	0.0062	0.0067	0.0068	0.0115	0.0121	0.0123	0.0124
τ_j (sec)	0.0434	0.434	4.34	43.4	434	4340	43400	434000
D_g (1/MPa) = 0.0006386								

The Prony coefficients are shown in Table 4.9.1while Figure 4.9.3 displays the fitted and the experimental creep test data. The data presented in this figure are the average of three specimen replications. The coefficient of determination for the Prony coefficients was found to be well-above 0.99. It certifies the accuracy of the proposed model.

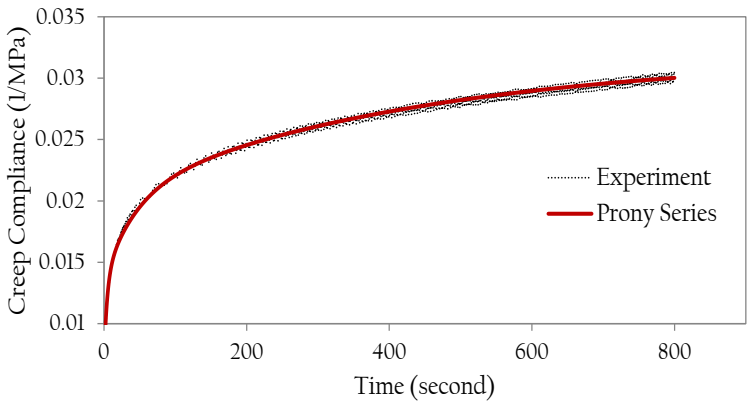

Figure 4.9-3 Prony series fit to experiment data

4.10 Interconversion Techniques

4.10.1 Conversion from Creep Compliance, D(t), to Relaxation Modulus, E(t)

As it was mentioned, there are two general approaches available in this regard. The conversion technique can be performed either by applying approximate interconversion methods [75, 105, 106] or by running the direct interconversion technique.

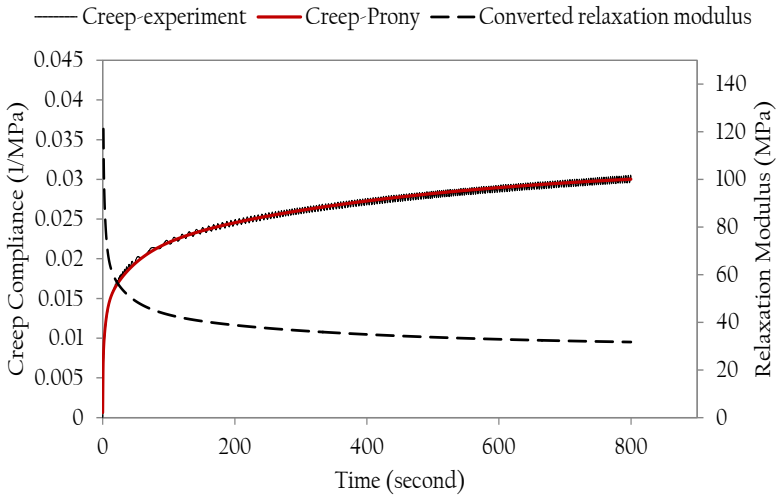

Figure 4.10-1 Converted relaxation modulus from experimental creep test

Various approximate interconversion approaches were investigated by Ebrahimi *et.al* [107]. The data have shown to match the exact solution quite acceptably. The approximate methods successfully handled the interconversion with well above 93% accuracy. The study suggests on considering the approximate technique as a promising alternative for the exact solution. As a result, in this part, *Park & Kim*, method was considered as a conversion approach.

Figure 4.10.1 displays the converted relaxation modulus from the experimental creep complex.

4.10.2 Conversion from Complex Modulus, E^*, to Relaxation Modulus, E(t)

In order to evaluate the compatibility of different conversion methods, the relaxation modulus was also converted from the complex modulus test. In this regard, of the most convenient approach would be simulating asphalt mixture's viscoelastic behaviour by a set of mechanical system consists of spring and dashpot. The differential equation in time is typically considered for this purpose. Therefore, for this research, the exact interconversion technique was applied to complex modulus test data. The model based on generalized Maxwell model (GMM) is shown in Equation 4.10.1:

$$E^*(\omega) = E_e + \sum_{j=1}^{n} E_j \frac{\omega^2 \rho^2}{1+\omega^2 \rho_j^2} + i \sum_{j=1}^{n} E_j \frac{\omega \rho_i}{1+\omega^2 \rho_j^2} \qquad 4.10\text{-}1$$

where,

E_e = equilibrium modulus,
E_j = relaxation strength,
ρ_j = relaxation time, and,
ω = Frequency (Hz).

To solve Equation 4.10.1, first, the Prony coefficients are fitted to the measured dynamic complex modulus as illustrated in Figure 4.10.2 plotted at reference temperature of 40 °C. Table 4.10.1 shows the 10-term Prony coefficient fitted to the complex modulus data. Basically, the same rationale was followed in order to find the Prony coefficients, this time, for the complex modulus master curve. Following the same concept and acknowledging the fact that the complex modulus test covers the wider time span, the higher term number would be, logically, required, therefore, the fitting process can be undertaken with highest possible accuracy. As can be seen from Figure 4.10.2, the Prony model fits perfectly with the measured complex modulus. The indication is that, the coefficients selected for the Prony series match thoroughly with the complex modulus data.

Table 4.10-1 Prony Series Coefficients-Complex Modulus

E_j (MPa)	ρ_j (second)
7868.74	0.00004
3890.62	0.0004
2849.25	0.004
884.68	0.04
321.16	0.4
105.91	4.0
78.96	40
12.61	400
17.49	4000
26.74	40000
E_e (MPa) = 4.96	

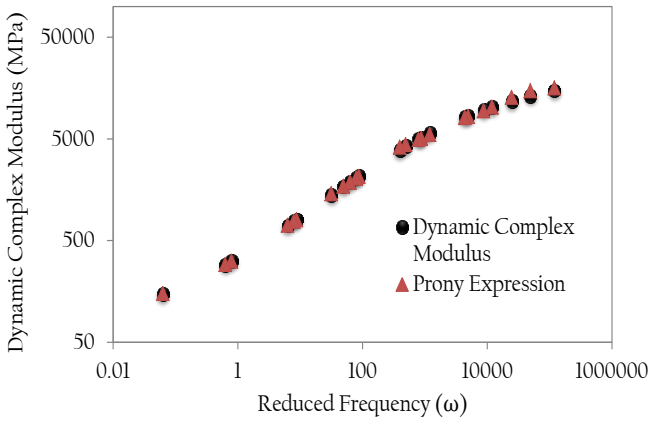

Figure 4.10-2 Prony series fitted to complex modulus master curve

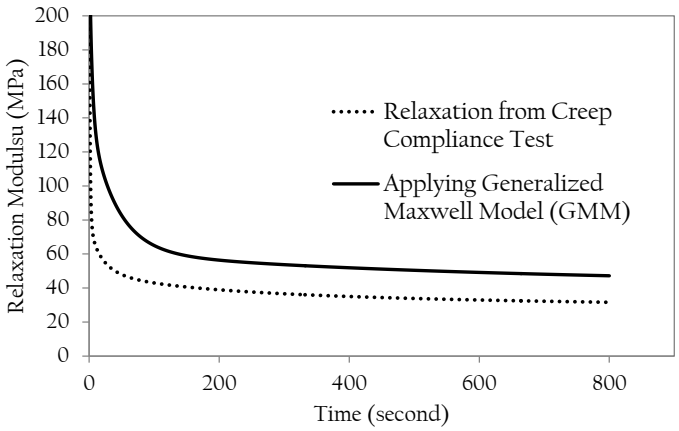

Figure 4.10-3 Interconverted relaxation modulus from complex modulus test versus static creep test

After finding the proper Prony coefficients, the final stage for this interconversion will be applying these coefficients to the relaxation modulus in time domain.

For relaxation modulus $E(t)$, the Prony series in time domain takes the following form which is referred to Wiechert model as shown in Equation 4.10.2;

$$E(t) = E_e + \sum_{j=1}^{M} E_j e^{-t/\rho_j} \qquad 4.10\text{-}2$$

where,

E_e = Equilibrium modulus (long-term relaxation modulus),
E_j = Prony regression coefficient, and,

ρ_j = Relaxation time.

Figure 4.10.3 shows the difference between the two interconversion methods. As observed, the resulted graphs do not match with each other. The relaxation modulus converted from the complex modulus test data seems to overestimate the one from the static creep test. These differences could be attributed to specimen to specimen variability since the samples used for the dynamic modulus test were not the same as those used in the creep test, however, the two groups of specimens had quite identical volumetric properties and made from the same mix under similar compaction method. Apart from the specimen to specimen differences, author also believes that the difference in the nature of the test domains should be the major cause for the existing deviation.

In order to analyse the converted data accurately, the interpretation is required to be undertaken with respect to the tests mechanism. As for the static creep test, the test is commonly performed for long period of time. Considering the static nature of the test, higher precision for long-term creep response can be envisaged in here. However, having an accurate quick-loading application could be considered unfeasible. That will display itself in less accurate measurement for short-term creep response. On the other hand, it is very difficult to run complex modulus test accurately for long loading times (i.e. low frequencies). Unlike the creep test, nature of the complex modulus test is for short-term loading.

Therefore, based on the observation above, long-term asphalt mixture response could be more accurately modelled by performing the static creep test, while short-term response could be, indeed, better simulated by the complex modulus test.

4.11 Combined Error Technique

As it was shown above, results from different interconversion techniques do not seem to be matched with each other considering the long term loading. Generally, the Prony coefficients are fitted separately to the relaxation modulus from creep and complex modulus tests. Therefore, error between these two conversion techniques could be minimised if the coefficients are fitted simultaneously. As a result in this study, fitting the Prony coefficients for relaxation modulus were done simultaneously for both creep and complex modulus tests by minimising the final error;

$$Error_{\text{Re}laxation} = \sum_{i=1}^{N_R} \left[E(t_i) - (E_e + \sum_{j=1}^{n} E_j e^{-t_i / \rho_j}) \right]^2 \quad \text{4.11-1}$$

$$Error_{Complex\_Modulus} = \sum_{i=1}^{N_E} \left[E^*(\omega_i) - \left(E_e + \sum_{j=1}^{n} E_j \frac{\omega_i^2 \rho_j^2}{1+\omega_i^2 \rho_j^2} + i \sum_{j=1}^{n} E_j \frac{\omega_i \rho_j}{1+\omega_i^2 \rho_j^2} \right) \right]^2 \quad \text{4.11-2}$$

$$\text{Total Error} = Error_{\text{Re}laxation} + Error_{Complex\_Modulus} \quad \text{4.11-3}$$

where, all the terms are as defined earlier in the text.

For this analysis, 10 term Prony coefficients were fitted to both relaxation and complex modulus by minimizing the total error, as brought in Equations 4.11.1, 4.11.2 & 4.11.3, respectively. Results from combining these two methods are presented in Table 4.11.1 and Figure 4.11.1. As can be seen, data are shown to be quite promising and noticeable improvement is observed by applying combined approach. As a result, the final graphs overlap through the entire loading time.

In order to check the effect of these new coefficients on complex modulus master curve, comparison was made between the complex modulus master curve experiment data and the one resulted from Prony fit as it is shown in Figure 4.11.2. As it was predicted, the Prony fit lags at the lower frequencies which simulate longer loading time.

Studying the converted data for static creep and complex modulus tests proves the aforementioned hypothesis. The data show that, the true conversion will be the result of determining short term relaxation modulus form the complex modulus test. Alternatively, long term modulus can be found by considering the static creep test data.

In conclusion and based on the observation presented above, as it was discussed earlier, it is generally believed that the relaxation modulus as a fundamental material properties could be determined from either static creep or complex modulus test. However, based on the data calculated in this thesis, it is determined that the complex modulus test is an effective test considering short term loading, while the static creep test result will be accurate for long term material characteristic determination. Combining these two tests showed to be a promising approach in determining true relaxation modulus.

Table 4.11-1 Prony Series Coefficients-
Combined Error Approach

E_j (MPa)	ρ_j (second)
7867.904	0.00004
3893.399	0.0004
2845.060	0.004
913.2120	0.04
382.3920	0.4
96.12200	4.0
19.38700	40
10.21900	400
12.65800	4000
15.46900	40000
E_e (MPa) = 4.96	

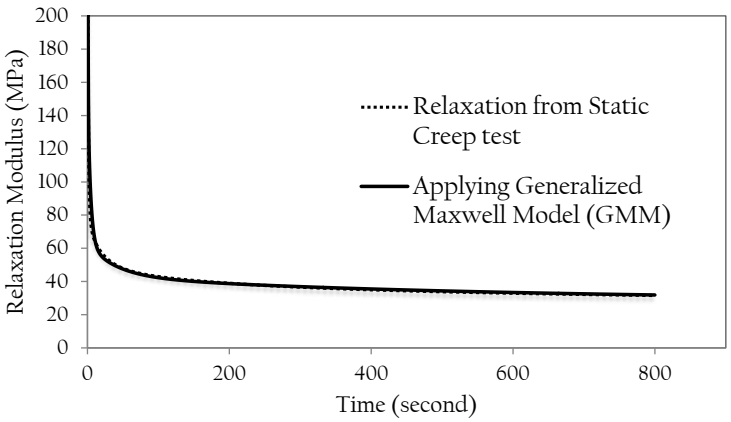

Figure 4.11-1 Interconverted relaxation modulus form complex modulus and static creep tests applying combined error technique

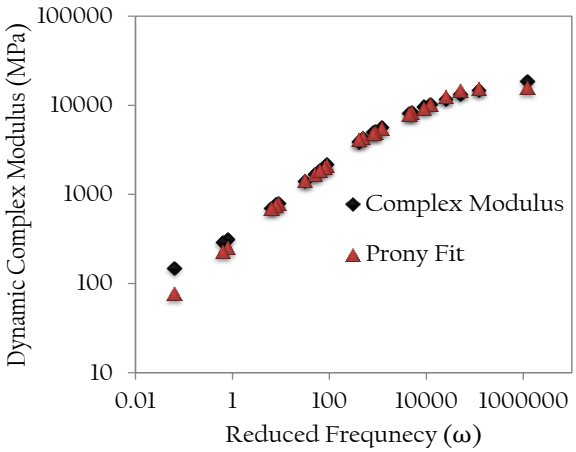

Figure 4.11-2 Complex modulus data versus Prony fit

4.12 Conclusions

Initially, the 5-term Prony series representation was fitted to the static creep data with and without power-law presmoothing. It was found that smoothing will not necessarily result in positive Prony coefficients. Various approximate interconversion methods between linear viscoelastic creep compliance and relaxation modulus were discussed using asphalt concrete data. It was observed that the Prony coefficients could influence the interconverted relaxation curve. Moreover, using the discretization of the slope n value (slope of log creep compliance with log t) over the time domain showed to be more accurate as the log creep - log time graph is not always a perfect straight line. The exact solution of the convolution integral by

Tikhonov regularization method was obtained and compared with approximate methods to check the validity of the approximation techniques. Considering the creep-relaxation constitutive model as ill-posed problem, Tikhonov regularization was selected in solution process. $L-curve$ method was also considered as a part of regularization procedure in order to find the best trade-off between acceptable residual and tolerable error. Relaxation modulus curve was plotted under "pre" and "post" process technique. Calculated data showed relatively acceptable resemblance. It was shown that the approximate methods are capable of producing results with more than 93% accuracy. If under any circumstances, the exact method cannot be utilized, "Park & Kim" approximate technique is suggested as the alternative method due to having the least deviation from the exact solution.

In addition, the Prony coefficients were also fitted to the complex modulus data that showed an accurate match with the measured values. However, the relaxation modulus converted from complex modulus test showed an obvious deviation from that converted from creep compliance test.

It is believed that the difference in the nature of the test domains, and specimen to specimen variations should be the major cause for the existing discrepancy. The graph interpretation is required to be accomplished concerning the tests mechanism. On that basis and by considering the nature of each test, a rather accurate result in long-term loading can be expected from the static creep test. On the other hand, complex modulus loading system can be considered with higher precision results for short-term loading.

At the end, the combined error approach was used to check the aforementioned hypothesis. It was shown that a quite promising data could be determined by simultaneously fitting the Prony coefficients to relaxation and complex modulus test data.

Chapter 5: Repeated Creep Test

5.1 Introduction

The following chapter covers the major portion of laboratory work for this research. The repeated creep test was conducted for hot mix asphalts covering various parameters (i.e. different levels of mix gradation, air void content, binder type and deviatoric stress). A total of 120 cylindrical specimens were utilised for this purpose. The reason behind the allocated number of specimens was to form a full factorial design of experiment to analyse the most significant factors and their interactions. As a result, the interrelation amongst the different factors (known as the interactions) as well as their level of significance would be statistically analysed.

5.2 Background

As it was discussed earlier, rutting shows itself through two major mechanisms; one dimensional densification (or, vertical compression) and plastic movement. The former is due to excessive amount of air void or lack of compaction while the latter is caused by inadequate shear strength. Studying the level of deterioration of each of these mechanisms reveals that, the vertical compression generally results in low to moderate rutting level whereas a high severity deformation is commonly observed as a consequence of the plastic movement.

Among the available laboratory test procedures, the repeated creep test is one of the most common laboratory tests with the ability to characterise the rutting phenomenon considering the shear behaviour.

The repeated creep test is employed for about 10,000 cycles and records the cumulative permanent strain as a function of the number of cycles (repetitions) over the testing period. A haversine pulse load cycle of 0.1s load and a 0.9s dwell time is applied for the test duration. Figure 5.2.1 shows a schematic data as a result of plotting permanent strain versus cycle number. As can be seen, the cumulative strain curve can be divided into three major zones; primary, secondary and tertiary zones. The primary zone is where the rapid accumulation of permanent strain with a decreasing rate takes place. With the continuation of the loading cycles, the primary zone will lead to the secondary zone which consists of a constant rate of

strain. Finally, the strain curve undergoes a sharp increase in the rate of strain at the onset of the tertiary zone. The cycle number at which the tertiary region begins is called the Flow Number (FN). What differentiates the tertiary zone from the other two regions and makes it essential for the purpose of this research is the fact that the material deformation in here occurs under the zero rate of volume change. In other words, the rate of change in the concluding zone is purely shear based (Figure 5.2.1)

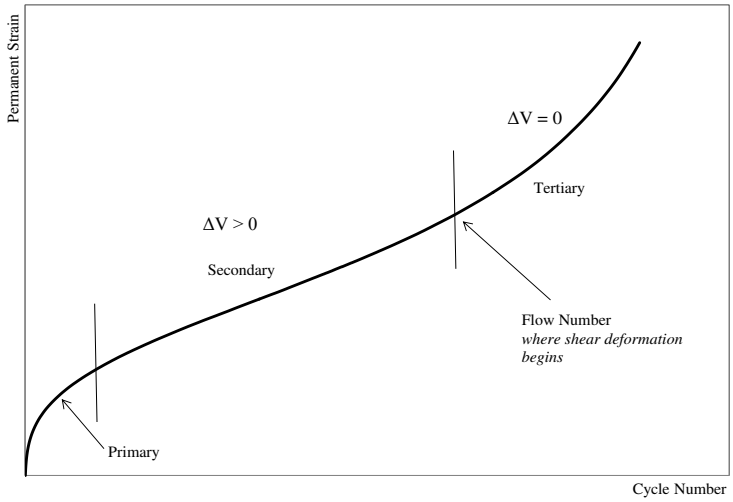

Figure 5.2-1 Repeated creep test result

As a result, by locating the tertiary point through the repeated creep test, the cycle number at which shear related rutting happens would be detected.

In general, the power-law model is used to analyse the test results;

$$\varepsilon_p = aN^b \qquad 5.2\text{-}1$$

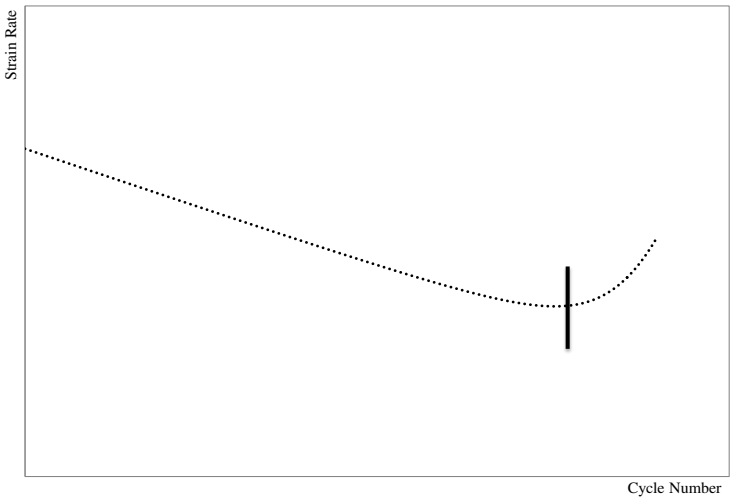

Figure 5.2-2 Plot of the rate of change in permanent strain versus loading time on a log–log scale for a repeated creep test

In Equation 5.2.1, ε_p is the permanent strain. "a" is called the intercept and represents the permanent strain at the first cycle, $N = 1$, while the slope "b" embodies the rate of change of the permanent strain as a function of the change in loading cycles.

Principally, the rate of change of the permanent strain is calculated and the point with the minimum rate governs the flow number as illustrated in Figure 5.2.2. However, following the traditional method could result in a misleading flow number due to presence of one or more low deceptive strain rates. For instance, Figure 5.2.3 depicts a typical creep test. The figure consists of the permanent strain curve plus its rate of change with respect to the number of cycle. As it is shown, one can observe several minimum values for the strain rate. National Cooperation Highway Research Program (NCHRP) report 513, Simple Performance Tester for Superpave Mix Design: First-Article Development and Evaluation, recommends to report the first such minimum point if more than one strain rate share the same value [53]. This approach might not necessarily result in a true flow number.

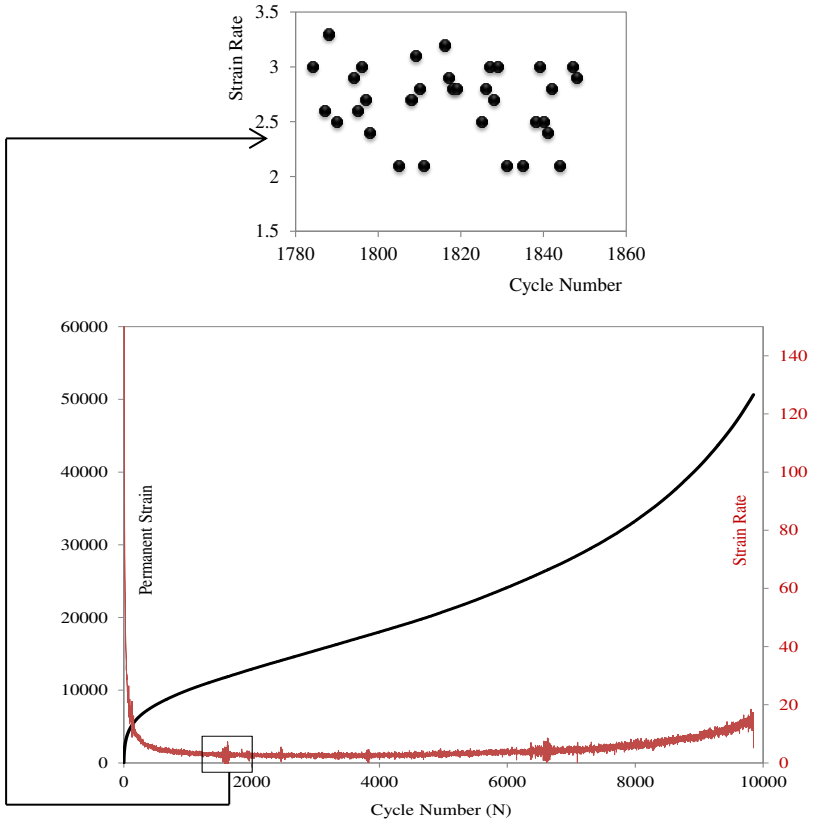

Figure 5.2-3 Typical repeated creep test and its strain rate

To overcome this obstacle, the Francken model was selected for this study. The model, as described in Equation 5.2.2, is a composite mathematical expression consists of power part

and exponential component. This combination is believed to be a very good representation in modelling all three stages of material behaviour in permanent deformation test [108].

$$\varepsilon_p(N) = AN^B + C(e^{DN} - 1) \qquad 5.2\text{-}2$$

where,

$\varepsilon_p(N)$ = Permanent deformation or permanent strain,
N = Cycle number, and
A, B, C and D = Regression constants.

To use the model, the regression constants are first estimated through nonlinear regression technique. Then, as shown in Equation 5.2.3, the first derivative with respect to N is calculated;

$$\varepsilon_p'(N) = \left(A * B * N^{(B-1)}\right) + \left(C * D * e^{(D*N)}\right) \qquad 5.2\text{-}3$$

Equation 5.2.3 defines the rate of change in the permanent strain.

Finally, the second derivative is determined to find the cycle number for the tertiary stage commencement.

$$\varepsilon_p''(N) = A * B * (B-1) * N^{(B-2)} + \left(C * D^2 * e^{(D*N)}\right) \qquad 5.2\text{-}4$$

Mathematically speaking, the derivative of a function switches the sign from negative to positive at the *point of inflection* on the curve of that function. Moreover, as already discussed, flow number is reported as the cycle at which the *minimum* strain rate occurs. Given the above, the flow number can be easily detected by taking the derivative of the strain rate curve (i.e. Equation 5.2.4) and finding the cycle number at which the negative strain slope gradient turns to positive value.

In this regard, Table 5.2.1 shows an example of a set of analysed test data. The table consists of four columns; cycle number, permanent strain, strain slope and the gradient of strain slope. As can be seen, the value for the first derivative of the permanent strain in the secondary stage is practically the same for the large number of loading cycles. However, it is rather easier to find the inflection point through the "gradient of the strain slope". For the data in Table 5.2.1, the cycle number of "3162" can be easily separated as the flow number by examining the last column.

Table 5.2-1Example for flow number determination – AC20 with 80/100 binder

Cycle Number	Permanent Strain%,	Strain Rate	Gradient of Strain Slope
3154	15948.8693	2.42085	-2.15E-06
3155	15951.2901	2.42085	-1.85E-06
3156	15953.7110	2.42085	-1.55E-06
3157	15956.1319	2.42085	-1.26E-06
3158	15958.5527	2.42085	-9.57E-07
3159	15960.9736	2.42085	-6.59E-07
3160	15963.3944	2.42085	-3.61E-07
3161	15965.8153	2.42085	-6.26E-08
3162	15968.2361	2.42085	2.35E-07
3163	15970.6570	2.42085	5.33E-07
3164	15973.0778	2.42085	8.31E-07
3165	15975.4987	2.42085	1.13E-06
3166	15977.9195	2.42085	1.43E-06

5.3 Sample Preparation and Testing

5.3.1 Material and Sample Preparation

In this study, AC 20 and AC14 mixes were utilised which are commonly used hot mix asphalts in New Zealand highway industry. These mixes have 20 and 14 mm maximum nominal aggregate size, respectively. Details for mix design and aggregate properties are provided in Appendix A. Two types of binders were used in this research; 60/70 and 80/100. The numbers suggest the penetration values for each class of binder. At least, two air void contents were chosen for the creep experiments; 3.0% and 5.0%. All the specimens were tested at two temperatures, 40 °C and 50 °C, and under two deviatoric stresses; 240 kPa and 600 kPa.

Cylindrical specimens with 100 mm in diameter by 150 mm in height were cut and cored from 150 mm in diameter and 170 mm height gyratory compacted specimens. The aggregates, binders and job mix formula were taken from a local contractor who designed these mixes for one of the Motorways in Christchurch – New Zealand. Asphalt mixtures were prepared based on the Australian standard AS 2891.2.1 “Methods of Sampling and Testing Asphalt” [109]. Accordingly, the asphalt samples were mixed and compacted at 150 °C. Following the Australian standard, all mixtures were also aged at 150 °C for one hour before compaction to simulate the short term ageing.

Compaction technique is another difference between the Australian and the Superpave method. As for the Superpave, vertical pressure, angle and speed of gyration are 600 kPa, 1.25 ° and 30 gyrations per minute, respectively. However, the counterparts for the Australian approaches are 240 kPa, 3.0° and 60 gyrations per minute, respectively. Aside from the material type and mixing methods, this modification in sample compaction is yet another parameter which prevents the researchers and the industry to simply adopt available meddles developed elsewhere.

5.3.2 Laboratory Experiment

The repeated creep test, as mentioned above, was considered in this stage of the study. The test is performed with haversine pulse loading cycle consists of a 0.1 s loading and a 0.9 s rest time, until specimen failure or capturing the tertiary point, whichever occurs first. The test setup is as shown Figure 5.3.1.

Figure 5.3-1The repeated creep test setup

To record the specimen deformation, three on specimen vertical Linear Variable Differential Transformers (LVDTs) were used to compensate for the error as a result of possible non-linear deformation. The LVDTs were mounted in an equally circumferential space with 100 mm gauge length. To maintain a uniform stress distribution and reduce the friction between the load platens and the specimen, two layers of friction reducers were used in this study. One layer was under the bottom face of the specimen and the other one is placed at the top of the specimen under the top load platen.

To control the temperature during the experiment, a temperature chamber with a temperature range from "-5 to 60 °C" and accuracy of "± 0.1 °C" was used. Dummy specimens with the

temperature sensors mounted at the centre were used in order to monitor the actual specimen temperature during testing process. Table 5.3.1shows the different factors and their levels that were considered in the repeated creep test. Five factors each at two levels were considered in the repeated creep test. The factors that considered in this investigation are mix type (i.e. maximum nominal aggregate size), binder type and air void content in the compacted mix and test temperature.

Table 5.3-1 Detail of repeated creep test

AC 14, 20							
Binders 60/70, 80/100							
VTM = 3.0%				VTM = 5.0%			
T = 40 °C		T = 50 °C		T = 40 °C		T = 50 °C	
240 kPa	600 kPa	240 kPa	600 kPa	240 kPa	600 kPa	240 kPa	600 kPa

5.4 Results and Analysis

5.4.1 Flow Number Model

The aim of undertaking the repeated creep test in this research was to identify the most significant factors involved in the shear-based permanent deformation phenomenon. Table 5.4.1 shows the measured responses, flow numbers, of two replicates for all the combinations of the creep test. The factors in this study are coded as (-1) for Binder 60/70, Temperature 40 °C, Deviatoric Pressure of 240 kPa and 3.0% Air Voids and (1) for Binder 80/100, Temperature 50 °C, Deviatoric Pressure of 600 kPa and 5.0% Air Voids . The codes will be of a great help in further statistical analysis.

The results in Table 5.4.1 suggest a clear trend. The specimens are shown to go under earlier failure, an equivalent of smaller flow numbers, as the factors move form (-1) to (+1). The indication is, preparing specimen with softer binder (i.e. 80/100), higher air voids percentage (i.e. 5.0%) or increasing the test temperature (40 to 50 °C) and pressure (240 to 600 kPa) will result in higher permanent deformation. Even though the raw data propose rather clear trend, the effect of each factor plus their plausible interactions were investigated through the statistical analysis approach.

Factorial design is widely used in the data assessment where the experiment involves several factors and it is necessary to study the joint effect of the factors on a nominated response.

One of the most special cases in the factorial design analysis is the case where "k" factors are tested each at *two levels* . These levels could be quantitative as well as qualitative [62].

Table 5.4-1 Flow number results for AC 20

Binder	Temperature - °C	Pressure - kPa	VTM - %	log (FN) - R1*	log (FN) - R2*
60/70	40	240	3.0	4.2443	4.2524
80/100	40	240	3.0	3.4833	3.4218
60/70	50	240	3.0	3.3345	3.3560
80/100	50	240	3.0	2.7634	2.7528
60/70	40	600	3.0	3.6458	3.5782
80/100	40	600	3.0	2.8169	2.8432
60/70	50	600	3.0	2.7033	2.5527
80/100	50	600	3.0	2.2068	2.0828
60/70	40	240	5.0	3.7966	3.7805
80/100	40	240	5.0	3.2017	3.1697
60/70	50	240	5.0	2.8319	2.6684
80/100	50	240	5.0	2.4843	2.4713
60/70	40	600	5.0	3.0983	2.7380
80/100	40	600	5.0	2.5514	2.4564
60/70	50	600	5.0	2.0607	1.9731
80/100	50	600	5.0	1.8751	1.8751

* R1 & R2; replicates one and two

For instance, in our case, the binder type possesses the qualitative characteristic whereas the rest of the factors are considered quantitative. A complete replicate of such a design requires $2*2*2*...*2=2^k$ observations and is called a 2^k *factorial design*. Therefore by having 4 factors, for each mix type separately, this study requires 2^4 or *16* observations as brought in their coded version in Table 5.4.1.

The null hypothesis for this statistical analysis is that, changes in the factors will not affect the test response: no significant difference in flow number would be observed for any combination of input level. The level of significance, "α" which is the probability of Type 1 error for the test is considered equal to 0.05. In order to reject or accept the hypothesis, the P-value is calculated and compared with "α". P-value indicates the probability of getting a mean difference between the groups as high as what is observed by chance. The lower the P-value is, the more significant the difference between the groups will be. Therefore, in this study a P-value greater than 0.05 indicates the statistical similarity amongst the responses. The statistical software package “Minitab version 17” was used to carry out the analysis of

variance and calculate the P-value [110]. Analysis of Variance (ANOVA) method is used in order to evaluate the statistical significance among the responses.

As shown in Table 5.4.2, all the factors are found significant. As for the joint effects, just, "Binder-Temperature" and "Binder-Air Voids" in two-way interactions are selected as significant. None of the higher level interactions are shown to be significant.

Table 5.4-2 Analysis of variance for AC 20

Source	DF	Adj SS	Adj MS	F-Value	P-Value
Binder	1	2.0801	2.08009	299.18	0.000
Temperature	1	5.3516	5.35161	769.73	0.000
Pressure	1	3.7504	3.75037	539.42	0.000
VTM	1	1.5338	1.53379	220.61	0.000
2-Way Interactions	6	0.3768	0.06280	9.03	0.000
Binder*Temperature	1	0.1541	0.15411	22.17	0.000
Binder*Pressure	1	0.0239	0.02386	3.43	0.082
Binder*VTM	1	0.1850	0.18505	26.62	0.000
Temperature*Pressure	1	0.0026	0.00261	0.38	0.549
Temperature*VTM	1	0.0000	0.00001	0.00	0.968
Pressure*VTM	1	0.0112	0.01116	1.60	0.223
3-Way Interactions	4	0.0167	0.00418	0.60	0.668
4-Way Interactions	1	0.0027	0.00275	0.40	0.538
Error	16	0.1112	0.00695		
Total	31	13.2233			

Based on the analysis above, temperature, pressure, binder type and air void content have all found to play a significant role in asphaltic material behaviour. What the result signifies is that, change in any of these parameters would potentially alter the material response toward permanent deformation under the applied load.

As it was expected, temperature appears to impose the highest impact on the deformation amongst the selected factors. The reason is that, increase in service temperature reduces the binder viscosity used in the mix. As a result, binder softens and begins acting as lubricant rather than binding agent. This phenomenon, consequently, softens asphalt mixtures which leads to excessive deformation.

Considering the material response, same rationale would be applied to the rest of the significant factors studied during the course of this research. Clearly, increasing the applied pressure accelerates the induced damage to the material. As for the air void content, one of

the main reasons to include it in asphalt mix design is providing just enough room to prevent bleeding. Presence of high air void undermines the mix strength by weakening its structure.

Another approach to study the significant factors is through the Normal and/or half-Normal probability plots. The probability plot is a graph which represents the effect of each studied factor versus the percent probability of that effect [62]. In this approach, the factors' significance is proportional to their distance from the probability line. The one which deviates the most illustrates the highest significant effect (i.e. Temperature, in this case).

The only difference between normal and half-normal probability effect is in displaying the effect estimate sign. In normal plot, the raw value of the effect estimates is used against their cumulative normal probability. Though, the absolute value of these effects is considered for half-Normal plot. Many analysts feel that the half-normal plot is easier to interpret since the pure effect regardless of positive or negative direction is plotted.

Figure 5.4.1illustrates the half-normal probability plot. It is clearly evident that, binder, temperature, pressure, air voids and binder-temperature and binder-air voids interactions are highly significant.

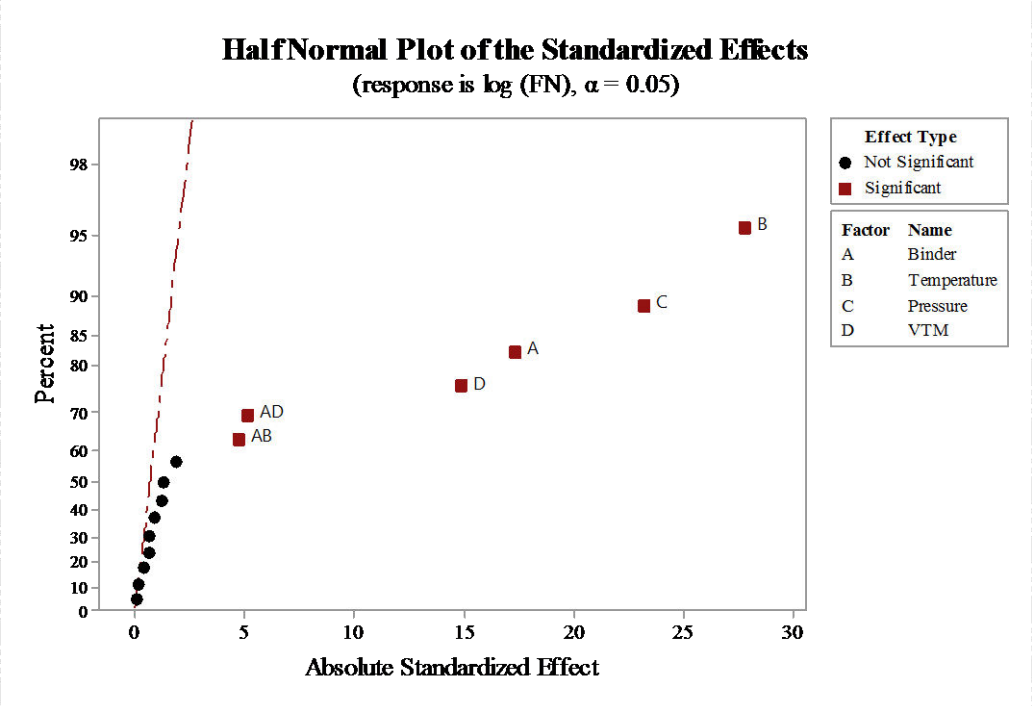

Figure 5.4-1 Half-normal probability plot, AC 20

By specifying the significant factors, the regression model can be constructed as below;

$$\log(\mathrm{FN}) = 2.9085 - 0.2550(\mathrm{B}) - 0.4089(\mathrm{T}) - 0.3423(\mathrm{P}) - 0.2189(\mathrm{VTM}) + 0.0694(\mathrm{B}*\mathrm{T}) + 0.0760(\mathrm{B}*\mathrm{VTM}) \quad R^2 = 0.96 \qquad 5.4\text{-}1$$

In Equation 5.4.1, FN is the flow number. B, T, P and VTM are binder type, temperature, pressure and void content in the total mix (air voids), respectively. $(B*T)$ and $(B*VTM)$ represent the pertinent interactions.

A potential concern in the 2^k factorial design method is the linearity assumption in the factor effects. Nevertheless, the method would work quite well even if the linearity assumption holds very approximately. That will be taken care of by including the interactions in the final model, as it is shown in Equation 5.4.1. As a result, the model accounts for some curvature (i.e. nonlinearity) in the response function [62].

Still, there are some cases where the response curvature cannot be simply modelled by first-order equation, such as the $\log(FN)$ equation. In such cases, logical model recommended to consider is second-order responses surface method;

$$y = \beta_0 + \sum_{j=1}^{k} \beta_j x_j + \sum\sum_{i<j} \beta_{ij} x_i x_j + \sum_{j=1}^{k} \beta_{jj} x_j^2 \qquad 5.4\text{-}2$$

where,

y = Response,
β = Regression coefficients, and
x = Regressor variables

To evaluate the acceptability of the traditional first-order approach, a number of *centre points* are added to the original 2^k design. The centre points consist of n_c replicates run at the points $x_i = 0 (i = 1,2,...,k)$. One important reason for adding the replicates at the design centre is that, centre points do not affect the usual effect estimates in 2^k design technique [62].

Air voids of three and five percentages are considered for the model proposed in Equation 5.4.1. Second order response surface method was undertaken to check the possible nonlinearity in air void distribution effect on the resulted flow number. In order to do so, new set of data including 16 extra runs at code (0), 4.0% air voids, were prepared for all the possible combinations of binder, temperature and pressure as shown in Table 5.4.3. Running the analysis shows that the quadratic effect of air void percentage is not significant. The "P"

value was found to be equal to 0.580. Therefore, this would support the sufficiency of the first-order model.

Table 5.4-3 New set of flow number, AC 20

Binder	Temperature - °C	Pressure - kPa	VTM - %	log (FN) - R1*	log (FN) - R2*
60/70	40	240	3.0	4.244	4.252
60/70	40	240	4.0	4.038	4.093
60/70	40	240	5.0	3.797	3.781
60/70	40	600	3.0	3.646	3.578
60/70	40	600	4.0	3.308	3.342
60/70	40	600	5.0	3.098	2.979
60/70	50	240	3.0	3.334	3.356
60/70	50	240	4.0	2.829	2.832
60/70	50	240	5.0	2.668	2.832
60/70	50	600	3.0	2.553	2.703
60/70	50	600	4.0	2.530	2.498
60/70	50	600	5.0	2.061	1.973
80/100	40	240	3.0	3.422	3.483
80/100	40	240	4.0	3.308	3.311
80/100	40	240	5.0	3.202	3.170
80/100	40	600	3.0	2.817	2.843
80/100	40	600	4.0	2.698	2.679
80/100	40	600	5.0	2.456	2.551
80/100	50	240	3.0	2.763	2.753
80/100	50	240	4.0	2.660	2.666
80/100	50	240	5.0	2.484	2.471
80/100	50	600	3.0	2.207	2.083
80/100	50	600	4.0	2.037	2.025
80/100	50	600	5.0	1.875	1.875

* R1 & R2; replicates one and two

5.4.2 Permanent to Resilient Strain Model

Asphalt mixture properties and indeed the permanent deformation are largely influenced by in-service temperature as well as deviatoric pressure. One approach to associate this effect is to develop a model based on permanent to resilient strain. Given that both of these parameters are controlled by pressure and temperature, normalising the permanent strain by the resilient strain should therefore capture most of pressure and temperature effects. This concept is the basis of the asphalt rutting model in the NCHRP Project 1-37A mechanistic-empirical design methodology [41]. Therefore, permanent to elastic strain model was also proposed in this study. The model and the half-normal plot are shown in Equation 5.4.3 and Figure 5.4.2, respectively.

$$\log\left(\frac{\varepsilon_p}{\varepsilon_r}\right) = 1.3788 - 0.0438(B) - 0.0778(T) - 0.0564(P) + 0.0229(B*T*VTM) \qquad 5.4\text{-}3$$

$$R^2 = 0.87$$

where, ε_p and ε_r are permanent and resilient modulus, respectively. The rest are as defined above.

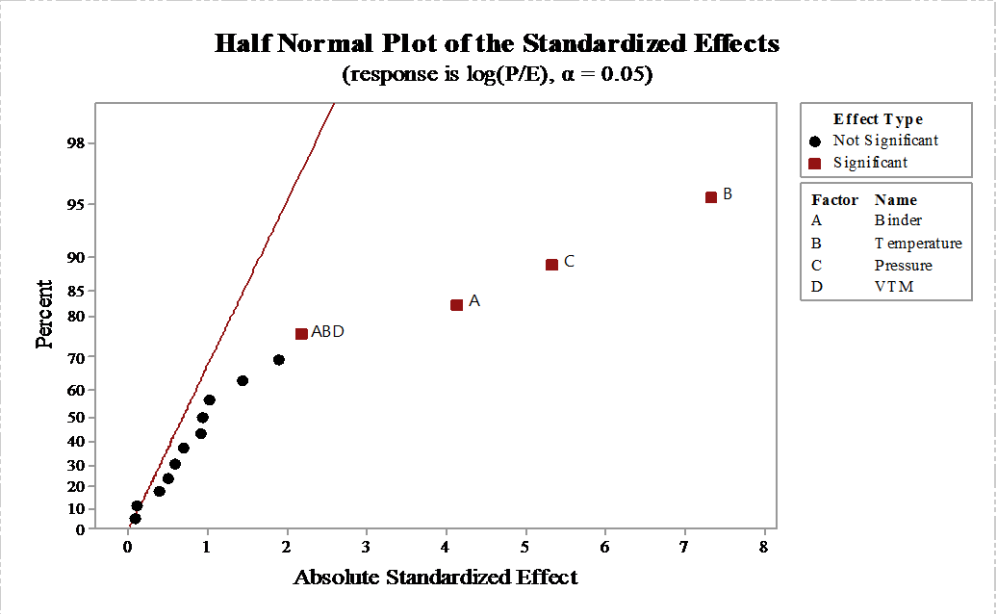

Figure 5.4-2 Half-normal plot - Permanent to Resilient Strain, AC 20

As shown in the figure, the "Air Void" main effect is cast out as a significant parameter while "Temperature", "Pressure" and "Binder" are still considered as highly effective on the response factor. As expected, temperature has by far the highest influence. Regarding joint effects, the three-way interaction of "Binder-Temperature-VTM" appears to be of significance. The implication is that, input of these parameters in material behaviour cannot be merely investigated on their own. To appreciate their applications in material response, these factors must be considered in conjunction with other parameters in joint effect. In other words, although air voids' main effect did not find its way amongst the significant factors, its interaction with binder and temperature proves otherwise. A significant interaction will often mask the significance of main effects [62]. What it means is the air voids ultimate effect is measured as a result of its interaction with binder and temperature.

Figure 5.4.1and Figure 5.4.2 essentially generate the same result. Even though the air voids' main effect is considered significant in the flow number analysis, it still contains the lowest significance level compared to the other three parameters. Nonetheless, the air void appears

again in “Binder-VTM” interaction. Generally speaking, the figures reveal the significance of temperature’s effect as the highest level of influence on permanent to resilient strain ratio plus the binder, temperature, VTM interactions.

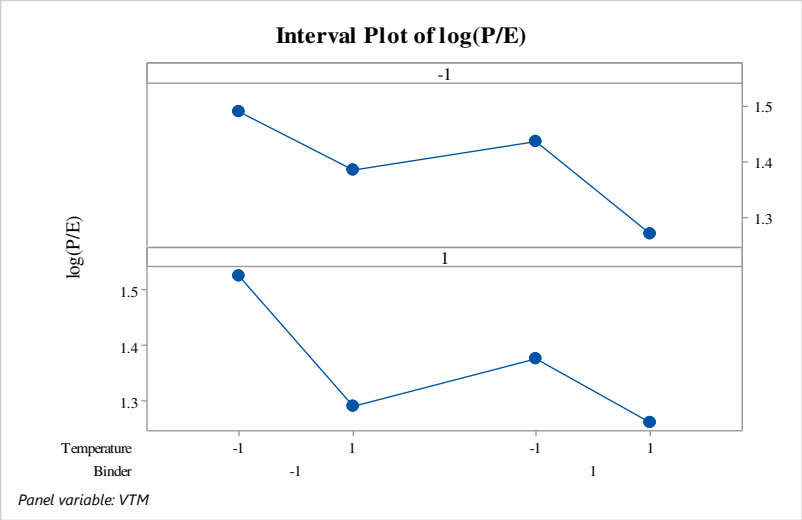

Figure 5.4-3 Three-way interaction, “Binder-Temperature-VTM”, AC20

Additional evaluation in the permanent to resilient strain can be undertaken by studying the three-way interaction effects. It is done by first; plotting the “Binder-Temperature-VTM” joint effect for the logarithm of permanent to resilient strain (i.e. $\log\left(P/E\right)$), as shown in Figure 5.4.3. The difference in factor influence, then, becomes noticeable when the very same plot is constructed and “VTM” is exchanged by “Pressure” as shown in Figure 5.4.4.

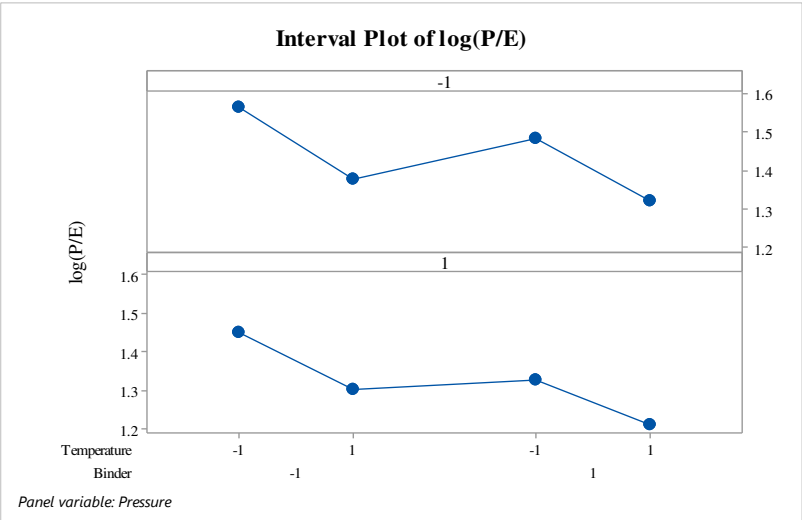

Figure 5.4-4 Three-way interaction, “Binder-Temperature-Pressure”, AC20

Comparisons between these two prove the significant effect of air voids involvement in response function in the presence of temperature and binder. It can be seen that, the permanent strain variation is more dramatic for air voids compare to pressure.

Table 5.4-4 Flow Number results for AC 14

Binder	Temperature - °C	Pressure - kPa	VTM - %	log (FN) - R1*	log (FN) - R2*
60/70	40	240	3.0	3.6001	3.5579
80/100	40	240	3.0	3.2672	3.2931
60/70	50	240	3.0	2.9590	2.9499
80/100	50	240	3.0	2.4914	2.5441
60/70	40	600	3.0	3.0792	3.1106
80/100	40	600	3.0	2.7959	2.8228
60/70	50	600	3.0	2.4518	2.4609
80/100	50	600	3.0	2.0607	2.1206
60/70	40	240	5.0	3.4228	3.3516
80/100	40	240	5.0	2.9380	2.9143
60/70	50	240	5.0	2.5821	2.4533
80/100	50	240	5.0	2.2878	2.2989
60/70	40	600	5.0	2.6946	2.6314
80/100	40	600	5.0	2.4639	2.4609
60/70	50	600	5.0	2.0414	1.9085
80/100	50	600	5.0	1.7482	1.7243

* R1 & R2; replicates one and two

Table 5.4.4 provides the measured FN of two replicates for AC 14 gradation. The factors are coded following the same trend as discussed in AC 20 analysis; (-1) for Binder 60/70, Temperature 40 °C, Deviatoric Pressure of 240 kPa and 3.0% Air Voids and (1) for Binder 80/100, Temperature 50 °C, Deviatoric Pressure of 600 kPa and 5.0% Air Voids.

Regression models for FN and permanent to elastic strain prediction for AC 14 gradation are brought in Equations 5.4.4 and 5.4.5 below;

$$\begin{aligned}\log(\mathrm{FN}) = 2.67 &- 0.1570(\mathrm{B}) - 0.3538(\mathrm{T}) - 0.2605(\mathrm{P}) - 0.1763(\mathrm{VTM}) \\ &- 0.0255(\mathrm{P} * VTM) + 0.0206(\mathrm{B} * \mathrm{P}) + 0.0164(B * VTM) \\ &+ 0.0260(\mathrm{B} * \mathrm{T} * \mathrm{VTM}) - 0.0208(B * T * P * VTM)\end{aligned} \qquad 5.4\text{-}4$$

$$\ldots\ldots\ldots\ldots\ldots\ldots\ldots\ldots\ldots\mathrm{R}^2 = 0.98$$

$$\begin{aligned}\log\left(\frac{\varepsilon_\mathrm{p}}{\varepsilon_\mathrm{r}}\right) = 1.360 &- 0.0319(B) - 0.0570(T) - 0.0462(P) - 0.03083(B * T) \\ &+ 0.0247(\mathrm{B} * \mathrm{P}) - 0.0250(B * P * VTM) + 0.0233(B * T * P).\end{aligned} \qquad 5.4\text{-}5$$

$$\ldots\ldots\ldots\ldots\ldots\ldots\ldots\ldots\ldots R^2 = 0.87$$

Similar to what observed for AC 20, all the major parameters were found significant in FN prediction. However, the interactions have greater role in AC 14 model. The implication is mixture’s higher sensitivity to simultaneous change of any of the major factors.

Air voids main effect is again cast out in the permanent to resilient strain model. Nevertheless, it shows its significance in three-way interaction of binder and temperature. Models for both gradations follow, roughly, the same trend with an identical coefficient of determination which indicates they both could predict the mix behaviour, quite accurately.

Finally, ANOVA analysis was undertaken for a combination of AC 14 and 20 combinations. As it was expected, the analysis outcome confirms the significant contribution of all the major effects to the response determination. The regression model for the FN prediction was devised in Equation 5.4.6 with the coefficient of determination of 0.97:

$$\begin{aligned}\log(\mathrm{FN}) = {} & 2.79 - 0.1185(\mathrm{A}) - 0.2060(\mathrm{B}) - 0.3814(\mathrm{T}) - 0.3014(\mathrm{P}) - 0.1976(\mathrm{VTM}) \\ & + 0.0490(\mathrm{A}*\mathrm{B}) + 0.0276(\mathrm{A}*\mathrm{T}) + 0.0409(A*P) + 0.0213(A*VTM) \\ & + 0.0341(\mathrm{B}*\mathrm{T}) + 0.0240(B*P) + 0.0462(B*VTM) + 0.0082(T*P) \\ & - 0.0057(T*VTM) - 0.0022(P*VTM)\end{aligned} \qquad 5.4\text{-}6$$

where, (A) indicates aggregate gradation. It is considered as (-1) for AC 20 and (1) for AC 14 considering the coded method. The rest are as defined in Equation 5.4.1. The permanent to elastic strain model was also constructed as shown in Equation 5.4.7;

$$\begin{aligned}\log\left(\frac{\varepsilon_{\mathrm{p}}}{\varepsilon_{\mathrm{r}}}\right) = {} & 1.3694 - 0.038(\mathrm{B}) - 0.067(\mathrm{T}) - 0.051(\mathrm{P}) - 0.016(\mathrm{VTM}) \\ & - 0.019(\mathrm{A}*\mathrm{B}*\mathrm{T}) - 0.015(\mathrm{B}*\mathrm{T}*\mathrm{VTM}) \ldots\ldots R^2 = 0.78\end{aligned} \qquad 5.4\text{-}7$$

5.5 Model Accuracy

Validation of the models' accuracy was checked by assessing the residual values and their trends. Examination of the residuals is calculated during the analysis of variance (ANOVA) [62]. If the model is adequate, the residuals should be structureless with no obvious patterns. One way to check the model adequacy is by studying the normality assumption. This is completed by plotting a normal probability plot of the residuals. If the normal distribution assumption of the errors is satisfied, this plot will fall upon the equality line. In general, moderate departures form normality is accepted for the data. Whereas, cases with error distribution consist of considerably thicker or thinner tails are of more concern. Figure 5.5.1 illustrates the normal probability plot of the residuals for AC 14. The general impression of the figure is that, the errors are approximately distributed with a normal pattern with no

outliers. The same conclusion is valid for AC 20 and the combined model as shown in Figures 5.5.2 and 5.5.3.

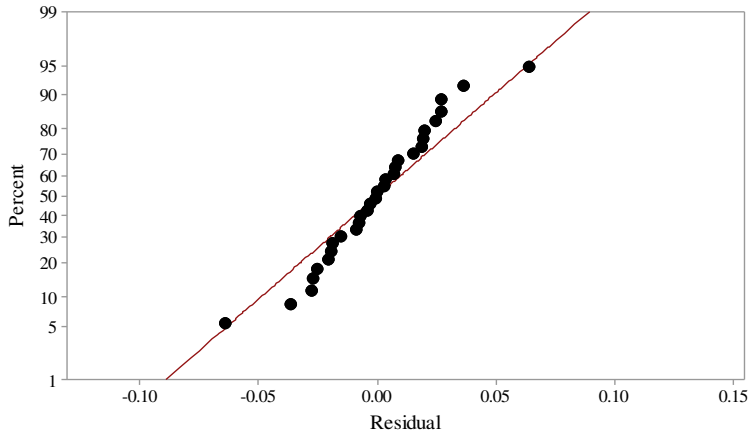

Figure 5.5-1 Normal probability plot of the residual, AC14

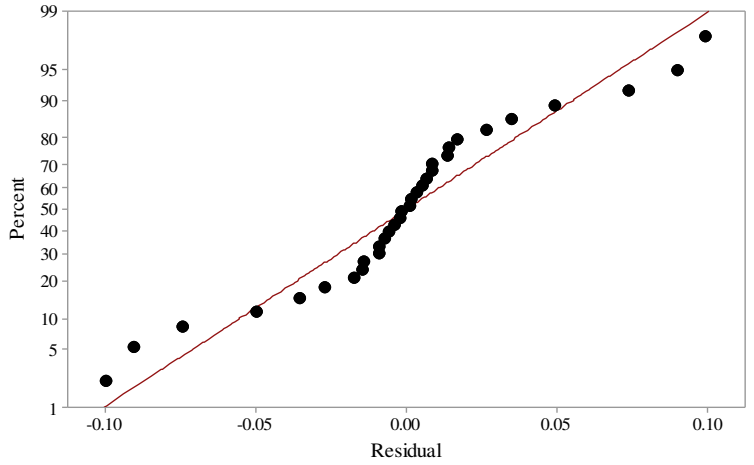

Figure 5.5-2 Normal probability plot of the residual, AC20

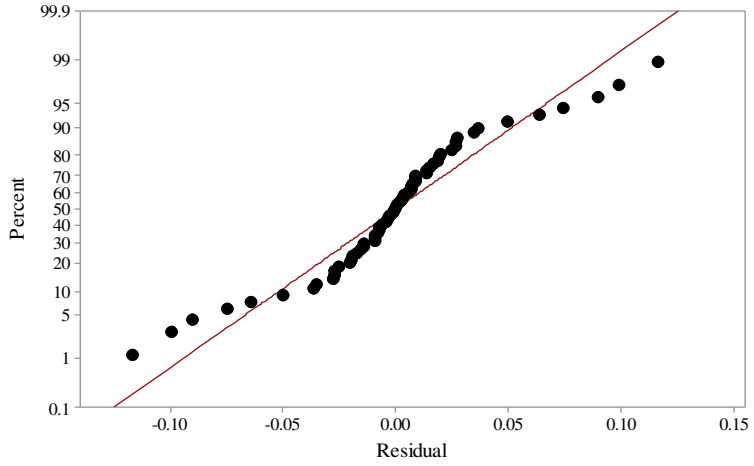

Figure 5.5-3 Normal probability plot of the residual, AC14 & 20 combined

Another approach in this regard is by plotting the residuals, this time, in response to their run order (or, the time equivalent). This method is helpful in detecting correlation among residuals. Sometimes, the data collection quality is affected through the course of time consequently altering the residuals. For instance, the skill of the experimenter may change as the experiment progresses.

Having the residual plot versus time would characterise any bias point in this process. This condition often causes the residual plot to spread more on one end than the other. Figures 5.5.4 to 5.5.6 present the residuals run order (or, time) for AC14, 20 and 14 & 20 combined, respectively. As can be seen, there is no reason to suspect any violation of the independence assumption.

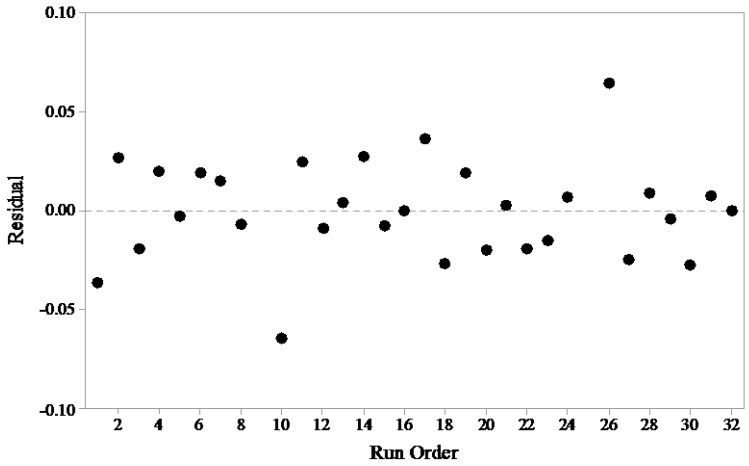

Figure 5.5-4 Plot of residual versus run order, AC14

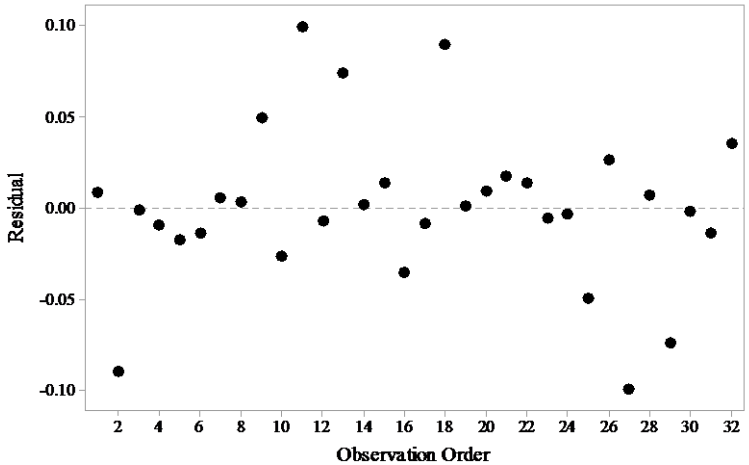

Figure 5.5-5 Plot of residual versus run order, AC20

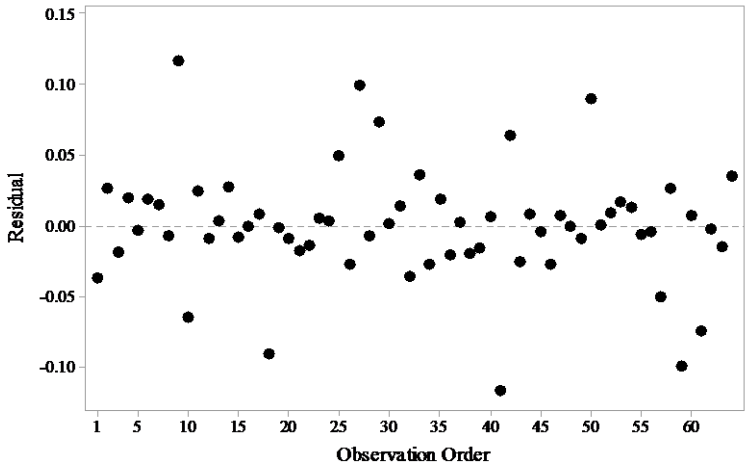

Figure 5.5-6 Plot of residual versus run order, AC 14 & 20

The proposed models in this study were also compared to the NCHRP 1-37 permanent to resilient strain ratio model discussed in Chapter 2 – Literature Review [41]. Figure 5.5.7 below shows the $\log\left(\frac{\varepsilon_p}{\varepsilon_r}\right)$ for these models. As can be seen from the figure, NCHRP 1-37 model tends to overestimate the permanent to strain ratio for New Zealand mix. The graph implies that, although, the method is adopted by AASHTO in their mechanistic empirical pavement design approach, it still cannot be directly implemented to other pavements with different mix designs and materials. As these methods have empirical basis, calibration is the least required modification for ever accurate data prediction.

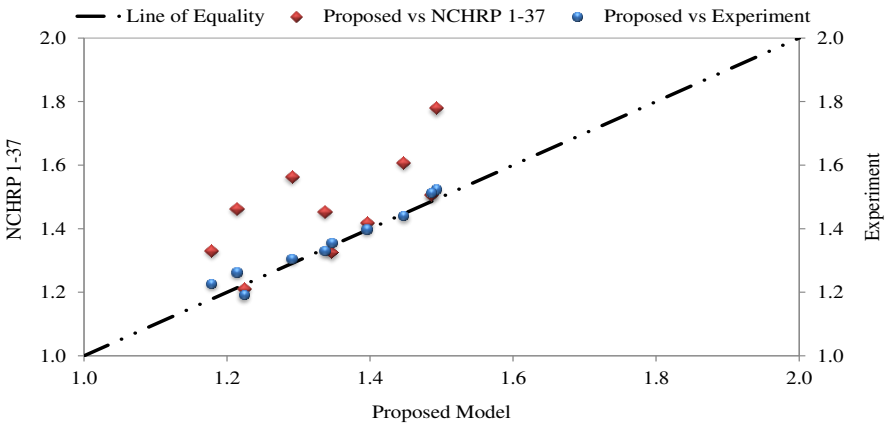

Figure 5.5-7 Model verification

It should be noted again that New Zealand and Australian mix design follows a different setting from that adopted by Superpave. Predicted data using the models from the current research are in complete agreement with the experimental ones. This, once again, verifies the model accuracy for the major New Zealand mixtures i.e. AC14 & 20.

5.6 Conclusion

A total of 120 cylindrical specimens were prepared for the repeated creep test. Cycle numbers at failure, the Flow Number (FN), were determined for various combinations of mix gradation, air void content, binder type and deviatoric stress in a full factorial design system of analysis.

The power-law model is the recommended technique for FN determination. Shortcomings of this approach were discussed and the relatively new solution, the Francken model, was taken into consideration instead. Francken model is composed of power as well as exponential components. This characteristic qualifies the model to truly represent the material behaviour under the creep test and as a consequence to determine an even more accurate FN.

Significant parameters were determined through ANOVA analysis. All the major parameters were found to have significant effect on the permanent deformation with Temperature having the greatest influence followed by Pressure and Binder type. Regression models were proposed to predict FN and permanent to resilient strain.

It is worth mentioning that, research outcomes conducted elsewhere cannot be simply implemented into New Zealand practice. Significant differences in mix property and specimen preparation are observed in New Zealand based mixtures. First of all, binder specification in New Zealand is based on penetration grade system. Moreover, mixing, pre-conditioning and compaction are conducted at the temperature of 150 °C with conditioning time duration of 60 ± 10 min. Finally, for the compaction phase, the gyration angle equals to 3 ± 1° with ram pressure of 240 ± 10 kPa. On the other hand, models developed in this study could accurately predict mix behaviours commonly used in New Zealand.

Chapter 6: Loaded Wheel Tracker Test

6.1 Introduction

The following chapter will cover the second and final set of the laboratory experiment conducted in this research. For this purpose, slab specimens prepared at different air void levels, binder types and aggregate gradations are tested in the wheel tracker at two temperatures.

Initially, the wheel tracker test was performed using the conventional test setup. In this setup, the wheel tracker tests were undertaken by having the slab specimens fitted in the same size steel mould that would cover their peripheries and prevent any lateral movement. However, after a number of preliminary experiments, it became evident that only the primary stage and part of the secondary stage of permanent deformation will occur under this setup and reaching high severity rutting, i.e. shear associated class of permanent deformation, will not be achieved through the current test setup. As a result, a new loaded wheel test setup was designed and manufactured for this research. Following the change in the test setup, the equivalent of the repeated creep test flow number (FN) was found for the wheel tracker test. Moreover, the major factors contributing to high severity rutting were also specified.

The wheel tracker test setup was also simulated by finite elements method utilising the viscoelastic and creep parameters determined in Chapter 4. The computer simulation was undertaken using the general purpose finite element software ABAQUS version 6.11 [111].

6.2 Background

Rutting, as it was covered in the literature, is classified as one of the main structural damage modes in pavement subject to mechanical loading [1]. This distress could be divided principally into three mechanisms; one dimensional deformation, mechanical deformation and lateral flow or plastic movement. Plastic movement is acknowledged by researchers as a major type of permanent deformation caused by inadequate shear strength. High rutting severity level is, predominantly, the result of this mechanism [10].

In order to study asphalt material behaviour, National Cooperative Highway Research Program (NCHRP) recommended the Simple Performance Test (SPT) [2]. As mentioned, in

rutting phenomenon, high severity damage takes place mainly as a result of shear deformation. The SPT accounts for shear deformation by measuring the flow number or flow time which will occur at the start of the “tertiary phase”. Studying asphalt material behaviour under the load application reveals that the asphalt mixture permanent deformation curve can be divided into three major zones known as; primary, secondary and tertiary zones. In general, permanent deformation accumulates rapidly in the primary zone. This increment decreases reaching a constant value in the secondary zone and finally, it increases rapidly at the onset of the tertiary zone [26]. The point with the lowest slope on the deformation curve is referred to tertiary point. The tertiary point has two significant characteristics; first, permanent deformation rate undergoes a dramatic increase right after this point. Second, it occurs under the constant volume which signifies the pure shear based deformation.

One issue regarding the SPT test series is that, they are rather time consuming and they also require elaborate testing equipment. In addition, they are not intended for quality control and quality assurance (QC\QA) either. More important, one can also observe that none of the test loading sequences is any close to the actual traffic load. As a result, the public and private sectors continued working on developing a test apparatus with unsophisticated test mechanism to be used in mix preparation step as well as the QC\QA of pavement construction [112]. Thus, wheel tracker test setup and its loading pattern could better simulate the action of moving traffic wheel [113, 114].

Figure 6.2.1 illustrates the conventional wheel tracker test setup. As shown in the figure, considering the current wheel tracker test setup, the asphalt sample is fully confined by the steel mould.

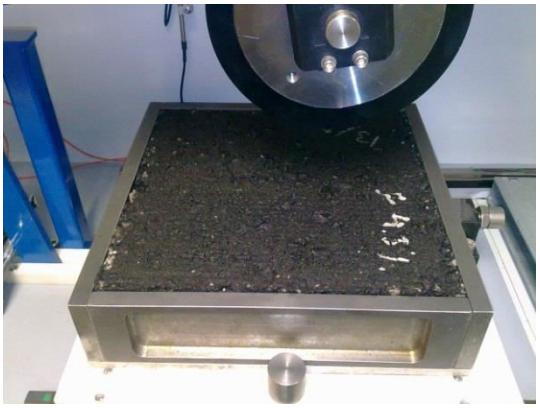

Figure 6.2-1 Current wheel tracker test mould

Having the specimen fully constrained at all sides will cause the mould to apply large reaction pressure which will severely limit the slab from lateral (shear) deformation that would have occurred for a similar but unconfined slab. Therefore, running the wheel tracker test and measuring the deformation in the existing setup would merely indicate measuring rutting caused by densification (i.e. compaction) as a result of air voids change as it will be explained in the sections ahead.

The aim of this step of the thesis is to introduce a new test setup for the wheel tracker test. The new setup in addition to measuring vertical deformation, will also take into account the lateral displacement. Removing the lateral constraints will allow for shear deformations to happen and this way, all three deformation zones in material behaviour can be truly captured. The differences between the results obtained from the conventional setup and the new setup will be discussed in Section 6.4.1.

6.3 Specimen Preparation

Asphalt mixes with *14* and *20 mm* nominal maximum aggregate size were prepared for the experimental stage. These are commonly used hot mix asphalts in New Zealand. Unlike the previous test plans, slab shape specimens are used in wheel tracker test. Slab specimens of *305*305*50* and *75* mm were considered for AC 14 and 20, respectively [115]. Asphalt mixtures were prepared with 60/70 and 80/100 penetration grade binder. The aggregates, binders, and job mix formula are the same as those used in Chapters 4 and 5. Asphalt mixtures were prepared based on Australian standard AS 2891.2.1 [56]. Accordingly, the asphalt cements were mixed and compacted at 150 °C. All mixtures were also aged at 150 °C for one hour before compaction. The mixtures are compacted using European standard roller compactor – steel roller shown in Figure 6.3.1.

Figure 6.3-1 Roller compactor for slab preparation

6.4 Test Setup and Specification

6.4.1 Introducing New Test Setup

At first, specimens were prepared and tested within the moulds of *305*305*50* and 75 *mm*. The steel moulds have identical dimensions to tested specimens. The specimens were fit in the exact same size moulds result in very limited lateral (shear) deformation. In order to investigate that, the preliminary tests were conducted for available binder types, 60/70 and 80/100, and aggregate gradations with maximum nominal sizes, 14 and 20 mm, at high temperatures (i.e. 50 and 60 °C) for 50,000 cycles and the total permanent deformations were recorded and are shown in Table 6.4.1.

Table 6.4.1 shows that the total permanent deformation accumulated after 50,000 cycles at 50 or 60 °C are quite small and reaching the Flow Number (FN) under the current test setup is impossible regardless of the material type used in sample preparation; e.g. coarse versus fine aggregate and hard versus soft binder. It also reveals that the present test setup is unable of even ranking the selected set of mixtures. Studying preliminary test results shown in the table, one will easily conclude that changes of the major parameters would have no significant effect on the permanent deformation mixtures response. In Chapter 4, it was found that aggregate gradation, temperature, binder type, plus air voids, all have significant influences on the material permanent deformation behaviour. However, under the current test setup, none of the above parameters plays any role on the vertical deformation. Wheel tracker test data with close proximity regardless of the test condition and material type is also reported in the literature [116, 117].

Table 6.4-1 Wheel Tracker test result - existing test setup

Gradation	Binder Type	Air Void %	Temperature °C	Rutting - mm
AC 14	60/70	5.5	50	2.1
AC 20	80/100	5.0	50	2.3
AC 20	60/70	7.7	50	2.2
AC 14	80/100	6.3	60	2.4
AC 20	80/100	5.6	50	2.5
AC 20	60/70	4.3	60	2.0

As for the next step, the very same mould sizes were used for the experiment. However, this time in order to ease the unnecessary side constraints, the specimens were cut for 20.0 mm on their lateral sides. Promising changes were observed accordingly and all three regions of the

permanent deformation curve were detected. Figure 6.4.2 to Figure 6.4.4 illustrate the deformation curves for AC 20 mixtures tested at 50 °C with and without lateral constraints.

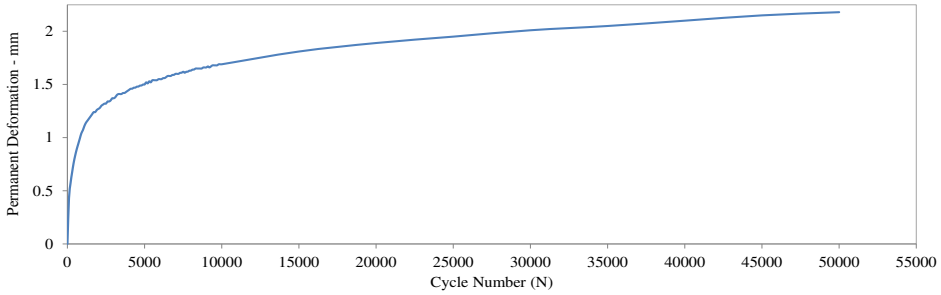

Figure 6.4-1 Wheel Tracker, Binder 80/100 - VTM =6.0% - before cutting

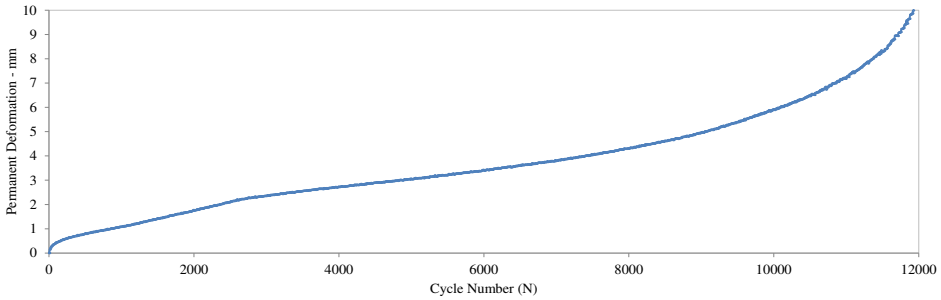

Figure 6.4-2 Wheel Tracker, Binder 80/100 - VTM =6.0% - after cutting

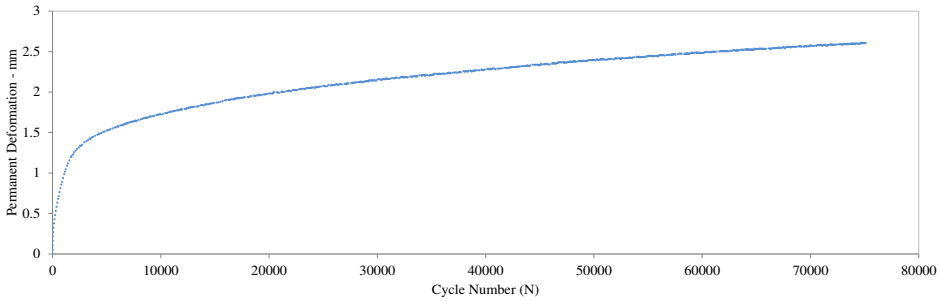

Figure 6.4-3 Wheel Tracker, Binder 60/70 - VTM =4.3% - before cutting

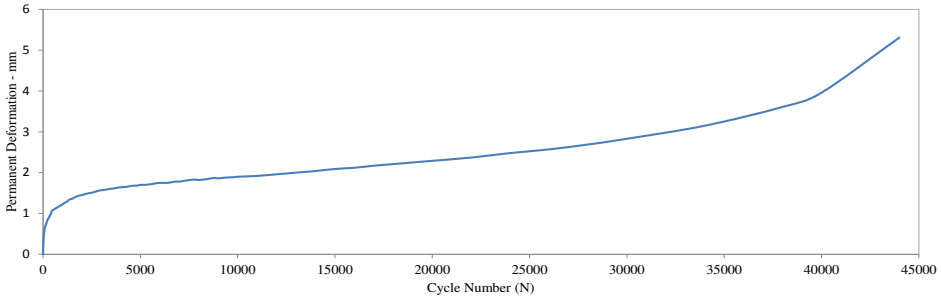

Figure 6.4-4 Wheel Tracker, Binder 60/70 - VTM =4.3% - after cutting

As can be seen, the figures above show that artificial lateral pressure is the single most important obstacle preventing the true material behaviour. Consequently, the decision was made to use the new test setup shown in Figure 6.4.5. The new setup would allow running the

experiment without altering the specimen size. Besides, the lateral deformation can also be recorded following the new test setup.

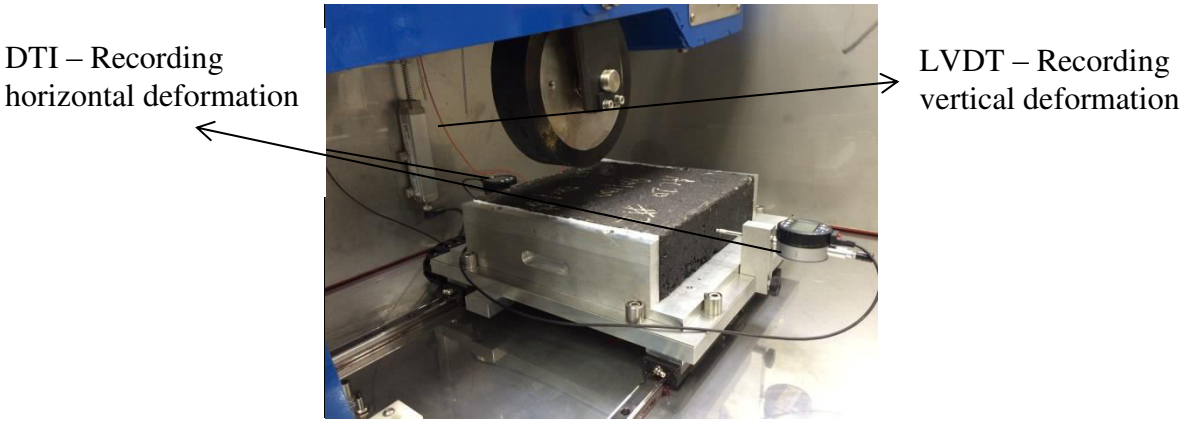

Figure 6.4-5 Proposed test setup

6.4.2 Experiment Specification

A modified version of the Auto Lift Arm ECO Cooper Wheel Tracker was designed at the Transportation Laboratory at University of Canterbury and it is used for the accelerated performance testing. The machine includes a single solid rubber wheel. The tyre width is 50 ± 1 mm which applies 700 N load. The average speed is 26.5 cycles per minute. The test is carried out in a temperature controlled chamber.

To record the horizontal deformation, two Dial Test Indicators (DTIs) are mounted on the specimen sides. One vertical Linear Variable Differential Transformer (LVDT) is also placed under the wheel tracker arm. The tests were run for two gradations, binder types, air void contents and at two temperatures as shown in Table 6.4.2.

Table 6.4-2 Detail of wheel tracker test

AC 14, 20			
Binders 60/70, 80/100			
VTM=3.5%		VTM=5.5%	
T=50 °C	T=60 °C	T=50 °C	T=60 °C

6.5 Experimental Results and Analysis

In order to guarantee capturing a complete deformation curve, the experiment was set up for 100´000 cycles or 15 mm vertical deformation, whichever occurs first.

Figures 6.5.1 to 6.5.6 show the permanent deformation versus the cycle number for a number of the tests while Table 6.5.1 covers flow numbers using Francken model, details of which is explained in Chapter 5. Data prepared are the average of two replicates.

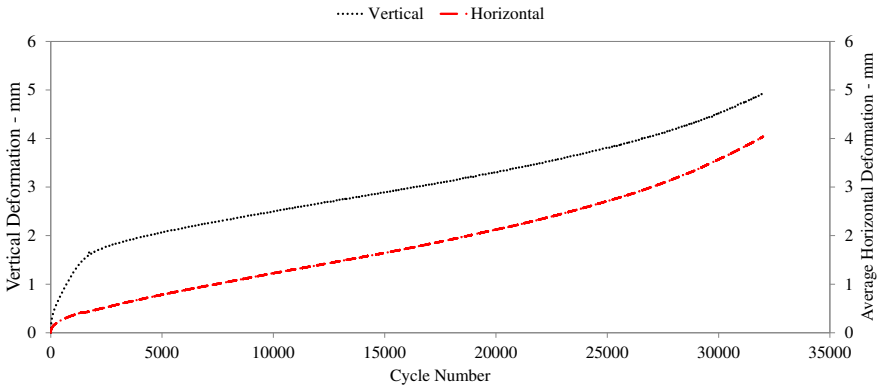

Figure 6.5-1 Permanent deformation versus cycle number – AC20[1]-60/70[2]-7.0[3]-50[4]

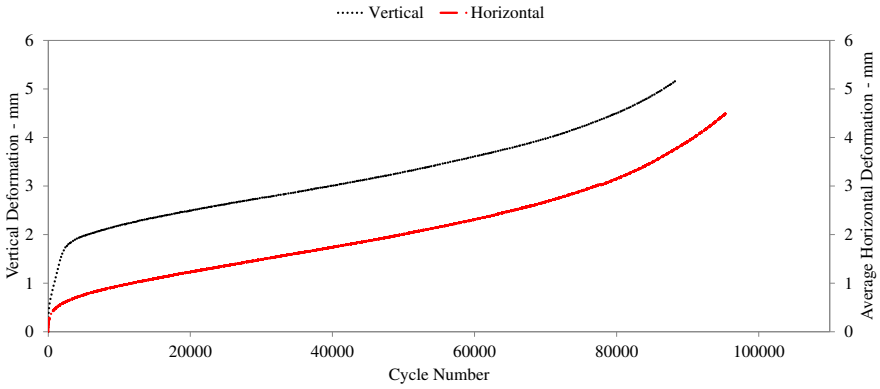

Figure 6.5-2 Permanent deformation versus cycle number – AC20[1]-60/70[2]-5.5[3]-50[4]

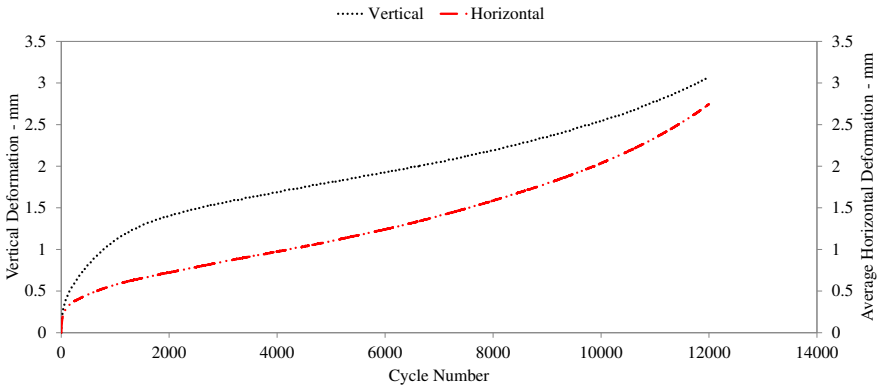

Figure 6.5-3 Permanent deformation versus cycle number - AC14[1]-60/70[2]-3.5[3]-60[4]

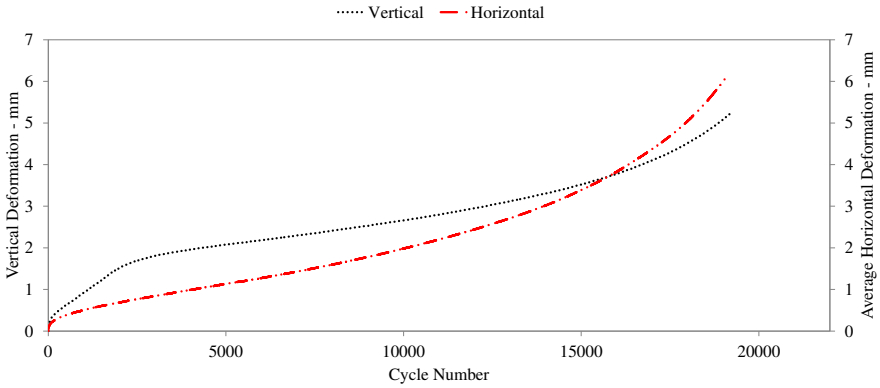

Figure 6.5-4 Permanent deformation versus cycle number - AC14[1]-60/70[2]-5.5[3]-50[4]

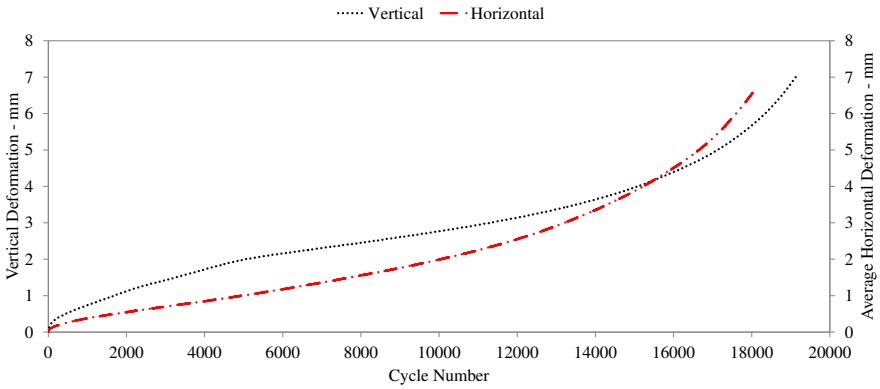

Figure 6.5-5 Permanent deformation versus cycle number - AC14[1]-60/70[2]-7.0[3]-50[4]

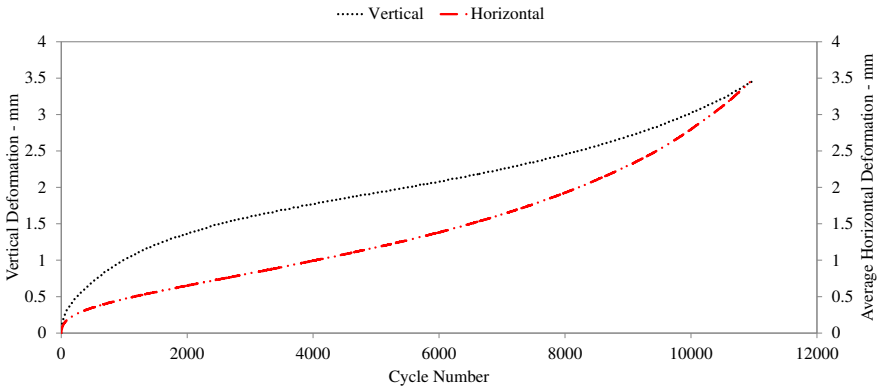

Figure 6.5-6 Permanent deformation versus cycle number - AC14[1]-80/100[2]-5.5[3]-50[4]

[1] Aggregate Gradation, [2] Binder Type, [3] Air Voids (%), [4] Testing Temperature (°C)

As the figures illustrate, by using the upgraded setup, every single slab reaches its failure point, with only very few exceptions. That was not the case for the conventional test method. Moreover, unlike the fully confined approach, the wheel tracker test becomes more sensitive to mix parameters such as air voids contents, aggregate gradation, binder type and also to the test temperature. Therefore, ranking the mixtures based on their permanent deformation behaviour becomes more reliable. As can be seen in Table 6.5.1, by moving from course to

fine aggregate, i.e. AC 20 to 14, the mix undergoes higher deformation rate. The conclusion also applies to binder, 60/7 to 80/100, air voids, 3.5 to 7.0%, and temperature, 50 to 60 °C.

In addition, the magnitude of permanent deformations under the loaded wheel test were also investigated at the onset of the tertiary zone for different mixes, test temperatures and slab thickness in order to provide a better understanding of the material behaviour. Exploring the deformation at the failure point reveals that the tertiary point predominantly takes place at around 2.4 mm based on the vertical deformation or 1.1 mm based on the lateral deformation at 50 °C. It is 1.7 mm and 0.90 mm for 60 °C, respectively. Therefore, based on the available data, it could be concluded that focusing on the horizontal deformation as a failure identification parameters could potentially drop the experiment time to half of what requires for the vertical deformation.

Table 6.5-1 Vertical and Horizontal flow number

T, °C	Gradation	Binder	Air Voids %	Vertical FN	Horizontal FN
50	AC 20	60/70	3.5	No failure	No failure
			5.5	33805	31850
			7.0	14660	10960
		80/100	3.5	No failure	No failure
			5.5	10300	7997
			7.0	3190	2600
	AC 14	60/70	3.5	14725	8900
			5.5	9530	5340
			7.0	8980	4600
		80/100	3.5	6430	3900
			5.5	5725	3360
			7.0	2910	1660
60	AC 20	60/70	3.5	17510	11110
			5.5	4000	2200
		80/100	3.5	15470	9100
			5.5	3440	2200
	AC 14	60/70	3.5	5420	3600
			5.5	1015	850
		80/100	3.5	3230	2300
			5.5	840	460

As a result, the following conclusions can be made observing the experiment data;

- The modified wheel tracker test is capable of ranking the specimens in regards to change in the major parameters such as temperature, air voids, aggregate gradation

and binder type. The conventional setup lacks the ability to detect the differences in mix behaviour.

- There is a rather noticeable difference between horizontal and vertical cycle number at failure. Using the lateral deformation data could potentially shorten the test length.
- By using the modified test setup, the true material failure point could be detected. Therefore, it will help pavement designers and practitioners by providing them with more reliable outcome.

6.6 Finite Element Simulation

The Finite Element Method (FEM) is a powerful technique in analysing material behaviour. Having the ability to analyse non-linear, three dimensional and plastic behaviour structures makes the method a desirable candidate in researching Hot Mix Asphalt (HMA) behaviour.

Abaqus is a general purpose finite element program. It is a powerful engineering simulation package that covers an extensive range of material from linear elastic to nonlinear plastic. Abaqus also has an extensive library of finite elements including continuum, shell, beam, truss and rigid elements [118]. In this study, ABAQUS/CAE was used. It is the complete Abaqus environment. It has both pre and post processors [119].

Generally speaking, the following steps are included in Abaqus simulation. The program, first, requires the user to create the geometry model. Then, the material properties is defined and assigned to the geometry prepared. After that, the boundary conditions and loading sequence is added. And, finally, the model is meshed and ready for the analysis. A critical step in the simulation step is the discretization. It is using small elements to represent the continuum body of the geometry selected. These elements are joined by shared nodes. The collection of nodes and the finite element forms the mesh and the number of elements used in a particular meshed is defined as mesh density. The displacement of these shared nodes is calculated by the software which eventually results in stress-strain determination [120].

6.6.1 Material Characterisation

Unlike the elastic materials which can be simply defined by specifying their Young's Modulus and Poisson's Ratio, the viscoelastic group, e.g. asphalt mixtures, requires more sophisticated data as their input.

To obtain the parameters for Abaqus/*Viscoelastic* option, first, the creep compliance test is carried out and fitted to generalized Kelvin model;

$$D(t) = D_g + \sum_{j=1}^{N} D_j \left[1 - e^{-t/\tau_j} \right] \qquad 6.6\text{-}1$$

where,

τ_j = Retardation time, D_j = Regression coefficients and, D_g = Glassy compliance.

The measured creep compliance is then used as the basis of conversion for Generalized Maxwell Model;

$$E(t) = E_e + \sum_{j=1}^{M} E_j e^{-t/\rho_j} \qquad 6.6\text{-}2$$

where,

E_e = Equilibrium modulus (long-term relaxation modulus),
E_j = Prony regression coefficient, and,
ρ_j = Relaxation time.

The conversion from creep to relaxation can be made by the help of interconversion techniques discussed in Chapter 4.

In viscoelastic option, the relaxation function in Abaqus is presented by shear $G(t)$ and bulk $K(t)$ modulus using Prony series [121];

$$G(t) = G_0 \left[1 - \sum_{k=1}^{N} \bar{g}_k^{\,p} \left(1 - e^{-t/\tau_k} \right) \right] \qquad 6.6\text{-}3$$

$$K(t) = K_0 \left[1 - \sum_{k=1}^{N} \bar{k}_k^{\,p} \left(1 - e^{-t/\tau_k} \right) \right] \qquad 6.6\text{-}4$$

where, G_0 and K_0 are the instantaneous shear and bulk moduli while $\bar{g}_k^{\,p}$ and $\bar{k}_k^{\,p}$ are dimensionless Prony coefficients. As a result, another conversion is again required from relaxation to shear relaxation modulus in order to finally obtain the input parameters required for the finite element simulation.

The next available method in calculating the permanent deformation is the viscoplastic technique by using the *Creep Model*. Creep behaviour in Abaqus is specified by the equivalent uniaxial behaviour – the creep law. The built-in constitutive equations for the power law creep model is considered relatively simple yet, appropriate approach in measuring irrecoverable strain for problem at hand [122, 123]. The model is active in Abaqus VISCO procedure. In this approach the creep strain ε_c is represented by Bailey-Norton law [121, 124]:

$$\varepsilon^c = \frac{A}{m+1}\sigma^n t^{m+1} \qquad 6.6\text{-}5$$

where, A, m and n are constants and are function of temperature.

Differentiating Equation 6.6.5 will result in *time-hardening* form of the creep model in which the creep strain rate depends on stress, time and temperature;

$$\dot{\varepsilon}^c = \frac{\delta\varepsilon^c}{\delta t} = A\sigma^n t^m \qquad 6.6\text{-}6$$

where,

$\dot{\varepsilon}^c$ = Creep strain rate,
σ = Uniaxial equivalent deviatoric stress,
t = Time,
A, n and m = Material constants.

σ is Mises equivalent stress. For physically reasonable behaviour, A and n must be positive and $-1 < m \leq 1$.

By rearranging Equation 6.6.6 and replacing "t" with $\left(\frac{\varepsilon^c(m+1)}{A\sigma^n}\right)^{\frac{1}{m+1}}$, the *strain-hardening* form is developed. The creep strain rate in here depends on stress, strain and temperature;

$$\dot{\varepsilon}^c = \left(A\sigma^n\left[(m+1)\varepsilon^c\right]^m\right)^{\frac{1}{m+1}} \qquad 6.6\text{-}7$$

Typically, the time hardening version of power-law creep model is recommended in cases when the stress state remains essentially constant. The strain hardening is mainly used when the stress state varies during the analysis [121].

If the creep model is used to describe the time dependent material behaviour, it can be shown that, given the same overall loading time, repeated and continuous loading pattern will result in the same predicted creep strain. In another word, static loading can be applied rather than applying the reparative action of moving load. Suppose that the creep property of material "x" is plotted in Figure 6.6.1. A load of constant magnitude is applied to the material with time durations of t_1, t_2 and t_3. Creeps resulting from these loading pattern are shown on the vertical axis as D_1, D_2 and D_3. Consequently, the total creep strain is simply the sum of the creeps associated to each loading. It is important to mention that the time duration used in the creep strain calculation is entered as a time in whole (i.e. Figure 6.6.1 - a) and is not calculated repeatedly from the origin (Figure 6.6.1 - b). The reason is that, the material is *worked* after each loading phase which makes it to react differently the next time it is loaded. Therefore, as long as creep model is to be used, the predicted response will be the same for moving and constant loading considering an identical total loading time.

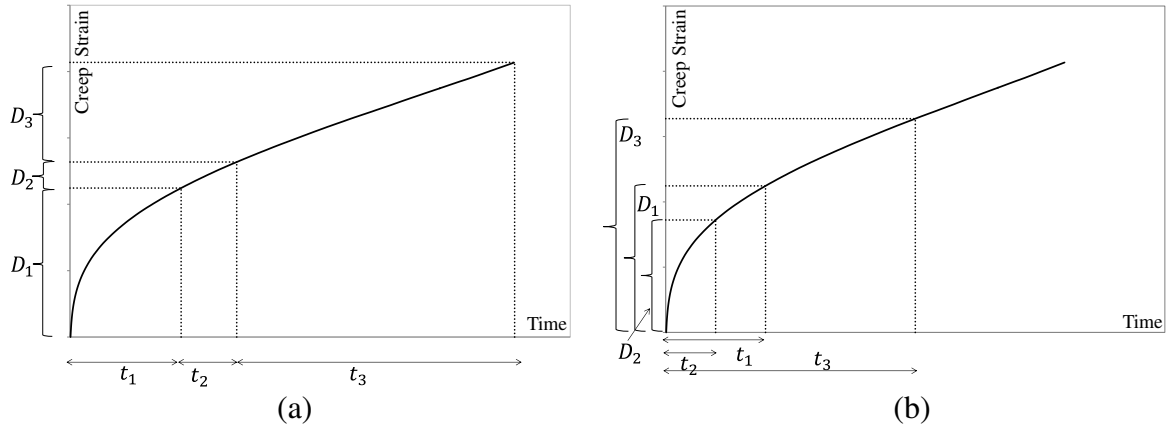

Figure 6.6-1 Correct loading time

6.6.2 Model Geometry

Two different model geometries were considered for this study. Initially, a three dimensional cylindrical specimen was designed to simulate the uniaxial creep compliance test. The reason behind this step was to validate the material properties accuracy as well as the simulation technique. A schematic of the cylindrical specimen is shown in Figure 6.6.2. Vertical pressure is applied to the top surface with the boundary condition mode of "ENCASTRE" at the bottom.

In the next step, the wheel tracker slab specimen simulation will be carried out. A 3D deformable solid beam was used in this step. Loading and the boundary condition is

illustrated in Figure 6.6.3. The “ENCASTRE” mode, similar to the cylindrical specimen simulation, is used for the bottom of the slab. For the side boundary conditions, vertical displacement is only allowed. Details on mesh and element type are covered in modelling and result section.

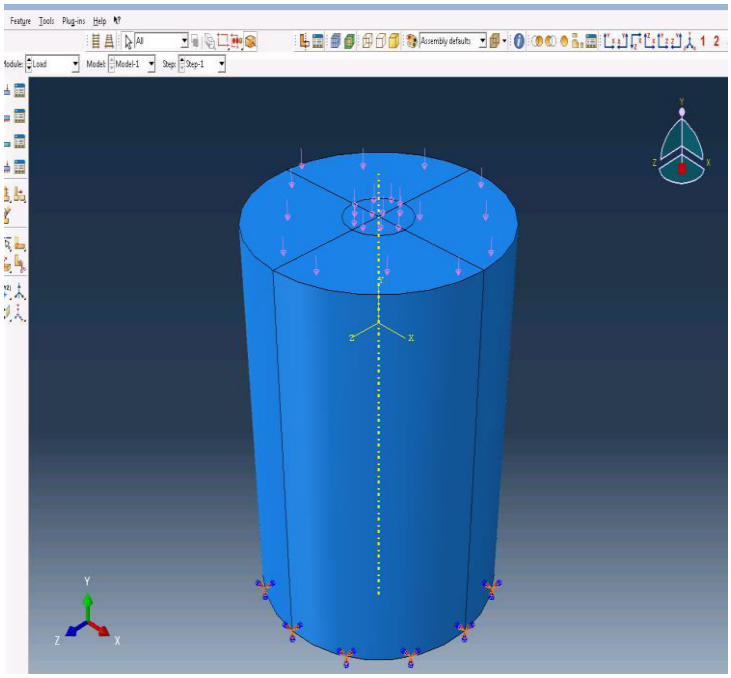

Figure 6.6-2 Boundary condition and loading for cylindrical specimen

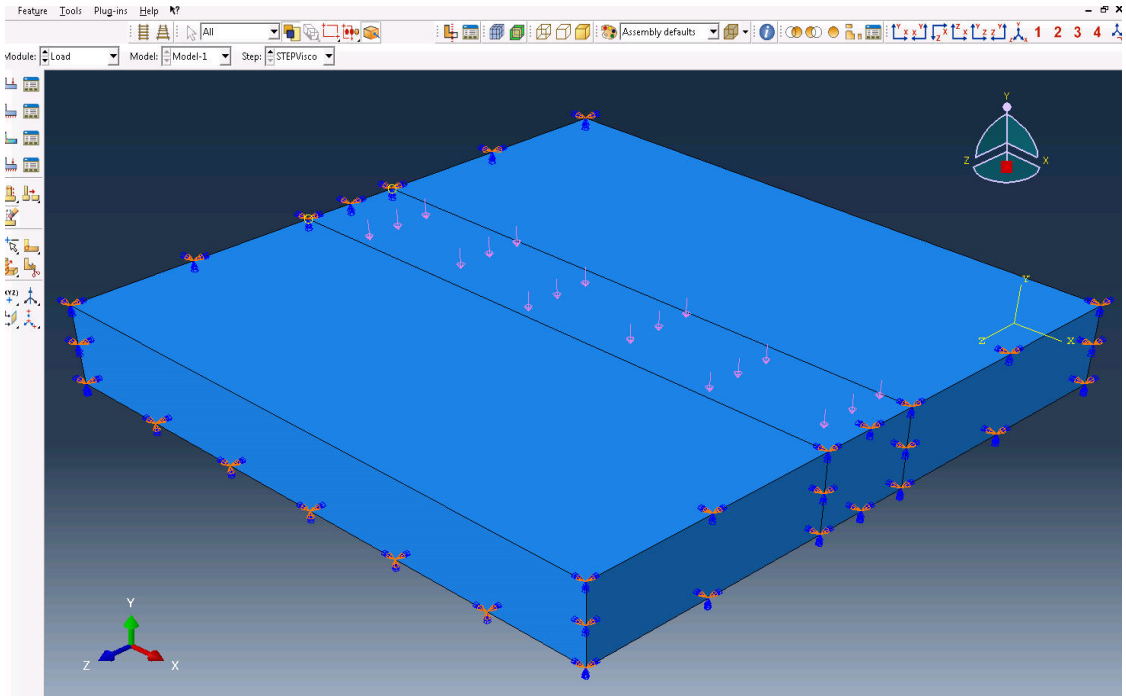

Figure 6.6-3 Boundary condition and loading for slab

6.6.3 Loading Method

The footprint of the wheel tracker rubber tyre on the asphalt slab surface has an average of 22.5 mm width by 50.0 mm length as shown in Figure 6.6.4. For the 700 N load applied the uniform pressure of 0.62 MPa is used in the simulation process.

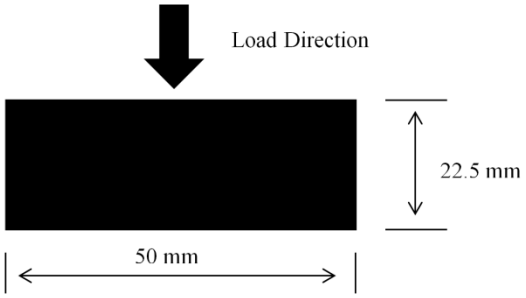

Figure 6.6-4 Wheel tracker rubber tire footprint

The step load function is applied to the first set of elements. It then moves forward till the wheel reaches the last element. Once the wheel returned to its original place through the same path, one cycle is completed. This will be repeated for the desired cycle number. Figure 6.6.5 shows the loading function sequence.

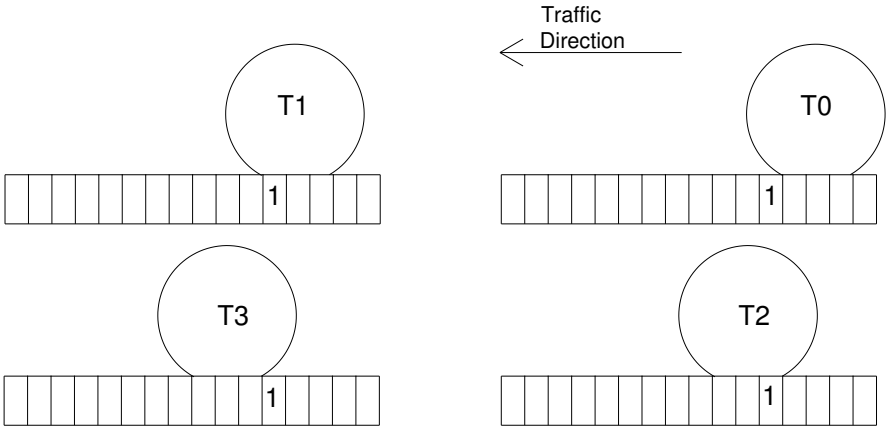

Figure 6.6-5 Wheel tracker loading pattern

It starts on time zero (T_0) from the edge of the element No.1. Subsequently, the wheel covers the whole element at time T_1. Time T_2 is when the rear edge of the tyre reaches element No.1. Notice that the max load magnitude is maintained during T_1 and T_2. Finally at time T_3, the wheel leaves the surface of element No.1 moving to the next element and so on until the end of the slab track. The duration can be calculated as follows;

$$T_0 \text{ to } T_1: \qquad t_1 = T_1 - T_0 = \frac{a}{v}$$

T_1 to T_2: $t_2 = T_2 - T_1 = \dfrac{b-a}{v}$

T_2 to T_3: $t_3 = T_3 - T_2 = \dfrac{a+b}{v} - \dfrac{b}{v} = \dfrac{a}{v}$

Total time duration; $T = \dfrac{a}{v} + \dfrac{b-a}{v} + \dfrac{a}{v} = \dfrac{a+b}{v}$

where, a is the element size, b is the tyre print and v is the wheel speed.

Studying the load magnitude reveals that the element would only bear the full magnitude during T_1 to T_2 time span. Whereas, the applied load changes from zero to full load and from full load to zero for T_0 to T_1 and T_2 to T_3, respectively. However, given that the wheel speed is constant, an equal time interval is considered for these two time intervals. Areas under the load-time diagram (for t_1 and t_3) can be simulated as the same size triangles with the height of maximum load magnitude. Consequently, a new loading order can be assumed for element No.1 as illustrated in Figure 6.6.6.

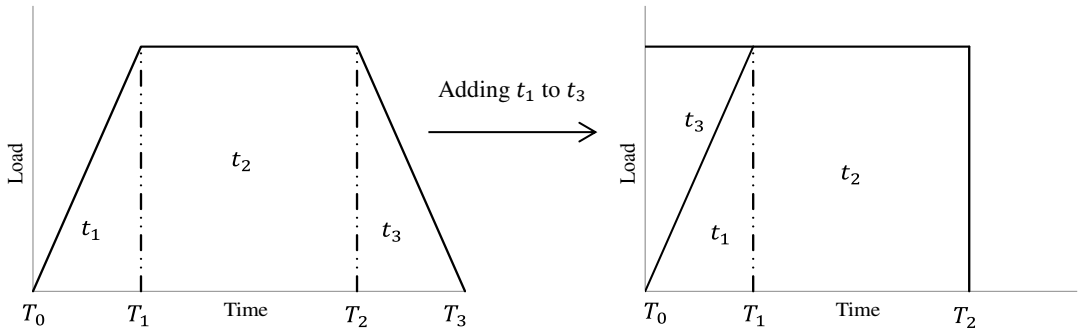

Figure 6.6-6 Load distribution used in simulation step

Now, the total loading time equals to $\left(b/v\right)$ that is calculated by dividing the tyre imprint length by the speed of the wheel regardless of the element size (a). The loading time is no longer dependent on the finite element size.

Initially, the step loading was considered for the Abaqus analysis. Preliminary investigations revealed a prolonged simulation time required for moving load approach. An alternate loading method was sought to overcome the obstacle. The adopted method consists of a single static load with the duration of an equivalent of the total cumulative loading time. This approach was originally considered by [122, 125-127] . Additional analysis confirmed the lengthy simulation effort for the moving load method. Table 6.6.1 below provides

compressive strain and the time summary for an example slab modelled and analysed for comparison purposes, only. The simulation was once undertaken by a moving load and then repeated for the static load of equivalent to 30 cycles. Data extracted from analysis show that the final strains resulted from these two approaches are quite similar while noticeable difference is observed in the computational efforts.

Table 6.6-1 Moving load versus static load simulation results

Loading Type	Cycle Number	Compressiove Strain	Computation Time (sec)
Moving	30	10.728*10^(-3)	16289
Static	30	11.112*10^(-3)	478.6

As a result, static load option was selected for this research instead of the moving load technique.

6.6.4 Modelling and Results

As discussed earlier, the creep compliance test was modelled prior to the wheel tracker analysis. This would help to validate the material parameters used in the finite element simulations. A 3D deformable solid was modelled with 150 mm height and 100 mm diameter. A 20 node quadratic brick element (C3D20) composed of 14200 elements was used as shown in Figure 6.6.7.

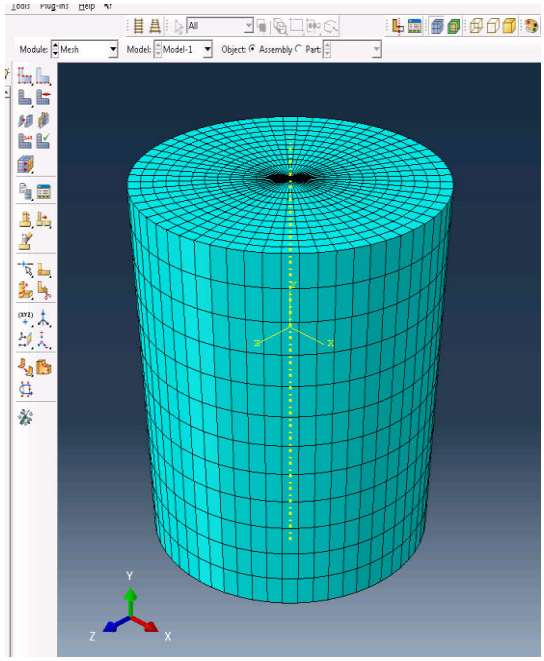

Figure 6.6-7 C3D20 – finite element mesh for creep compliance test

The instantaneous modulus and Poisson's ratio at the testing temperature have to be determined as a part of material properties input. The Poisson's ratio is assigned as 0.4 based on the New Zealand and Australian standard. For the modulus determination, the relaxation modulus explained by the generalized Maxwell model (Equation 6.6.2) is used. The instantaneous modulus is determined by equating "$t = 0$" in the formula.

On the other hand, the master curve can also be used for the modulus verification. In this approach, first, the curve is plotted at the prescribed temperature (i.e. 50.0 °C for this study). Subsequently, the dynamic modulus associated to 0.44 Hz (equivalent to the wheel tracker loading frequency) is then read from the graph. The creep parameters were developed using Equation 6.6.5 as reviewed in the "*Material Characterisation*". The elastic and creep modulus parameters for the simulation step are covered in Table 6.6.2.

Table 6.6-2 Asphalt mix – material parameters

AC 14 Binder 80/100 Temp 50 °C	Material Parameters				
	Elastic		Creep		
	Instantaneous Modulus (MPa)	Poisson's Ratio	A	n	m
Model Verification	70.50	0.4	1.99E(-4)	0.254	-0.811

The analysis was undertaken for the duration of 120 seconds. Figure 6.6.8 compares the laboratory experiment versus Abaqus prediction. The figure illustrates excellent matching between the experiment and the simulation results validating the accuracy of the selected material properties.

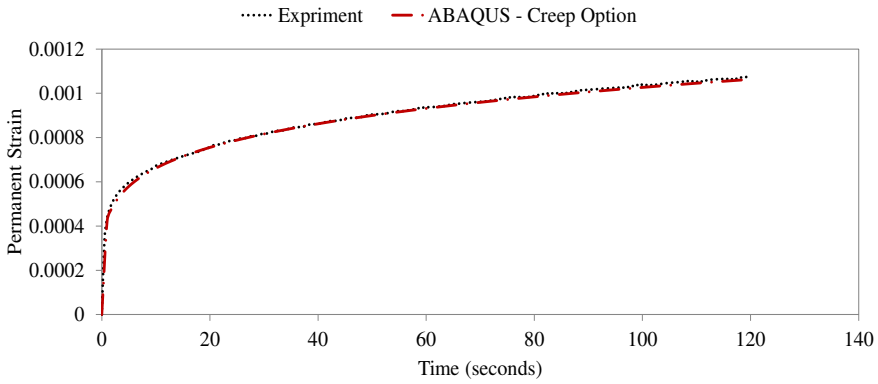

Figure 6.6-8 Experiment versus simulation

As for the wheel tracker simulation, the time of loading can be calculated using the machine loading frequency. Given the wheel speed is 26.5 cycle/min, the load duration will be equal

to 0.0837 sec for each pass. The loading time for each wheel pass is then summed up to produce the total cumulative loading time.

Of the major steps in the finite element simulation is the mesh size selection. In general, mesh dimension must be small enough to provide accurate responses from the simulation model. On the other hand, it should be also coarse enough to prevent a dramatic increase in computer hardware requirements and computational time. Four different finite element meshes were trialled in for this research in order to find the optimum mesh density. Figure 6.6.9 illustrates the effect of the degree of mesh density and their computational effort.

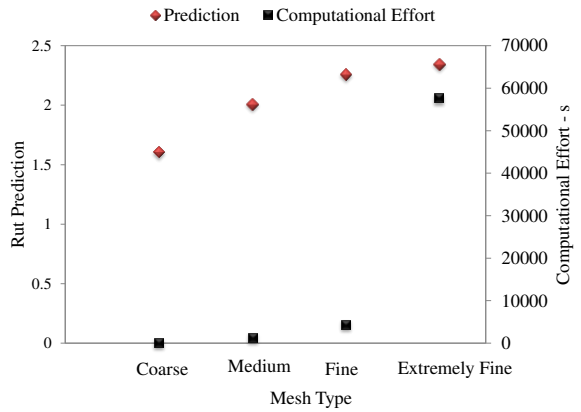

Figure 6.6-9 Mesh density effect on prediction/computational effort

The figure reveals that the prediction improvement is observed only up to a certain limit of mesh size reduction. While after that, there will be merely a marginal change in the result with a significant increase in the computational effort. As a result, “fine” mesh distribution was considered for the simulation. It includes 3078 elements as shown in Figure 6.6.10. As can be seen from the figure, to ensure accurate prediction, the area with high stress concentration is meshed with significantly greater density.

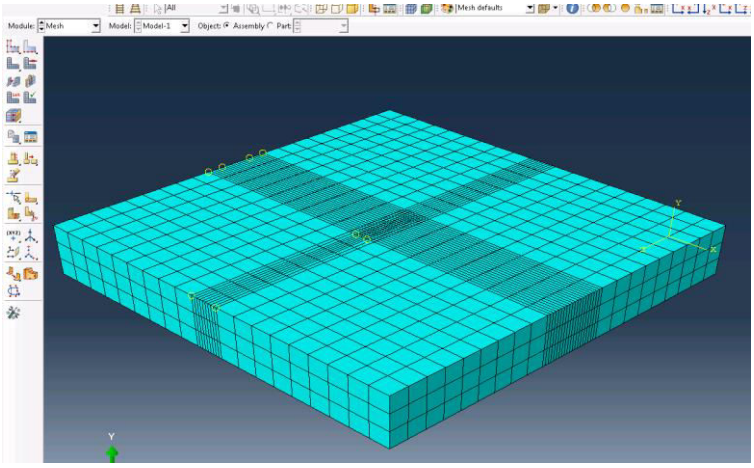

Figure 6.6-10 Mesh used in finite element simulation

The last step will be to determine the material properties for each mix. As covered earlier, von-Mises stress is used in the creep plasticity model. Analysis showed that, the von-Mises stress resulted from the wheel tracker is roughly equal to 0.32 MPa for the slab specimen. Therefore, the creep compliance test was performed at 50 °C under the uniaxial stress of 320 kPa deviator stress. The material parameters were determined and are shown in Table 6.6.3.

Table 6.6-3 Material properties used in simulation

Mix; Gradation – Binder	Material Parameters				
	Elastic		Creep		
	Instantaneous Modulus (MPa)	Poisson's Ratio	A	n	m
AC 14 – 60/70	81.3	0.4	1.98E(-3)	0.339	-0.727
AC 14 – 80/100	70.5	0.4	1.92E(-3)	0.347	-0.697
AC 20 – 60/70	201.5	0.4	8.04E(-4)	0.319	-0.845

Figures 6.6.11 to 6.6.13 show the measured rut depth and their comparison with the predicted ones. The data seem to be quite promising. The figures confirm the ability of the plastic creep model to, reasonably, predict the permanent deformation resulted from wheel tracker test.

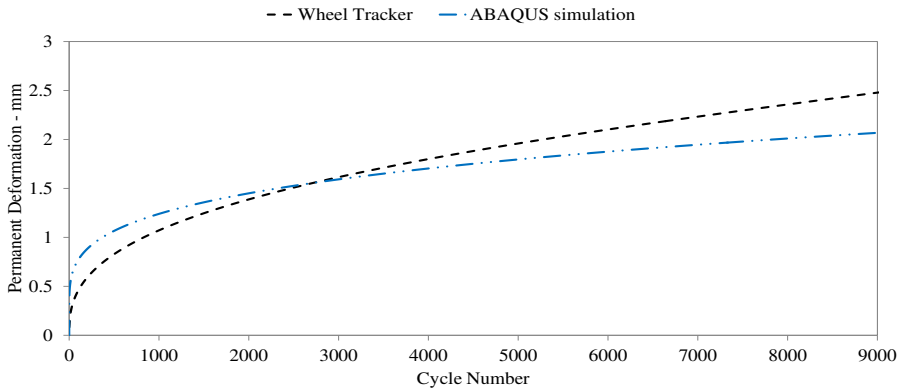

Figure 6.6-11 Measured deformation versus prediction AC 14 – 60/70

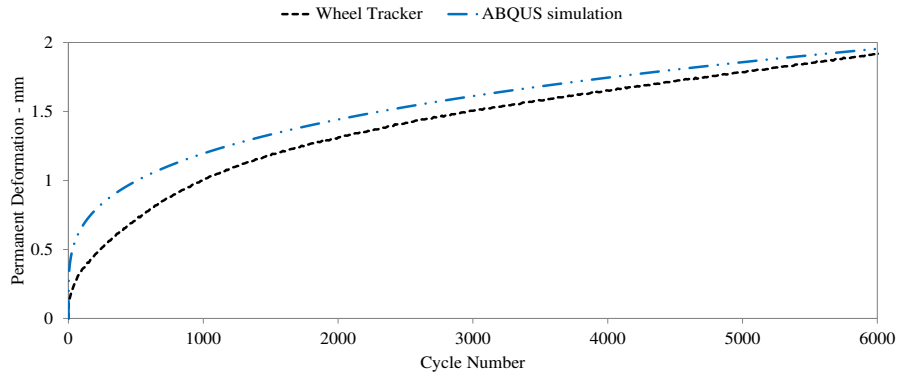

Figure 6.6-12 Measured deformation versus prediction AC 14 – 80/100

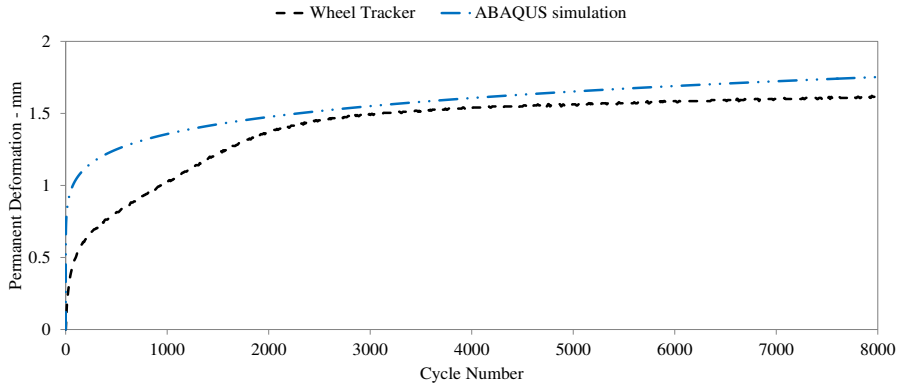

Figure 6.6-13 Measured deformation versus prediction AC 20 – 60/70

6.6.5 Comparison to Burger's Model

The Burger's Model is also used in the simulation of the permanent deformation behaviour of the asphaltic material. The model is a combination of Maxwell and Kelvin in series. The differential equation of the constitutive model governing Burger's model is shown in Equation 6.6.8 [128];

$$\sigma + p1\dot{\sigma} + p2\ddot{\sigma} = q1\dot{\varepsilon} + q2\ddot{\varepsilon} \qquad 6.6\text{-}8$$

As $p1, p2, q1$ and $q2$ are defined as;

$$p1 = \frac{\eta_M}{E_M} + \frac{\eta_M}{E_K} + \frac{\eta_K}{E_K}, \quad p2 = \frac{\eta_M \eta_K}{E_M E_K}$$

$$q1 = \eta_M, \qquad q2 = \frac{\eta_M \eta_K}{E_K}$$

where, E_M, η_M and E_K, η_K are spring and dashpot constants for Maxwell and Kelvin part, respectively.

It should be noted that Abaqus assumes the viscoelastic material state is defined by dimensionless relaxation modulus, therefore, in order to determine Burger's model constants that can be implemented to Abaqus software some variable transformations will be required. The shear relaxation modulus in Burger's term after Laplace transformation/inversion can be expressed by Equation 6.6.9 [129];

$$G(t) = \frac{G_M}{(\alpha - \beta)}\left[\left(\frac{G_k}{\eta_k'} - \beta\right)\cdot e^{-\beta t} + \left(\alpha - \frac{G_k}{\eta_k'}\right).e^{-\alpha t}\right] \qquad 6.6\text{-}9$$

where,

$$G_M = \frac{E_M}{2(1+\nu)},\ G_K = \frac{E_K}{2(1+\nu)}$$

$$\eta_M' = \frac{\eta_M}{2(1+\nu)},\ \eta_K' = \frac{\eta_K}{2(1+\nu)}$$

$$\alpha, \beta = \frac{p1 \mp \sqrt{p1^2 - 4p2}}{2 * p2}$$

Considering the shear relaxation modulus as;

$$G(t) = G_\infty + \sum_{i=1}^{n} G_i.e^{-t/\tau_i} \qquad 6.6\text{-}10$$

And, comparing it to Equation 6.6.9;

$$G_\infty = 0, \qquad G_1 = \frac{G_M}{(\alpha - \beta)}\left(\frac{G_K}{\eta_K'} - \beta\right),$$

$$G_2 = \frac{G_M}{(\alpha - \beta)}\left(\alpha - \frac{G_k}{\eta_K'}\right), \qquad \tau_1 = \frac{1}{\beta}, \qquad \tau_2 = \frac{1}{\alpha}$$

The dimensionless variable for Abaqus can be found as follows;

$$g_1 = \frac{1}{(\alpha - \beta)}\left(\frac{G_K}{\eta_K'} - \beta\right), \qquad g_2 = \frac{1}{(\alpha - \beta)}\left(\alpha - \frac{G_k}{\eta_K'}\right)$$

Therefore, g_1, g_2, τ_1 and τ_2 are parameters of Burger's model which can be directly inserted into Abaqus.

The static creep test was performed under 320 kPa deviator stress (equivalent to what observed under the wheel tracker test). The test was conducted for the duration of 80 seconds. Table 6.6.4 covers the Burger's model parameters used in the simulation process. Figure

6.6.14 shows the simulation result. As it appears, Burger's model underestimates the strain curve.

Table 6.6-4 Burge's model parameters

Mix	G_m	α	β	G_k	η'_k
AC 20 - 80/100 - Temp 50	25.180	0.197	0.004	0.0034	0.0307

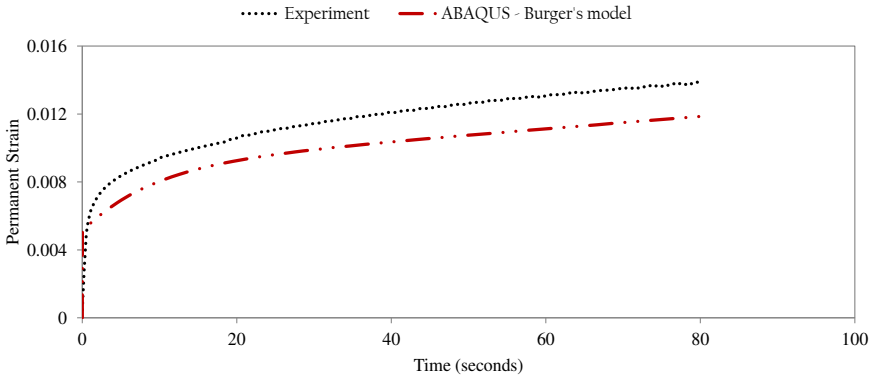

Figure 6.6-14 Experiment versus simulation – Burger's model

It is believed that, linear viscoelastic models such as Burger's Model would quite accurately represent asphalt materials behaviour. However, this statement applies only to the conditions with low state of stress. And, as long as the applied pressure remains within linearity limit, whereas, the wheel tracker test includes intense load application which goes beyond the linearity limit.

The viscoelastic simulation modelling represented in this chapter could be implemented in the mechanistic empirical design procedure. The finite element analysis can be used to describe material behaviour with higher level of accuracy. As shown in Figures 6.6.11 to 6.6.13, the viscoplastic creep model is capable of predicting asphaltic material response where permanent deformation is of concern.

6.7 Conclusion

The wheel tracker test and the finite element modelling were covered in this chapter. At first, the conventional test setup, which includes placing the specimen inside fully confined steel mould of the same internal dimension as the slab specimen, was employed for the laboratory experiment. However, the preliminary studies showed that undertaking the experiment under the existing setup will only lead to permanent deformation as a result of specimen densification (i.e. reduction in the air voids content). To overcome this obstacle, a new test

setup was introduced. In this method, all three phases of deformation, densification and shear related deformation can be recorded successfully. This was achieved by removing the barriers parallel to the loading path from the testing mould.

ABAQUS simulation was also carried out. The uniaxial creep compliance test was performed for the material properties determination used in the simulation. To study the accuracy of the extracted factors, the uniaxial creep test was first simulated. After determining the material properties, the wheel tracker simulation was then carried out. The plastic creep model was considered for this stage. One of the advantages of using the creep model is that the moving load can be replaced by static loading which will result in significant shortening in the computational effort.

Burger's Model was also considered in the simulation stage. The model which is a series combination of Maxwell and Voigt model can be used directly in the Abaqus program after some variable transformations.

Data resulted from the Burger simulation method were not as accurate as the creep plastic model. The reason is believed to be the state of stress in the wheel tracker test. Asphalt materials tend to behave nonlinearly under high pressure. They will no longer follow the linear viscoelastic rules.

Plastic creep simulation showed to be promising. Comparing the measured data form experiments with the predicted ones confirm the validity of the plastic creep option.

Chapter 7: Conclusions and Recommendations

The objectives of this thesis are to improve the state of the art of permanent deformation modelling in the current Mechanistic empirical pavement design adopted by the New Zealand and Australian industry, in addition to provide a thorough viscoelastic characterisation of the hot mix asphalt commonly used on New Zealand roads. The current Mechanistic empirical design used by New Zealand and Australia is based on the subgrade compressive strain criterion in which the permanent deformation is assumed to result mainly from the subgrade provided the control of the pavement layers thicknesses, material quality and construction of pavement layers. However, researches carried out by others have proven that at least 50% of the total permanent deformation occurs in the upper pavement layers.

Therefore, current mechanistic empirical pavement design methods have shifted away from the subgrade compressive strain criterion approach and instead these new methods consider the total permanent deformation as the sum of each pavement layer in addition to the subgrade. However, to model the permanent deformation for each pavement layer separately, a comprehensive research and modelling of the permanent deformation for different pavement materials will be essential. Therefore, this research work is ultimately focused on the viscoelastic characterisation and permanent deformation modelling of commonly used hot mix asphalts in New Zealand. The viscolelastic modelling of permanent deformation relies on material parameters such as dynamic modulus, creep compliance and relaxation modulus. Dynamic modulus test is not a common or popular test with New Zealand industry, instead the indirect resilient modulus test is the most popular test. Therefore, this study introduced a conversion from the IDT test using the Australian/NZ setup to dynamic modulus to provide practical and simple method for roading industry without requiring radical changes. The following steps were taken to address the objectives above.

The Indirect Tensile (IDT) test is widely popular with New Zealand researchers as well as the pavement industry. It is used in material characterization for design and quality control purposes. The test is considered as an alternative method in modulus determination. Simplicity and applicability to field cores are the main reasons contribute to the test's popularity. Nevertheless, the Dynamic Modulus Test is the one recommended for the modulus calculation.

To bridge this gap, the complex modulus and the indirect tensile test were both undertaken for a number of New Zealand asphalt mixtures. The dynamic modulus for the IDT test was calculated through the theory of linear viscoelasticity. The results were then compared to the ones recorded in the dynamic modulus test.

The statistical analysis showed that the results are identical for well above 90% of the data. Accordingly, the dynamic modulus determined from the IDT test is likely to be the same as the one measured from the axial compression test.

As a result of the above analysis, use of ME design procedure could be considered by the New Zealand industry. Dynamic modulus, for the ME design, can be obtained simply through IDT test result and without the necessity of adopting new test setup.

For the next step, the static creep test was performed in order to study the material properties. Dynamic modulus, relaxation modulus and creep compliance are considered as the major parameters in material characterisation. Theoretically speaking, it is well-known that all these material functions should be mathematically interrelated by using the interconversion techniques. However, experience has revealed that, the interconverted data do not necessarily match the one resulted from laboratory experiment. As a result, various interconversion techniques were taken into consideration to investigate true relationship among viscoelastic functions.

Data from the static creep test were converted to relaxation modulus through exact as well as approximate techniques. The relaxation modulus was also calculated using the complex modulus test outcome.

It was shown that the approximate techniques could carry out the viscoelastic interconversion with well above 93% accuracy. As for the complex, the combined error technique was also implemented to minimize possible errors.

To develop a new model, the repeated creep test covering a wide range of factors (mix gradation, air voids, binder type and deviatoric stress) was performed in a full factorial design of analysis. As a result, the relation amongst these factors plus their level of contribution was studied.

The repeated creep test is used as a means to reveal the cycle number at which rutting as a result of shear deformation takes place (known as Flow Number). Given the deformation at flow number plus the significance level of the factors mentioned above, regression models were developed for the rut depth prediction. Temperature was found by far the most significant factor governing the permanent deformation phenomenon following, largely, by deviatoric stress and binder type. Models developed in this study could accurately predict mix behaviours commonly used in New Zealand. This is not necessary the case with the ones developed elsewhere. It was shown that these models tend to overestimate NZ mix behaviour in regards to permanent deformation.

The laboratory experiments were concluded by performing the Wheel Tracker (WT) test. Initially, the test was conducted using the conventional test setup. The test is done by fitting the slab specimen within the same size mould which, was argued that, might result in very limited or no shear permanent deformation. The initial investigation, as it was presumed, revealed a decisive shortcoming in the current test method. It was found that following the conventional procedure, a very limited lateral (shear) related deformation, as a main contributor to high severity level permanent deformation, would be recorded. To overcome this obstacle, a new test setup was proposed by removing the side barriers along the loading track. Data produced as a result of this modification covered all three regions on the deformation curve (i.e. primary, secondary and tertiary zones of deformation) validating the rationale behind upgrading to the proposed setup.

The application of the new test setup has several advantages over the current method. It is, now, possible for the industry to undertake WT test for the purpose of rankling various asphalt mixtures. Ranking specimens could not be accomplished successfully as rather identical depth of rutting is recorded by the current setup of the wheel tracker test method. In addition, results from the proposed modified test setup method showed to be in greater compatibility with the true mix behaviour observed in practice.

Three-dimensional (3D) finite element simulation in ABAQUS program was used to describe asphalt mixture behaviour under the wheel tracker test. The time dependent material behaviour was accounted for through the creep model option. The approach provides user with direct implementation of the creep compliance parameters derived from the static creep test. It also has the advantage of static load simulation. The static load modelling would significantly shorten the simulation effort.

Burger's Model was also considered for viscoelastic simulation. Data resulted from the Burger simulation method were not as accurate as the creep plastic approach. The reason is believed to be the state of stress governed in the wheel tracker test. Asphalt materials tend to behave nonlinearly under high pressure. As a result, they would no longer follow the linear viscoelastic rules.

Finally, the simulation results were compared to the wheel tracker test. Promising data were recorded. Comparing the measured data form experiments with the predicted ones confirmed the validity of the plastic creep option.

It is important to mention that, this research should be treated as the first step in understanding and modelling New Zealand asphalt mixture behaviour where permanent deformation is of concern. The permanent deformation models introduced in Chapter 5 are based on air voids variation of 3 to 5%. The model precision and applicability could enhance significantly by including more comprehensive data points at higher air void content.

It is also recommended that the future studies enhance the wheel tracker test method by altering the applied lateral pressure. The proposed test setup in this study has improved the ability of the test to better capture the asphalt mixture response under the repeated load by eliminating the lateral pressure. However, there exists a noticeable lateral pressure in practice; either from nearby lane or existing shoulder. Therefore, proposing a modified setup with adjustable lateral pressure could potentially enrich the accuracy of material response under the load pressure.

In addition, modelling and analysis included in this study are developed solely based on the laboratory conducted experiments. Future studies are required to calibrate these models with the field data prior to use in any mechanistic empirical design methods.

References;

1. Archilla, A.R. and S. Madanat, *Development of a pavement rutting model from experimental data.* Journal of Transportation Engineering, 2000. **126**(4): p. 291-299.

2. Witczak, M.W., Kaloush, K., Pellinen, T., El-Basyouny, M., & Von Quintus, H., *Simple Performance Test for Superpave Mix Design*, 2002: Washington, D.C.

3. Sebaaly, P.E., McNamara, W. M., Epps, J.A., *resistance of SUPERPAVE and HVEEM mixtures volume -introduction and background*, 2000: Carson.

4. Druta, C., *A micromechanical approach for predicting the complex shear modulus and accumulated shear strain of asphalt mixtures from binder and mastics*. 2006, Louisiana State University: Louisiana.

5. Mohammad, L.N., Saadeh, S., Obulareddy, S. and Cooper, S., *Characterization of Louisiana asphalt mixtures using simple performance tests.* Journal of Testing and Evaluation, 2008. **36**(1): p. 1-12.

6. Austroads, *Guide to pavement technology, Part 2: Pavement Structural Design*. 2010, Sydney: Austroads Incorporated.

7. Monismith, C.L., Sousa, J. & Lysmer, L. *Modern Pavement Design Technology Including Dynamic Load Conditions*. in *Truck and Bus Meeting and Exposition*. 1988. Society of Automotive Engineers.

8. Kandhal, P.S., Mallick, R.B. & Brown, E.R., *Hot mix asphalt for intersections in hot climates*, 1998: Aurburn.

9. Garba. Rabbira., *Permanent Deformation Properties of Asphalt Concrete Mixtures*, in *Department of Road and Railway Engineering*2002, University of Science and Technology: Norwegian University of Science and Technology.

10. Witczak, M.W., *Specification Criteria for Simple Performance Tests for Rutting Volume I: Dynamic Modulus (E*) Volume II: Flow Number and Flow Time*, 2007: WASHINGTON, D.C.

11. OECD, *Heavy trucks, climate and pavement damage*. 1998, Washington, D.C.: OECD scientific experts group.

12. Asphalt Institute, *Superpave Mix Design manual, Superpave Series No. 2 (SP – 2).* 1996: Asphalt Institute.

13. You, Z., *Development of Specification for the Superpave Simple Performance Tests (SPT)*, 2009: Michigan.

14. Anderson, R.M. and R.B. McGennis. *Ruggedness evaluation of the shear frequency sweep test for determining the shear modulus of asphalt mixtures*. in *Asphalt Paving Technology 2003, March 10, 2003 - March 12, 2003*. 2003. Lexington, KY., United states: Association of Asphalt Paving Technologist.

15. Zhou, F. and T. Scullion. *Preliminary Field Validation of Simple Performance Tests for Permanent Deformation: Case Study*. 2003. National Research Council.

16. Airey, G.D., Hunter, A. E., &RAHIMZADEH, B. *The influence of geometry and sample preparation on dynamic shear rheometer testing*. in *Performance of bituminous and hydraulic materials in pavements*. 2002.

17. Kok, B.V., M. Yilmaz, and M. Guler, *Evaluation of high temperature performance of SBS + Gilsonite modified binder.* Fuel, 2011. **90**(10): p. 3093-3099.

18. Mark, R.E., Habeger, C. C., Borch, J. and Lyne, M. B., *Handbook of Physical Testing o Paper*. 2 ed. Vol. 1. 2002, Switzerland.

19. Roberts, F.L., Kandahl, P.S., Brown, E.R., Lee, D.Y., & Kennedy, T.W., *Hot Mix Asphalt Materials, Mixture Design and Construction*. 1996, Lanham, MD: NAPA Research and Education Foundation.

20. American Society for Testing and Materials, *Determining the Rheological Properties of Asphalt Binder Using a Dynamic Shear Rheometer*, 2008.

21. McGennis, R.B., Shuler, S., & Bahia, H.U., *Background of Superpave asphalt binder test methods*, 1994.

22. Witczak, M.W., K.E. Kaloush, and H. Von Quintus. *Pursuit of the simple performance test for asphalt mixture rutting*. in *Asphalt Paving Technology 2002, March 18, 2002 - March 20, 2002*. 2002. Colorado Springs, CO, United states: Association of Asphalt Paving Technologist.

23. Austroads Pavement Research Group., *Selection & design of asphalt mixes: Australian provisional guide* 97.

24. Kim, J., Sholar, G. A., and Kim, S., *Determination of Accurate Creep Compliance and Relaxation Modulus at a Single Temperature for Viscoelastic Solids.* Journal of Material in Civil Engineering, 2008. **20**: p. 147-156.

25. Huang, Y.H., *Pavement analysis and design*. 2004, PEARSON.

26. Witczak, M.W., *Simple Performance Tests: Summary of Recommended Methods and Database*, 2005, Transportation Research Board: Washington, D.C.

27. Kaloush, K.E., & Witczak, M.W, *Tertiary Flow Characteristics of Asphalt Mixtures*, in *Asphalt Paving Technology* 2002.

28. Kandhal, P.S., & Cooley, L.A., *Accelerated laboratory rutting tests: evaluation of the asphalt pavement analyzer*, 2003, TRANSPORTATION RESEARCH BOARD: WASHINGTON, D.C.

29. Tu, W., *Response modelling of pavement subjected to dynamic surface loading based on stress-based multi-layered plate*. 2007, Ohio: The Ohio State University.

30. Barber, E.S. *Application of Triaxial Compression Test Results to the Calculation of Flexible Pavement Thickness*. 1946. Highway Research Board.

31. Yoder, E.J., & Witczak, M. W, *Principles of pavement design*. 2nd ed. 1975, New York: A Wiley-Interscience publication.

32. Huang, Y.H., *Stresses and Displacements in Nonlinear Soil Media.* Journal of the Soil Mechanics and Foundations Division, 1968. **94**: p. 1-20.

33. Schwartz, C.W., and Kaloush, K.E., *Permanent Deformation Assessment for Asphalt Concrete Pavement and Mixture Design*, in *Modeling of Asphalt concrete*, R.Y. Kim, Editor. 2010, McGraw-Hill Construction: New York.

34. Sousa, J.B., Craus, J., and Monismith., C. L., *Summary report on permanent deformation in asphalt concrete*, 1991: Washington, D.C.

35. Chen, D.H., Zaman, M., & Laguros, J.G.,. *Assessment of Distress Models for Prediction of Pavement Service Life*. in *Proceedings of the 3rd Materials Engineering Conference*. 1994.

36. Pidwerbesky, B.D., Steven, B. D., & Arnold. G. *Subgrade Strain Criterion for Limiting Rutting in Asphalt Pavements*. in *Proceedings, 8th International Conference on Asphalt Pavement*. 1997.

37. Quintus, H.L.V., & Killingsworth, B.,, *Analyses Relating to Pavement Material Characterizations and Their Effects on Pavement Performance*, 1998: Washington, DC.

38. Kenis, W.J., & Wang, W. *Calibrating Mechanistic Flexible Pavement Rutting Models from Full Scale Accelerated Tests*. in *Proceedings, 8th International Conference on Asphalt Pavements*. 1997.

39. May, R.W., & Witczak, M.W. *An Automated Asphalt Concrete Mix Analysis System*. in *Proceedings of the Association of Asphalt Paving Technologists*. 1992.

40. Deacon, J.A., et al. *Analytically based approach to rutting prediction*. 2002. National Research Council.

41. NCHRP, *Mechanistic-Empirical Design of New and Rehabilitated Pavement*, 2004, National Research Council: Washington, D.C.

42. Kaloush, K.E., *Simple Performance Test for Permanent Deformation of Asphalt Mixture*, 2001, Arizona State University: Arizona.

43. Kim, Y.R., *Modeling of Asphalt Concrete*. 2010: McGraw-Hill Construction.

44. Qayoum, M.M., *Investigations for Using the Repeated Load Permanent Deformation Test in a Design Criteria fro Asphalt Mixtures*, 2004, Arizona State University: Arizona.

45. Secor, K.E., & Monismith, C.L. *Analysis of Triaxial Test Data on Asphalt Concrete Using Viscoelastic Principles*. in *Highway Research Board Proceedings*. 1961. Washington, D. C.: Highway Research Board.

46. Liao, Y., *Viscoelastic FE Modeling of Asphalt Pavements and Its Application to U.S. 30 Perpetual Pavement*, in *Russ College of Engineering and Technology* 2007, Ohio University: Ohio.

47. Barnes, H.A., Hutton, J.F, & Walters, K., *An Introduction to Rheology*. 1989, New York, NY: Elsevier.

48. Elseifi, M.A., I.L. Al-Qadi, and P.J. Yoo, *Viscoelastic modeling and field validation of flexible pavements.* Journal of Engineering Mechanics, 2006. **132**(2): p. 172-178.

49. Schapery, R.A., *Correspondence principles and a generalized J integral for large deformation and fracture analysis of viscoleastic media.* International Journal of Fracture, 1984. **25**: p. 195-223.

50. The Asphalt Institute, *Superpave mix design*. 1996.

51. The Asphalt Institute, *Mix Design Methods for Asphalt Concrete and Other Hot-Mix Types*. 1997, Lexington, KY: The Asphalt Institute.

52. ARA Inc, *Guide for Mechanistic-Empirical Design OF NEW AND REHABILITATED PAVEMENT STRUCTURES*, 2001: Illinois.

53. Bonaquist, R.F., Christensen, D.W., & Stump. W., *Simple Performance Tester for Superpave Mix Design: First-Article Development and Evaluation*, 2003: WASHINGTON, D.C.

54. Kim, Y.R., Seo, Y., King, Mark, & Momen, M., *Dynamic modulus testing of asphalt concrete in indirect tension mode.* Journal of the Transportation Research Borad, 2004: p. 163-173.

55. Hondros, G., *Evaluation of Poisson' ratio and the modulus of materilas of a low tensile resistance by the Brazilian (indiret tensile) test with particular references to concrete.* Ausralian Journal of Applied Science, 1959. **10**: p. 243-268.

56. Australian Standard, *Methods of Sampling and Testing Asphalt*, 1995.

57. Di Benedetto, H., and de la Roche, C., *State of the Art of Stiffness Modulus and Fatigue of Bituminous Mixtures*, in *RILEM Report 17, Bituminous Binders and Mixes*1998: London.

58. Australian Standard, *Determination of the resilient Modulus of asphalt - Indirect Tensile Method*, 1995: Australia.

59. Kim, Y.R., Momen, M., & King, M., *Typical Dynamic Moduli for North Carolina Asphalt Concrete Mixes*, 2005, North Carolina Department of Transportation Research and Analysis Group.

60. Bonaquist, R., *Refining the Simple Performance. Tester for Use in Routine Practice*, 2008, TRANSPORTATION RESEARCH BOARD: WASHINGTON, D.C.

61. Ebrahimi, M., Saleh, M., and Gonzalez, M. . *The Interrelationship between Indirect Resilient Modulus and Dynamic Modulus for Dense Graded Hot Mix Asphalt*. in *8th*

International Conference on Road and Airfield Pavement Technology (8th ICPT) 2013. Taipei-Taiwan.

62. Montgomery, C.D., *Design and Analysis of Experiments*. 2005: John Wiley & Sins, Inc.

63. McCarthy, L.M.B., T., *Comparing HMA Dynamic Modulus Measured by Axial Compression and IDT Methods*, 2012, Transportation Research Board of the National Academies.

64. Mirza, M.W., Graul, R. A., Greoger, J. L., and Lopez, A., *Theoretical Evaluation of Poisson's Ratio and Elastic Modulus Using Indirect Tensile Test with Emphasis on Bituminous Mixtures.* Journal of the Transportation Research Board, 2007. **1590**(Volume 1590 / 1997): p. 34-44.

65. Delaporte, B., Di Benedetto, H., Chaverot, P. and Gauthier, G., *Linear viscoelastic properties of bituminous materials including new products made with ultrafine particles.* Road Materials and Pavement Design, 2009. **10**(1): p. 7-38.

66. Di Benedetto, H., Sauzéat, C. and Sohm, J., *Stiffness of bituminous mixtures using ultrasonic waves propagation.* Road Materials and Pavement Design, 2009. **10**(4): p. 789-814.

67. Olard, F.a.D.B., H., *General "2S2P1D" model and relation between the linear viscoelastic behaviors of bituminous binders and mixes.* Road Materials and Pavements Design, 2003. **4**(2): p. 185-244.

68. Pouget, S., Sauzéat, C., Di Benedetto, H. and Olard, F., *From the behaviour of constituent materials to the calculation and design of orthotropic steel bridge structures.* Road Materials and Pavement Design, 2010. **11**: p. 111-144.

69. Chehab, G.R., & Kim, Y.R., *Interrelationships among Asphalt Conceret Stiffnesses*, in *Modeling of Asphalt Concrete*, Y.R. Kim, Editor. 2010, McGraw-Hill Construction. p. 139-159.

70. Sohm, J., Gabet, T., Hornych, P., Piau, J. M. and Di Benedetto, H, *Creep tests on bituminous mixtures and modelling.* Road Materials and Pavement Design, 2012. **13**(4): p. 832-849.

71. Nilsson, B.R., Chehab, G.R. and Kim, R, *Application of a viscoelastoplastic continuum damage tensile model to asphalt mixes in Sweden.* Road Materials and Pavement Design, 2004. **5**: p. 133-161.

72. Kim, J., Roque, R., and, Birgisson, B., *Obtaining Creep Compliance Parameters Accurately from Static or Cyclic Creep Tests.* Journal of ASTM International, 2005. **2**(8).

73. Ebrahimi, M., Saleh, M., & Gonzalez, M, *Investigating the Applicability of Complex Modulus and Creep Compliance Interconversion in Asphalt Concrete.* Advances in Civil Engineering Materials, 2014. **3**(1): p. 106-121.

74. Leaderman, H., *Viscoelasticity phenomena in amorphous high polymeric systems.* Rheology, 1958. **2**: p. 1-6.

75. Denby, E.F., *A note on the interconversion of creep, relaxation and recovery.* Rheologica Acta, 1975: p. 591-593.

76. Cheristensen, R.M., *Theory of viscoelasticity*, ed. 2nd. 1982, New York.

77. Schapery, R.A., *A Simple Collocation Method for Fitting Viscoelastic Models to Experimental Data*, 1961: Pasadena, California.

78. Tschoegl, N.W., *The Phenomenological Theory of Linear Viscoelastic Behavior*. 1989, Berlin: Springer-Verlag.

79. Park, S.W., Kim, Y. R., and Schapery, R. A. , *A Viscoelastic Continuum Damage Model and Its Application to Uniaxial Behavior of Asphalt Concrete.* Mechanics of Materials, 1996. **24**(4): p. 241-255.

80. Haddad, Y.M., *Viscoelasticity of Engineering Materials*. 1995, Great Britian: Chapman & Hall.

81. Cost, T.L., and Becker, E. B, *A Multi-Data Method of Approximate Laplace Transform Inversion.* International Journal for Numerical Methods in Engineering, 1970. **2**(2): p. 207-219.

82. Park, W.S., and, Schapery, R. A. , *Methods of interconversion between linear viscoelastic material functions. Part I-a numerical method based on Prony series.* International Journal of Solids and Structures, 1998. **36**: p. 1653-1675.

83. Schapery, R.A., and Park, W. S. , *Methods of interconversion between linear viscoelastic material functions. Part II-an approximate analytical method.* International Journal of Solids and Structures, 1998. **36**: p. 1677-1699.

84. Silva, H.N., Sousa, P. C., Holanda, A. S., and Soares, J. B, *a computer program for linear viscoelastic characterization using prony series*, 2008, Federal University of Alagoas.

85. Sousa, P.C., Silva, H. N., and S, J. B, *Prony series study for viscoelastic characterization of asphalt mixtures*, 2008, Instituto Brasileiro de Petróleo, Gás e Biocombustíveis – IBP.

86. Feng, W.W., and Hallquist, J. O. , *on the Prony relaxation function*, in *11thInternational LS_DYNA Users Conference*2011: Michigan.

87. Park, S.W., and Kim, Y. R., and Schapery, R. A., *Fitting Prony-series viscoelastic models with Power-law presmoothing.* Journal of Materials in Civil Engineering, 2001. **13**: p. 26-32.

88. Williams, M.L., *Fundamental studies relating to system analysis of solid propellants*, in *SM 61-5*1961: California Institute of Technology, Pasadena, California. p. 1-293.

89. Mun, S., Chehab, G., and Kim, Y. R., *Determination of Time-Domain Viscoelastic Functions Using Optimized Interconversion Techniques.* Road Materials and Pavement Designs 2007. **8**: p. 351-365.

90. Lawson, C.L.a.R.J.H., *Solving Least Squares Problems*. 1974, United States of America: Prentice-Hall.

91. Flintsch, G.W., and Katicha, S. W., *Hot-Mix Asphalt Linear Viscoelastic Response.* Road Materials and Pavement Design, 2010. **11**(2): p. 489-498.

92. Findely, W.N., Lai, J. S. and K. Onaran, *Creep and Relaxation of Nonlinear Viscoelastic Materials*. 1989, New York.

93. Hansen, P.C., Davies, A. R., and de Hoog, F. R., *On the Volterra Integral Equation Relating Creep and Relaxation* IOPScience, 2008. **24**(3): p. 1-13.

94. Sorvari, J., and Malinen, M., *On the Direct Estimation of Creep and Relaxation Functions.* Mechanics of Time-Dependent Materials, 2007. **11**: p. 143-157.

95. Linz, P., *Analytical and Numeriocal Methods for Volterra Equations*. 1985, Philadelphia: SIAM.

96. Hansen, P.C., *REGULARIZATION TOOLS: A Matlab package for analysis and solution of discrete ill-posed problems.* Numerical Algorithms, 1994. **6**(1): p. 1-35.

97. Honerkamp, J.a.W., J., *Tikhonov Regularization Method for Ill-Posed Problems.* Continuum Mechanics and Thermodynamics, 1990. **2**(1): p. 17-30.

98. Sorvari, J., and Malinen, M., *Numerical interconversion between linear viscoelastic material functions with regularization.* International Journal of Solids and Structures, 2007. **44**(3-4): p. 1291-1303.

99. Hansen, P.C., *Rank-Deficient and Discrete Ill-Posed Problems: Numerical Aspects of Linear Inversion*. 1998, Philadelphia: Society for Industrial and Applied Mathematics.

100. Hansen, P.C., *The L-Curve and its use in the numerical treatment of inverse problems*, in *Computational Inverse Problems in Electrocardiography*, P.R. Johnston, Editor. 2001, WIT Press.

101. Hansen, P.C.a.O.L., D.P, *The Use of the L-Curve in the Regularization of Discrete Ill-Posed Problems.* SIAM Journal on Scientific Computing, 1993. **14**(6): p. 1487-1503.

102. Kim, Y.R., and Park, S. W. , *Interconversion between relaxation modulus and creep compliance for viscoelastic solids.* Journal of Material in Civil Engineering, 1999. **11**: p. 76-82.

103. ARA, I., *Guide for Mechanistic- Empirical Design of New and Rehabilitated Pavement Structures*, H.R. Program, Editor 2004.

104. Jahromi, S.G., and Khodaii A. , *Master Curve for Stiffness Asphalt Concrete.* International Journal of Pavement Research and Technology, 2009.

105. Leaderman, H., *Viscoelasticity Phenomena in Amorphous High Polymeric Systems,*. Vol. Vol. II. 1958, New York.

106. Christensen, R.M., *Theory of Viscoelasticity*. 1982: New York.

107. Ebrahimi, M., Saleh, M., and Gonzalez, M, *Interconversion between Viscoelastic Functions using Tikhonov Regularization Method and its Comparison with Approximate Techniques.* Road Materials and Pavement Design, 2014. **15**(4).

108. Biligiri, K.P., Kaloush, K. E., Mamlouk, M. S., and Witczak, M. W., *Rational Modeling of Tertiary Flow for Asphalt Mixtures.* Transportation Research Record: Journal of the Transportation Research Board, 2007: p. 63-72.

109. Australian Standard, *Methods of Sampling and Testing Asphalt* 1995: Australia.

110. Inc., M., *Minitab 17 Statistical Software*, 2010, State College, PA: Minitab, Inc. .

111. ABAQUS, I., *ABAQUS Version 6.11*, 2011, Dassault Systèmes: Providence, RI, USA.

112. Kandhal, P.S., and Cooley, L. A., *Accelerated Laboratory Rutting tests: Evaluation of the Asphalt Pavement Analyzer*, 2003: Washington D.C.

113. Ahmad, J., Abdul Rahman, M,Y., and Hainin, M., R., *Rutting Evaluation of Dense Graded Hot Mix Asphalt Mixture.* International Journal of Engineering & Technology 2011. **11**(05).

114. lu, Q., and Harvey, J.T., *Evaluation of Hamburg Wheel-Tracking Device Test with Laboratory and Field Performance Data.* Transportation Research Record: Journal of the Transportation Research Board, 2006.

115. Australian Standard, *Commentary to AG:PT/T220 - Sample Preparation - Compaction of Asphalt Slabs Suitablel for Characterisation*, 2005, Standards Australia: Sydney.

116. Shami, H., I., Lai, J,S., D'angelo J,A, and Harman, T.P., *Development of Temperature-Effect Model for Predicting Rutting of Asphalt Mixtures Using Georgia Loaded Wheel Tester.* TRANSPORTATION RESEARCH RECORD, 1997.

117. Yildirim, Y., Jayawickrama, P., Hossain, M., Alhabshi, A., Yildirim, C., Smit, A., and Little, D., *Hamburg Wheel-Tracking Database Analysis*, 2007, Texas Department of Transportation.

118. ABAQUS, *Abaqus 6.11 Getting Started with ABAQUS: Interactive Edition*. 2011.

119. ABAQUS, *Abaqus 6.11, ABAQUS/CAE User's Manual*. 2011.

120. Roberts, F.L., Mohammad, L.N., Oin, H. and Huang, B., *Comparative Performance of Rubber Modified Hot Mix Asphalt under AFL Loading*, 2003.

121. ABAQUS, *ABAQUS Documentation*. 2011, Providence, RI, USA: Hibbitt, Karlsson & Sorensen, Incorporated.

122. Hua, J., *Finite Element Modeling and Analysis of Accelerated Pavement Testing Devices and Rutting Phenomenon*, 2000, Purdue University: Purdue University.

123. White, T.D., Haddock, J. f., Hand, A. J. T., and Fang, H., *Contributions of Pavement Structural Layers to Rutting of Hot Mix Asphalt Pavements*, 2002, National Cooperative Highway Research Program: Washington, D.C.

124. Kraus, H., *Creep Analysis*. 1980: A Wiley-Interscience Publication.

125. Huang, H.M., *Analysis of Accelerated Pavement Tests and Finite Element Modeling of Rutting Phenomenon*, 1995, Purdue University: Purdue University.

126. Pan, C.L., *Analysis of Bituminous Mixtures Stripping/Rutting Potential*, 1997, Purdue University: Purdue University.

127. Uzarowski, L., *The Development of Asphalt Mix Creep Parameters and Finite Element Modeling of Asphalt Rutting*, in *Civil Engineering*2006, University of Waterloo: Waterloo, Ontario, Canada.

128. Findely, W.N., Lai, J. S. and K. Onaran, *Creep and Relaxation of Nonlinear Viscoelastic Materials*. 1976, New York: Dover Publications, Inc.

129. Juan, K.J.-y., Y., *Application of Linear Viscoelastic Differential Constitutive Equation in ABAQUS*, in *International Conferencve on Computer Design and Application (ICCDA 2010)*2010.

Appendix A: Mix Design and Material Properties

A.1 Mix AC 14

Table C.1.1 Aggregate properties

Aggregate	SC 14	SC 10	Concrete Sand	BARMAC AP5cr100	HP APcr100
Sieve Size (mm)	% Passing				
13.2	100	100	100	100	100
9.5	12	99	100	100	100
6.7	0	31	100	100	100
4.75	0	0	99	98	99
2.36	0	0	77	59	67
1.18	0	0	64	40	45
0.600	0	0	56	29	32
0.300	0	0	34	21	23
0.150	0	0	7	14	16
0.075	0	0	1	9	10
Bulk SG	2.63	2.62	2.64	2.63	2.61
Bulk SG SSD	2.65	2.65	2.66	2.65	2.64
Apparent SG	2.69	2.69	2.69	2.69	2.69
Absorption (%)	0.8	0.9	0.7	0.8	1.0
Blend Ratio	15	15	15	33	22

Table A.1.2 Mix blend properties

Sieve Size (mm)	Percentage Passing	
	Blend Result	AC 14 Specification
16.0	100	100
13.2	100	-
9.5	87	79 - 95
6.7	75	69 - 84
4.75	69	58 - 75
2.36	46	43 - 61
1.18	33	32 - 48
0.600	25	21 - 36
0.300	17	15 - 26
0.150	9	10 - 17
0.075	5	5 - 11
Bulk SG	2.63	
Bulk SG SSD	2.65	
Apparent SG	2.69	
Absorption (%)	0.8	

Table A.1.3 Asphalt concrete mix results

Sample ID	I	II	III	IV	V
Total Binder Content (%)	4.5	5.0	5.5	6.0	6.5
Maximum SG	2.469	2.447	2.433	2.412	2.395
Bulk SG	2.297	2.322	2.342	2.381	2.375
Air Voids (%)	7.0	5.1	3.7	1.3	0.8
VMA (%)	16.5	16.0	15.7	14.8	15.4
VFB (%)	57.7	68.0	76.2	91.3	94.6
Film Index (%)	6.9	7.8	8.6	9.6	10.4
Effective Binder (%)	4.3	4.82	5.26	5.83	6.33
Stability (KN)	15.3	14.85	15.65	16.60	16.15
Flow (mm)	2.75	2.75	2.75	3.0	3.0

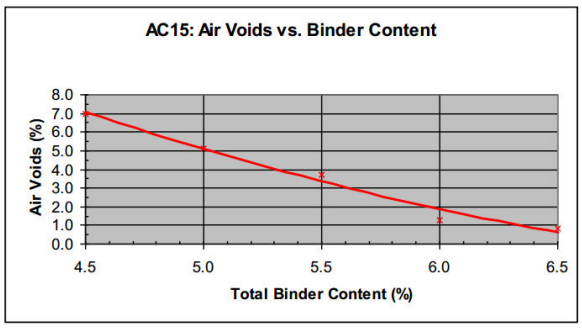

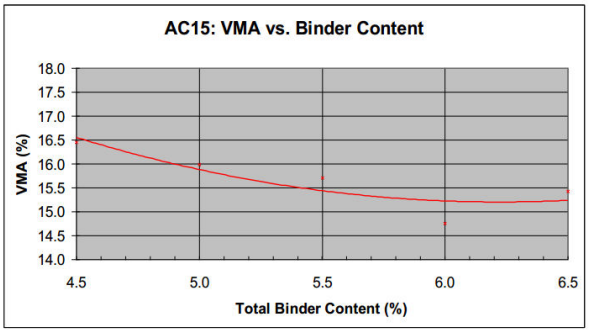

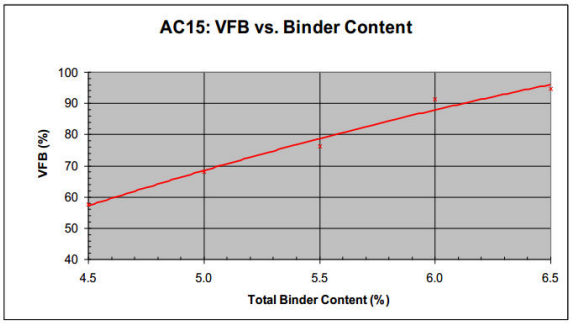

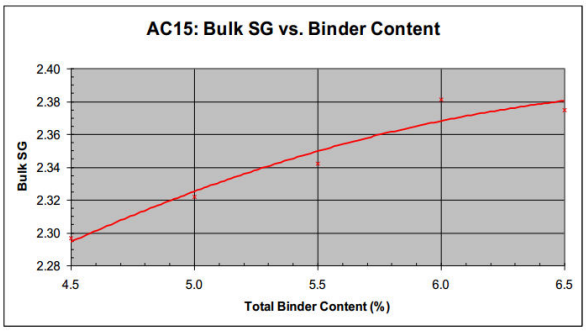

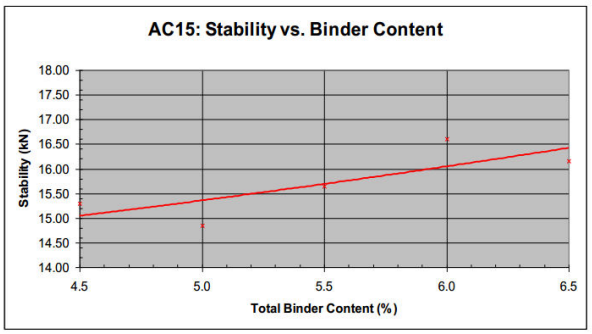

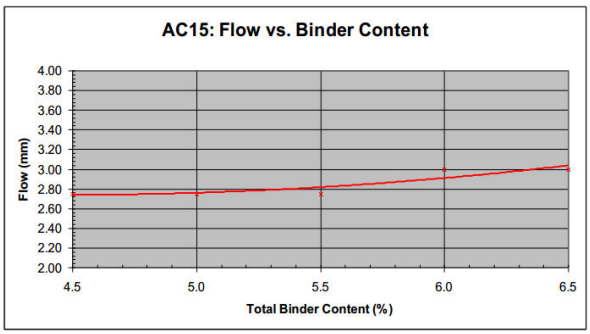

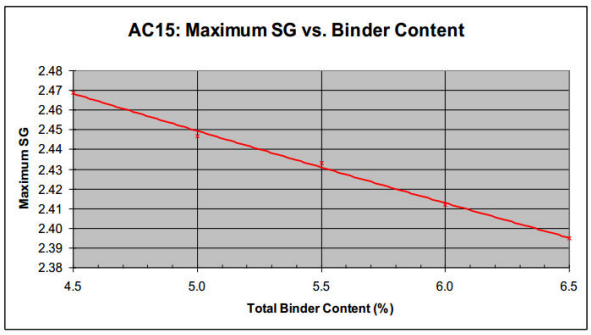

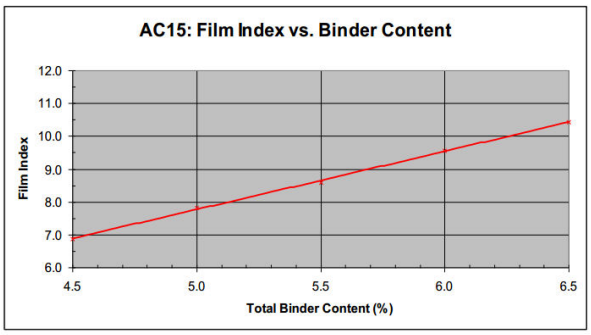

Figure A.1.1 Asphalt concrete mix result

Table A.1.4 Mix specification

	Results	AC 14 Specification
Total Binder Content (%)	5.5	-
Air Voids (%)	3.7	3.0 - 4.0
VMA (%)	15.7	14 minimum
VFB (%)	76.2	-
Film Index (%)	9.6	-
Stability (KN)	15.65	6.65 minimum
Flow (mm)	2.75	2.0 - 4.5

A.2 Mix AC 20

Table A.2.1 Aggregate properties

Aggregate	SC 19	SC 14	SC 10	Concrete Sand	BARMAC AP5cr100	HP APcr100
Sieve Size (mm)	% Passing					
19.0	100	100	100	100	100	100
13.2	37	100	100	100	100	100
9.5	1	12	99	100	100	100
6.7	0	0	31	100	100	100
4.75	0	0	0	99	98	99
2.36	0	0	0	77	59	67
1.18	0	0	0	64	40	45
0.600	0	0	0	56	29	32
0.300	0	0	0	34	21	23
0.150	0	0	0	7	14	16
0.075	0	0	0	1	9	10
Bulk SG	2.65	2.63	2.62	2.64	2.63	2.61
Bulk SG SSD	2.67	2.65	2.65	2.66	2.65	2.64
Apparent SG	2.7	2.69	2.69	2.69	2.69	2.69
Absorption (%)	0.6	0.8	0.9	0.7	0.8	1.0
Blend Ratio	15	8	10	15	30	22

Table A.2.2 Mix blend properties

Sieve Size (mm)	Percentage Passing	
	Blend Result	AC 14 Specification
19.0	100	100
13.2	91	83 - 95
9.5	78	70 - 90
6.7	70	60 - 79
4.75	66	52 - 70
2.36	44	40 - 55
1.18	32	29 - 43
0.600	24	20 - 32
0.300	17	13 - 23
0.150	9	8 - 16
0.075	5	4 - 10
Bulk SG	2.61	
Bulk SG SSD	2.63	
Apparent SG	2.67	
Absorption (%)	0.8	

Table A.2.3 Asphalt concrete mix results

Sample ID	I	II	III	IV	V
Total Binder Content (%)	4.0	5.0	5.5	6.0	6.5
Maximum SG	2.481	2.453	2.436	2.422	2.397
Bulk SG	2.288	2.310	2.352	2.365	2.382
Air Voids (%)	7.8	5.8	3.4	2.4	0.6
VMA (%)	15.8	15.5	14.4	14.4	14.2
VFB (%)	50.9	62.3	76.0	83.6	95.6
Film Index (%)	6.9	7.2	8.1	8.8	10.0
Effective Binder (%)	3.63	4.30	4.79	5.24	5.88
Stability (KN)	13.10	12.45	15.45	14.90	14.65
Flow (mm)	2.50	2.75	2.75	2.75	3.0

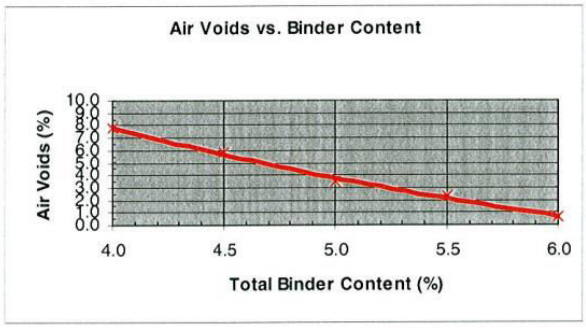

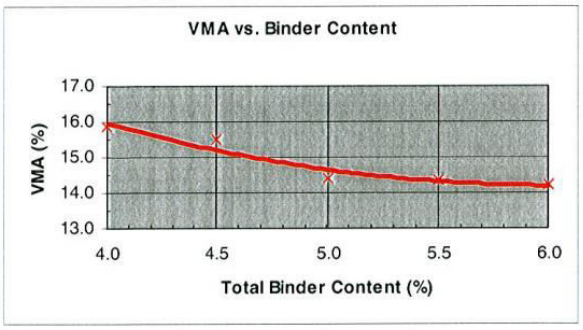

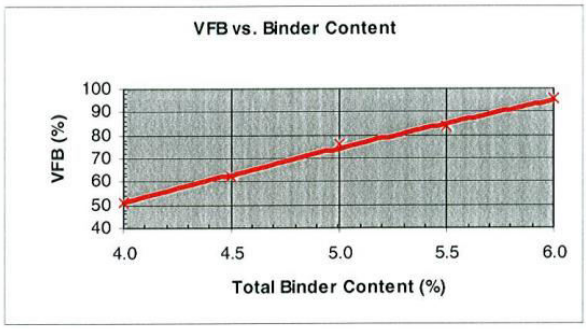

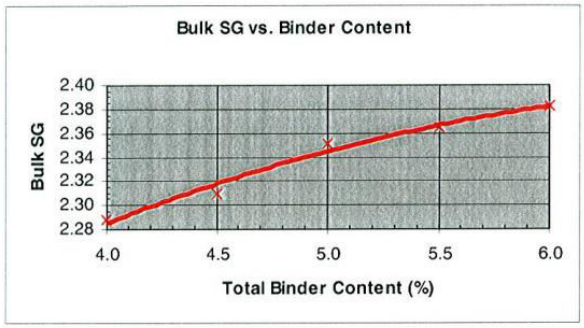

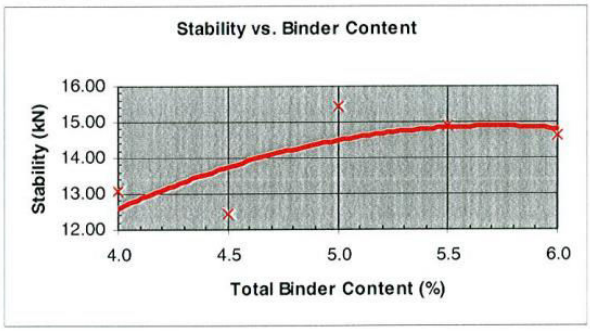

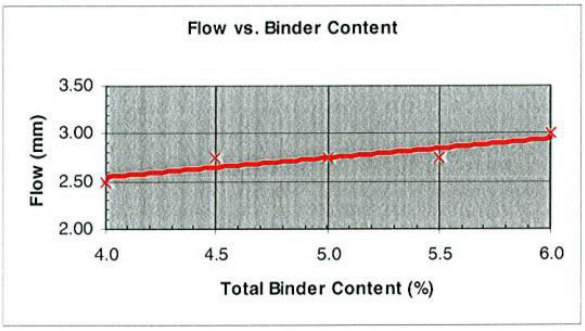

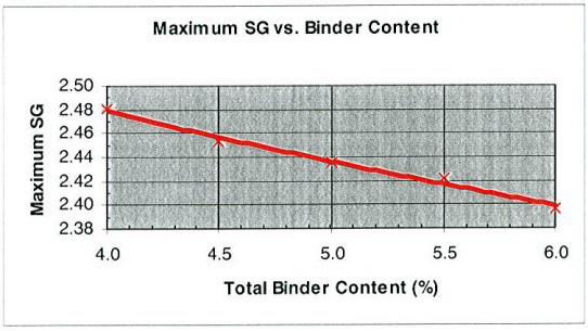

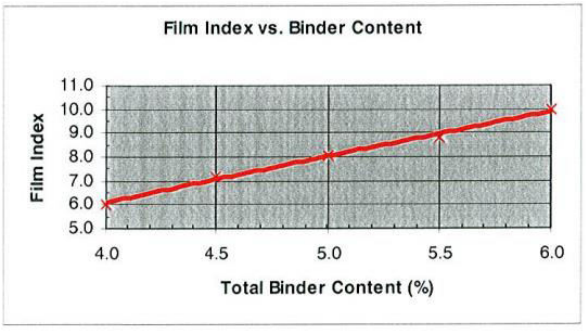

Figure A.2.1 Asphalt concrete mix result

Table A.2.4 Mix specification

	Results	AC 14 Specification
Total Binder Content (%)	5.0	-
Air Voids (%)	3.4	3.0 - 4.0
VMA (%)	14.4	13 minimum
VFB (%)	76.0	-
Film Index (%)	8.1	4.0 – 6.0
Stability (KN)	15.45	6.65 minimum
Flow (mm)	2.75	2.0 - 4.5

Appendix B: Data accuracy check for complex modulus test

B.1 Mix; AC 20 – Binder 60/70 – VTM = 4.0%

Table B.1 Shift factor

Temp (°C)	log (at)
-25	7.399713
-20	6.447609
-15	5.532387
-10	4.651945
-5	3.804336
0	2.987758
4.4	2.293507
15	0.708057
21.1	-0.152543
30	-1.346043
37.8	-2.335856
40	-2.606119
46.1	-3.336002
54.4	-4.285461

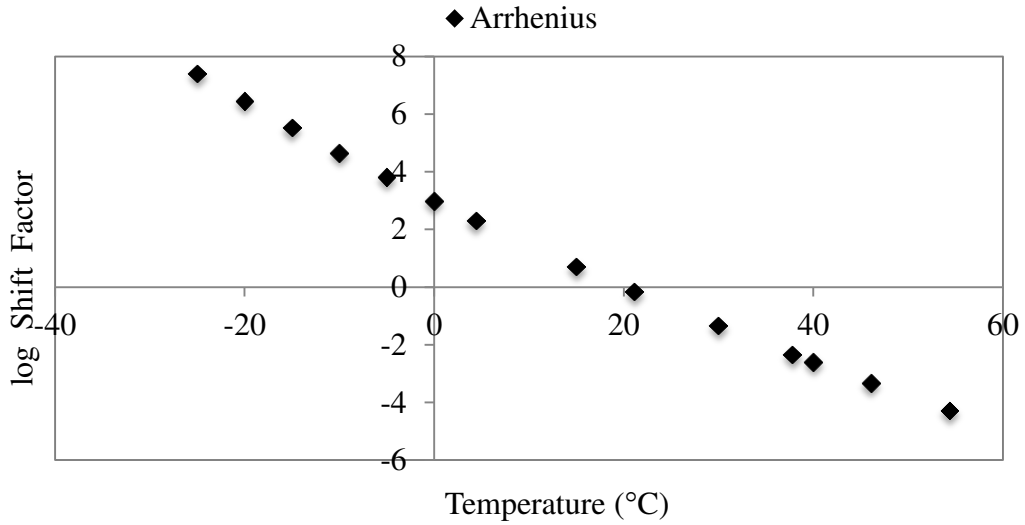

Figure B.1 Shift factors as a function of temperature

Table B.2 Master curve parameters

Fitting Parameters	
δ	3.85873
ß	-1.196
γ	-0.5955
ΔEa	229040

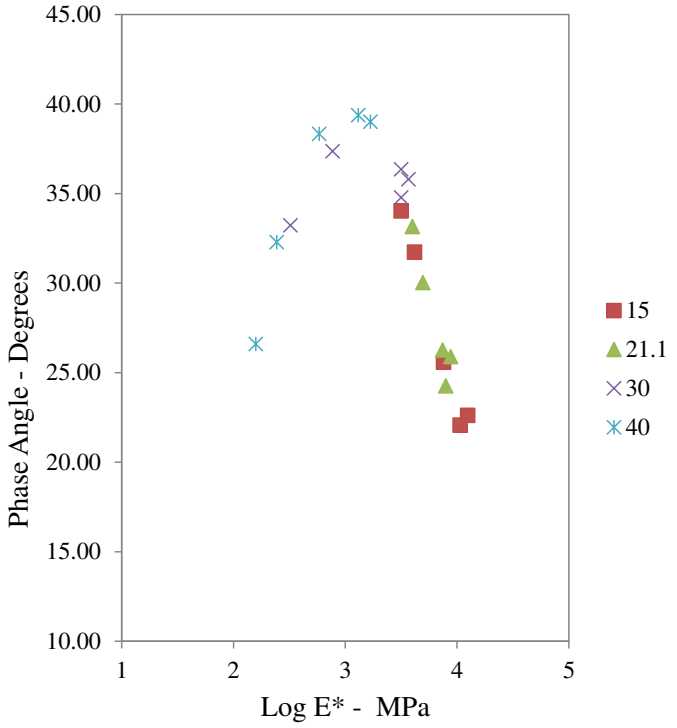

Figure B.2 Black space

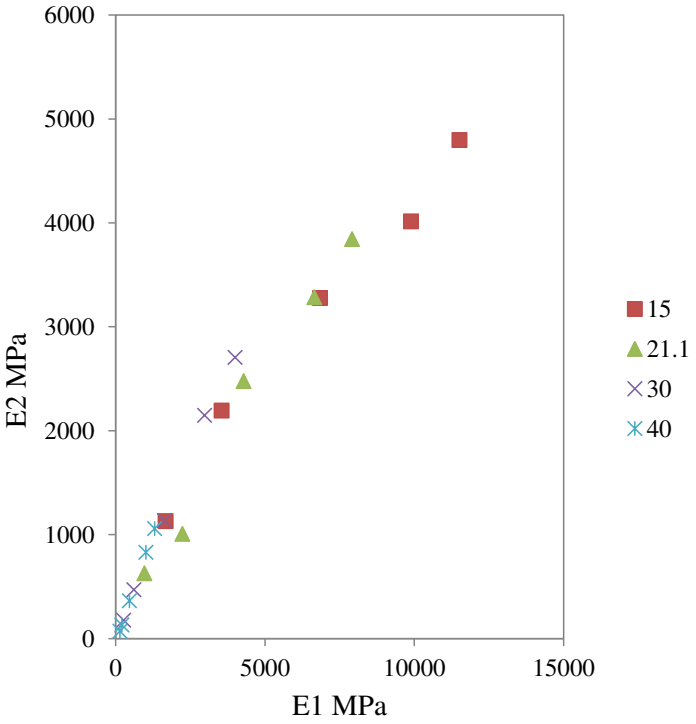

Figure B.3 Complex plane

B.2 Mix; AC 20 – Binder 60/70 – VTM = 5.0%

Table B.3 Shift factor

Temp (°C)	log (at)
-25	7.27170
-20	6.33607
-15	5.43668
-10	4.57147
-5	3.73852
0	2.93607
4.4	2.25383
15	0.69581
21.1	-0.14990
30	-1.32276
37.8	-2.29545
40	-2.56103
46.1	-3.27829
54.4	-4.21132

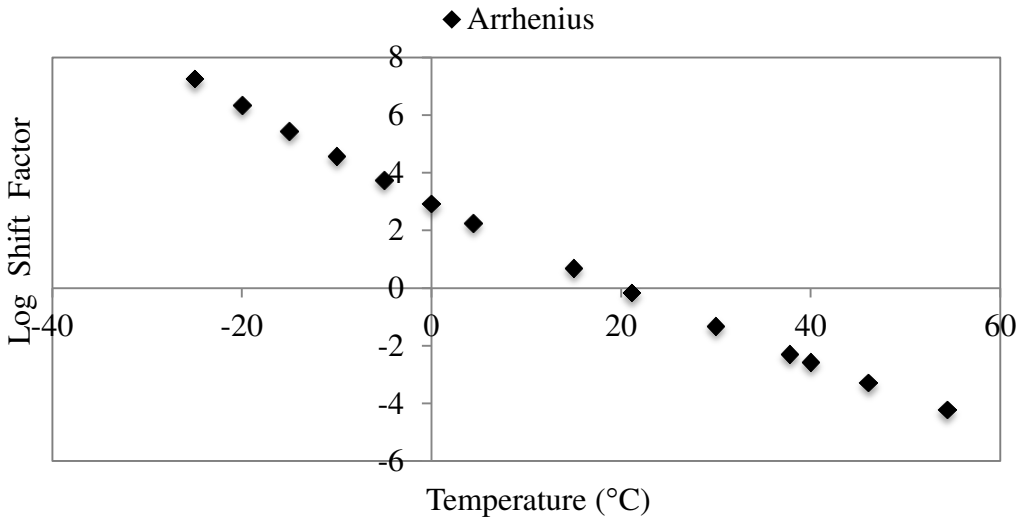

Figure B.4 Shift factors as a function of temperature

Table B.4 Master curve parameters

Fitting Parameters	
δ	4.22432
ß	-0.91623
γ	-0.67376
ΔEa	225077.1

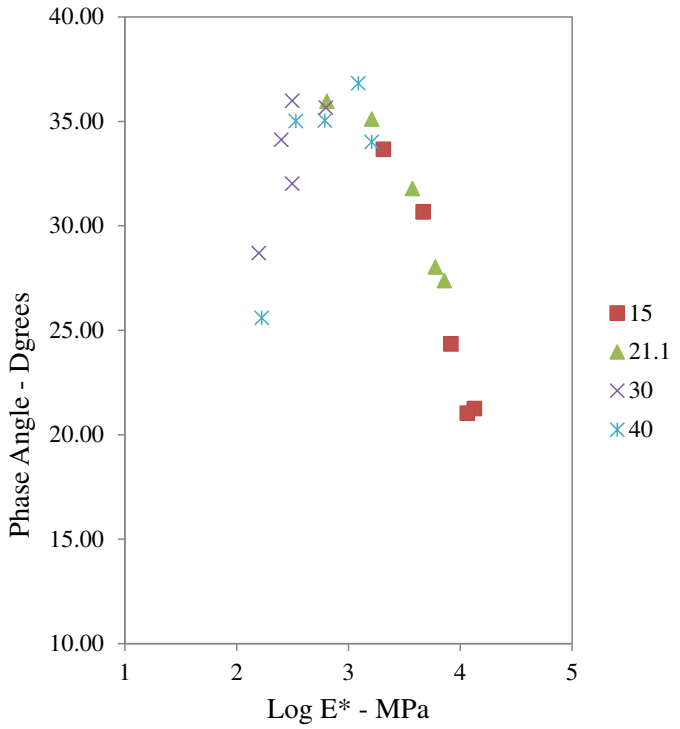

Figure B.5 Black space

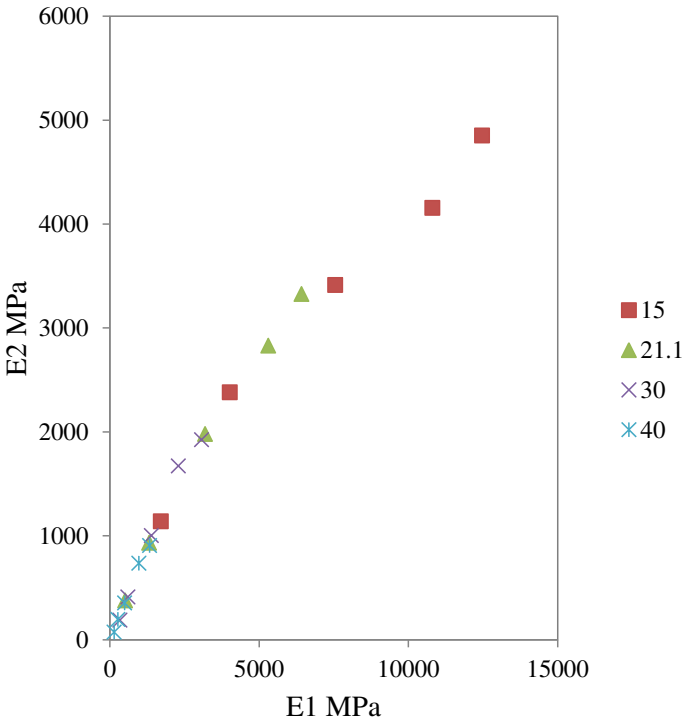

Figure B.6 Complex plane

B.3 Mix; AC 20 – Binder 80/100 – VTM = 4.0%

Table B.5 Shift factor

Temp (°C)	log (at)
-25	7.85473
-20	6.84408
-15	5.87258
-10	4.93800
-5	4.03827
0	3.17148
4.4	2.43454
15	0.75160
21.1	-0.16192
30	-1.42881
37.8	-2.47949
40	-2.76637
46.1	-3.54114
54.4	-4.54898

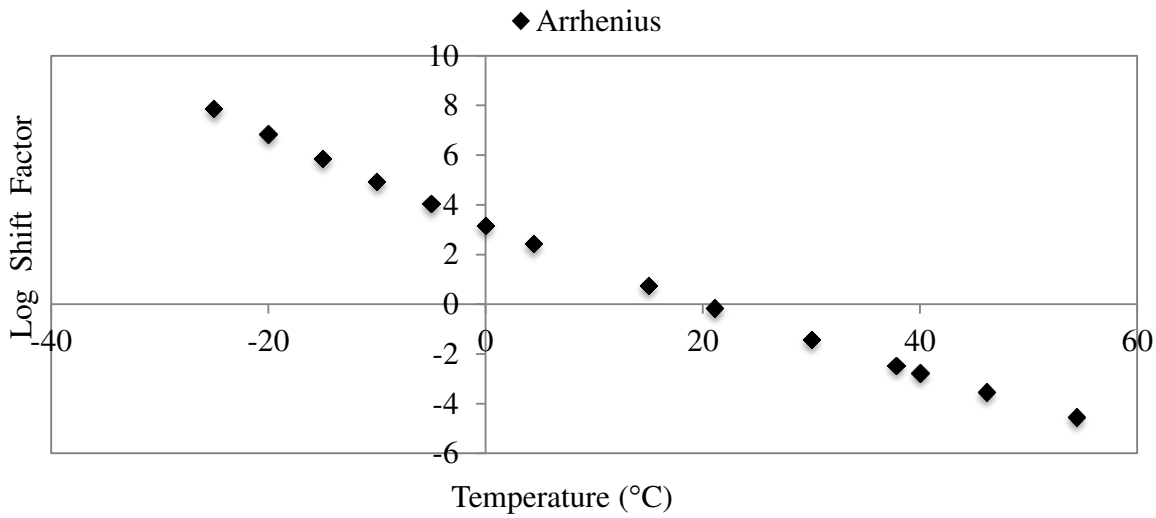

Figure B.7 Shift factors as a function of temperature

Table B.6 Master curve parameters

Fitting Parameters	
δ	4.103597996
ß	-0.75559943
γ	-0.59561111
ΔEa	243123.3841

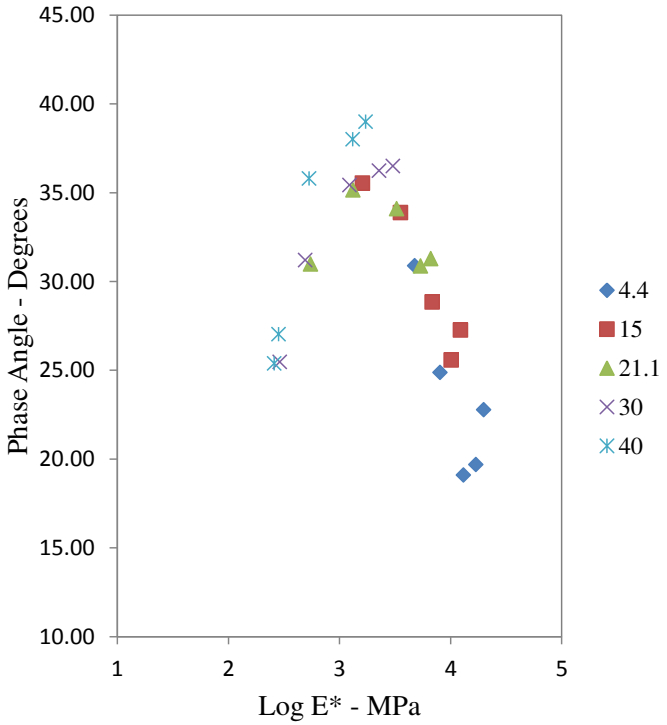

Figure B.8 Black space

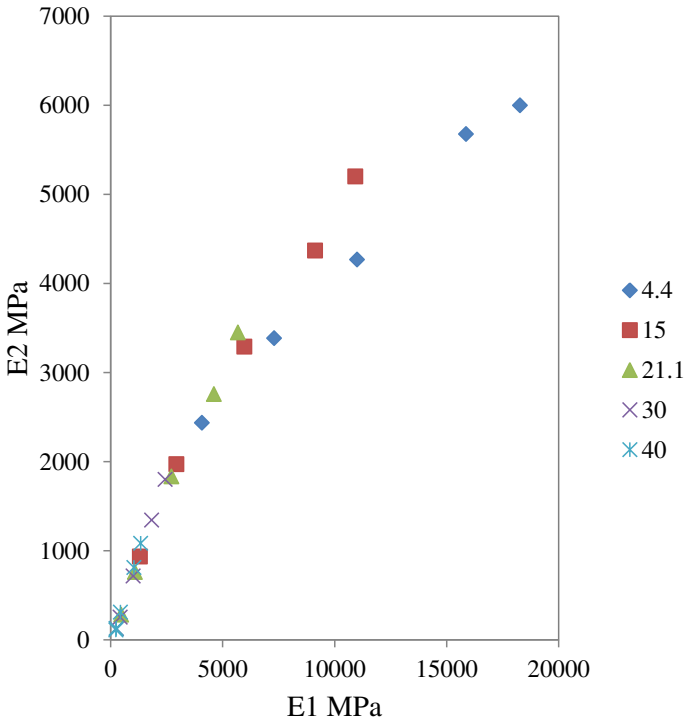

Figure B.9 Complex plane

B.4 Mix; AC 20 – Binder 80/100 – VTM = 5.0%

Table B.7 Shift factor

Temp (°C)	log (at)
-25	7.10859
-20	6.19395
-15	5.31473
-10	4.46893
-5	3.65467
0	2.87021
4.4	2.20328
15	0.68020
21.1	-0.14654
30	-1.29309
37.8	-2.24396
40	-2.50359
46.1	-3.20476
54.4	-4.11686

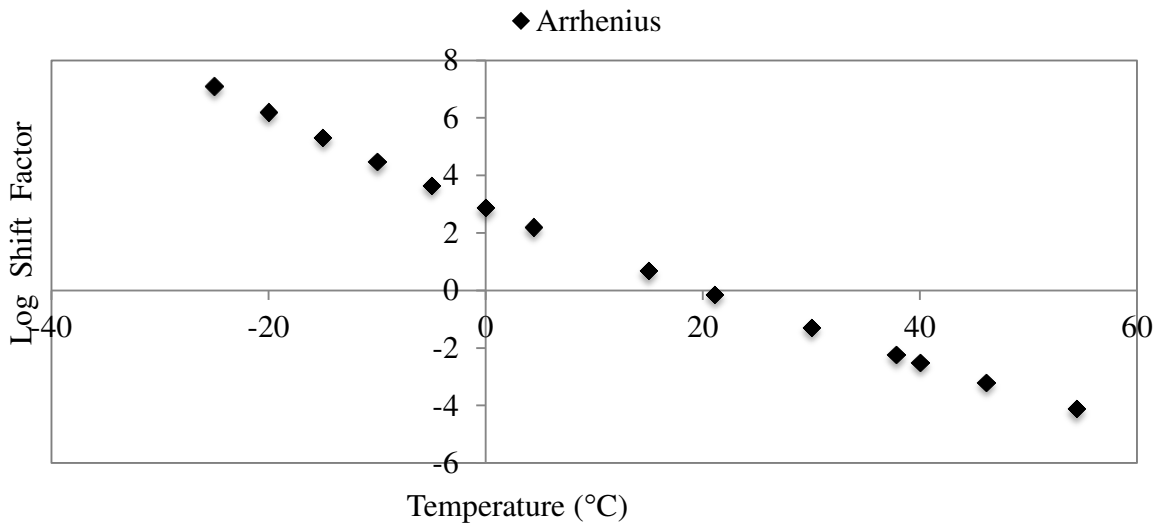

Figure B.10 Shift factors as a function of temperature

Table B.8 Master curve parameters

Fitting Parameters	
δ	3.618318314
ß	-0.92442935
γ	-0.60100463
ΔEa	220028.6316

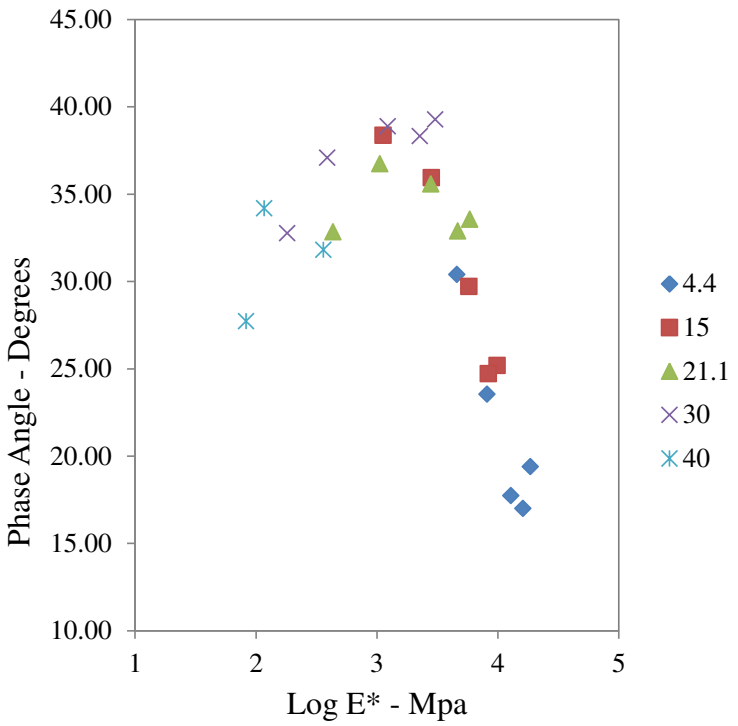

Figure B.11 Black space

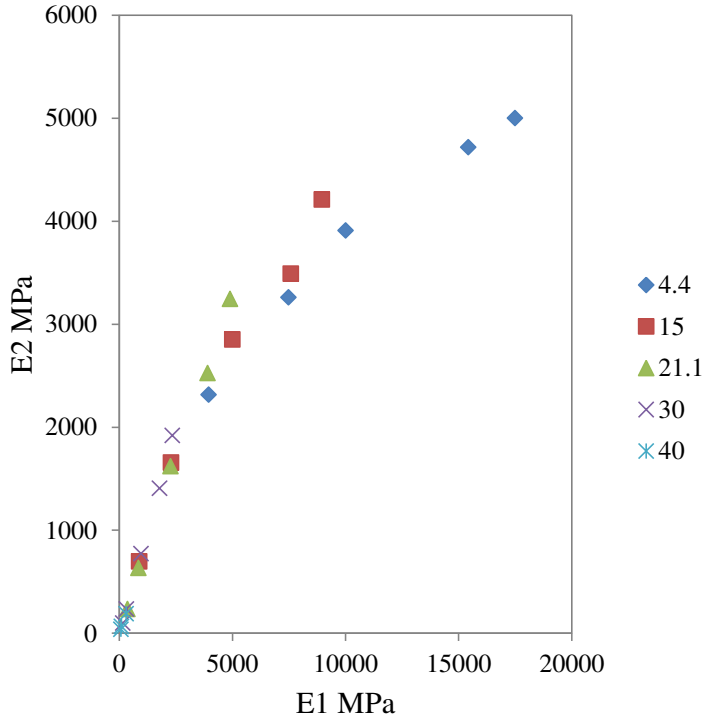

Figure B.12 Complex plane

Appendix C: Statistical Analysis

1. Australian Method

C.1 Mix; AC 20 – Binder 80/100 – VTM = 4.0%

Table C.1.1 Reduced Frequency, 0.0004Hz

Reduced Freq. 0.0004 Hz	*Variable 1*	*Variable 2*
Mean	249.3921845	291.9564622
Variance	7502.36378	8140.35641
Observations	2	3
Hypothesized Mean Difference	0	
df	2	
t Stat	-0.52938703	
P(T<=t) one-tail	0.324712071	
t Critical one-tail	2.91998558	
P(T<=t) two-tail	0.649424143	
t Critical two-tail	4.30265273	

Table C.1.2 Reduced Frequency, 0.4Hz

Reduced Freq. 0.4 Hz	*Variable 1*	*Variable 2*
Mean	3031.931481	3316.834188
Variance	24634.62866	779296.3482
Observations	2	3
Hypothesized Mean Difference	0	
df	2	
t Stat	-0.546192913	
P(T<=t) one-tail	0.319859989	
t Critical one-tail	2.91998558	
P(T<=t) two-tail	0.639719978	
t Critical two-tail	4.30265273	

Table C.1.3 Reduced Frequency, 10Hz

Reduced Freq. 10 Hz	*Variable 1*	*Variable 2*
Mean	8043.944694	9533.752971
Variance	158746.3845	2145673.447
Observations	2	3
Hypothesized Mean Difference	0	
df	2	
t Stat	-1.671308947	
P(T<=t) one-tail	0.118310131	
t Critical one-tail	2.91998558	
P(T<=t) two-tail	0.236620262	
t Critical two-tail	4.30265273	

Table C.1.4 Reduced Frequency, 100Hz

Reduced Freq. 100 Hz	*Variable 1*	*Variable 2*
Mean	12583.89866	14127.99848
Variance	1217922.477	751643.6561
Observations	2	2
Hypothesized Mean Difference	0	
df	2	
t Stat	-1.55598385	
P(T<=t) one-tail	0.129992421	
t Critical one-tail	2.91998558	
P(T<=t) two-tail	0.259984841	
t Critical two-tail	4.30265273	

C.2 Mix; AC 20 – Binder 80/100 – VTM = 5.0%

Table C.2.1 Reduced Frequency, 0.0005Hz

Reduced Freq. 0.0005Hz	*Variable 1*	*Variable 2*
Mean	143.112416	230.8063597
Variance	57.38352128	1914.315759
Observations	2	2
Hypothesized Mean Difference	0	
df	1	
t Stat	-2.792957066	
P(T<=t) one-tail	0.10944208	
t Critical one-tail	6.313751515	
P(T<=t) two-tail	0.218884159	
t Critical two-tail	12.70620474	

Table C.2.2 Reduced Frequency, 0.05Hz

Reduced Freq. 0.05Hz	*Variable 1*	*Variable 2*
Mean	1161.605537	1250.230974
Variance	4147.810414	271.2011093
Observations	2	2
Hypothesized Mean Difference	0	
df	1	
t Stat	-1.885431775	
P(T<=t) one-tail	0.15522609	
t Critical one-tail	6.313751515	
P(T<=t) two-tail	0.310452179	
t Critical two-tail	12.70620474	

Table C.2.3 Reduced Frequency, 1Hz

Reduced Freq. 1Hz	*Variable 1*	*Variable 2*
Mean	3499.506839	4392.681448
Variance	28792.96527	194697.7323
Observations	2	2
Hypothesized Mean Difference	0	
df	1	
t Stat	-2.671908865	
P(T<=t) one-tail	0.113994882	
t Critical one-tail	6.313751515	
P(T<=t) two-tail	0.227989764	
t Critical two-tail	12.70620474	

Table C.2.4 Reduced Frequency, 100Hz

Reduced Freq. 100Hz	*Variable 1*	*Variable 2*
Mean	11843.5079	13377.07404
Variance	95095.0164	1222908.952
Observations	2	2
Hypothesized Mean Difference	0	
df	1	
t Stat	-1.889118271	
P(T<=t) one-tail	0.154968856	
t Critical one-tail	6.313751515	
P(T<=t) two-tail	0.309937713	
t Critical two-tail	12.70620474	

2. AAHTO Method

C.3 Mix; AC 20 – Binder 60/70 – VTM = 4.0%

Table C.3.1 Reduced Frequency, 0.0002Hz

Reduced Freq. 0.0002Hz	*Variable 1*	*Variable 2*
Mean	469.1943288	216.2237097
Variance	19581.70625	7558.144959
Observations	2	2
Hypothesized Mean Difference	0	
df	2	
t Stat	2.171607587	
P(T<=t) one-tail	0.081013619	
t Critical one-tail	2.91998558	
P(T<=t) two-tail	0.162027238	
t Critical two-tail	4.30265273	

Table C.3.2 Reduced Frequency, 0.2Hz

Reduced Freq. 0.2Hz	*Variable 1*	*Variable 2*
Mean	1416.288277	1526.958876
Variance	20048.26172	4070.340605
Observations	2	2
Hypothesized Mean Difference	0	
df	1	
t Stat	-1.007792655	
P(T<=t) one-tail	0.24876458	
t Critical one-tail	6.313751515	
P(T<=t) two-tail	0.49752916	
t Critical two-tail	12.70620474	

Table C.3.3 Reduced Frequency, 10Hz

Reduced Freq. 10Hz	*Variable 1*	*Variable 2*
Mean	4237.742509	6668.340179
Variance	37560.30024	46991.02284
Observations	2	2
Hypothesized Mean Difference	0	
df	2	
t Stat	-11.82137164	
P(T<=t) one-tail	0.003539997	
t Critical one-tail	2.91998558	
P(T<=t) two-tail	0.007079994	
t Critical two-tail	4.30265273	

C.4 Mix; AC 20 – Binder 60/70 – VTM = 5.0%

Table C.4.1 Reduced Frequency, 0.001Hz

Reduced Freq. 0.001Hz	*Variable 1*	*Variable 2*
Mean	311.3675	248.0926
Variance	1192.204	9.96876
Observations	2	2
Hypothesized Mean Difference	0	
df	1	
t Stat	2.580849	
P(T<=t) one-tail	0.117666	
t Critical one-tail	6.313752	
P(T<=t) two-tail	0.235331	
t Critical two-tail	12.7062	

Table C.4.2 Reduced Frequency, 0.01Hz

Reduced Freq. 0.01Hz	*Variable 1*	*Variable 2*
Mean	802.8361172	745.9874759
Variance	19572.76643	3.850555115
Observations	2	2
Hypothesized Mean Difference	0	
df	1	
t Stat	0.574600851	
P(T<=t) one-tail	0.33399049	
t Critical one-tail	6.313751515	
P(T<=t) two-tail	0.66798098	
t Critical two-tail	12.70620474	

Table C.4.3 Reduced Frequency, 10Hz

Reduced Freq. 10Hz	*Variable 1*	*Variable 2*
Mean	8593.958078	10435.955
Variance	2518983.434	159392.7668
Observations	2	3
Hypothesized Mean Difference	0	
df	1	
t Stat	-1.607751616	
P(T<=t) one-tail	0.177116997	
t Critical one-tail	6.313751515	
P(T<=t) two-tail	0.354233995	
t Critical two-tail	12.70620474	

Table C.4.4 Reduced Frequency, 100Hz

Reduced Freq. 100Hz	*Variable 1*	*Variable 2*
Mean	12855.65185	14998.94224
Variance	3182250.123	35802.38401
Observations	2	3
Hypothesized Mean Difference	0	
df	1	
t Stat	-1.692802294	
P(T<=t) one-tail	0.169843857	
t Critical one-tail	6.313751515	
P(T<=t) two-tail	0.339687714	
t Critical two-tail	12.70620474	

C.5 Mix; AC 20 – Binder 80/100 – VTM = 4.0%

Table C.5.1 Reduced Frequency, 0.0004Hz

Reduced Freq. 0.0004Hz	*Variable 1*	*Variable 2*
Mean	143.112416	277.3191043
Variance	57.38352128	1439.631534
Observations	2	2
Hypothesized Mean Difference	0	
df	1	
t Stat	-4.905418601	
P(T<=t) one-tail	0.064012335	
t Critical one-tail	6.313751515	
P(T<=t) two-tail	0.12802467	
t Critical two-tail	12.70620474	

Table C.5.2 Reduced Frequency, 0.004Hz

Reduced Freq. 0.004Hz	*Variable 1*	*Variable 2*
Mean	388.5289533	511.1568496
Variance	463.2288111	19142.85519
Observations	2	2
Hypothesized Mean Difference	0	
df	1	
t Stat	-1.238536604	
P(T<=t) one-tail	0.216208676	
t Critical one-tail	6.313751515	
P(T<=t) two-tail	0.432417352	
t Critical two-tail	12.70620474	

Table C.5.3 Reduced Frequency, 4Hz

Reduced Freq. 4Hz	*Variable 1*	*Variable 2*
Mean	5663.552905	5384.22822
Variance	56631.11319	242912.8211
Observations	2	2
Hypothesized Mean Difference	0	
df	1	
t Stat	0.721762063	
P(T<=t) one-tail	0.300998211	
t Critical one-tail	6.313751515	
P(T<=t) two-tail	0.601996423	
t Critical two-tail	12.70620474	

Appendix D: Interconversions for the various asphalt mixtures

D.1 AC 14 @ 30.0 °C

Table D.1 Properties of asphalt mixes

Mix type	Binder	Air void percentage	Temperature
AC 14	60/70	3.0 ± 0.5%	30.0 °C

Table D.2 Prony series coefficients

j	$\boldsymbol{\tau_j}$ **sec**	$\boldsymbol{D_j}$ **1/MPa**
1	0.1	0.0033747
2	1	0.0034304
3	10	0.0027461
4	100	0.0036481
5	1000	0.0040152
$D_g = 0.000144\ (1/MPa)$		

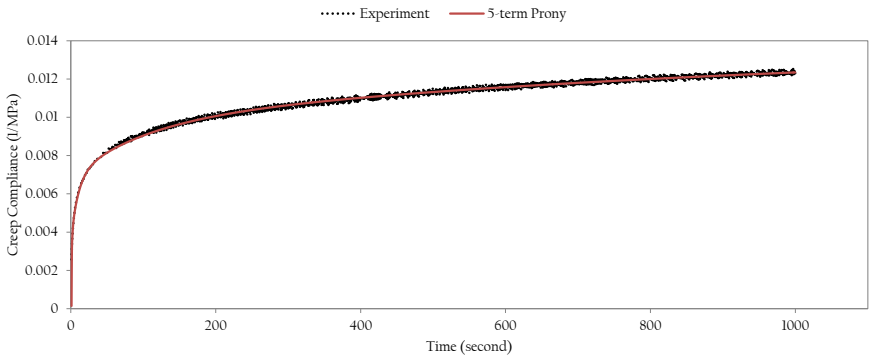

Figure D.1 Prony series fit to experimental data

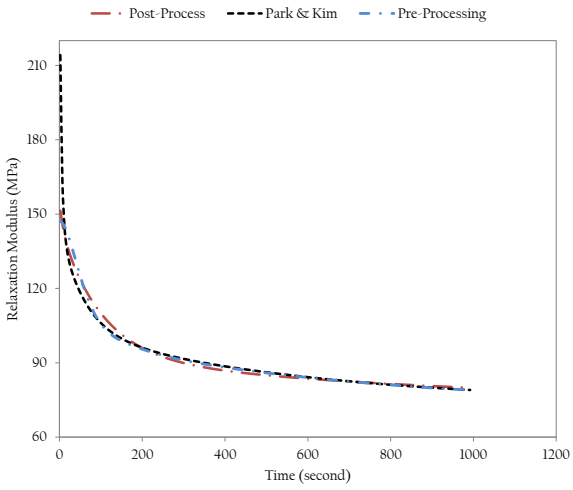

Figure D.2 approximate method versus "Pre" and "Post" processing techniques

D.2 AC 14 @ 25.0 °C

Table D.3 Properties of asphalt mixes

Mix type	Binder	Air void percentage	Temperature
AC 14	80/100	3.0 ± 0.5%	25.0 °C

Table D.4 Prony series coefficients

j	$\boldsymbol{\tau_j}$ **sec**	$\boldsymbol{D_j}$ **1/MPa**
1	10	0.0017845
2	10	0.0028026
3	100	0.0081256
4	1000	0.0109186
5	10000	0.0113110
$D_g = 0.000283\ (1/MPa)$		

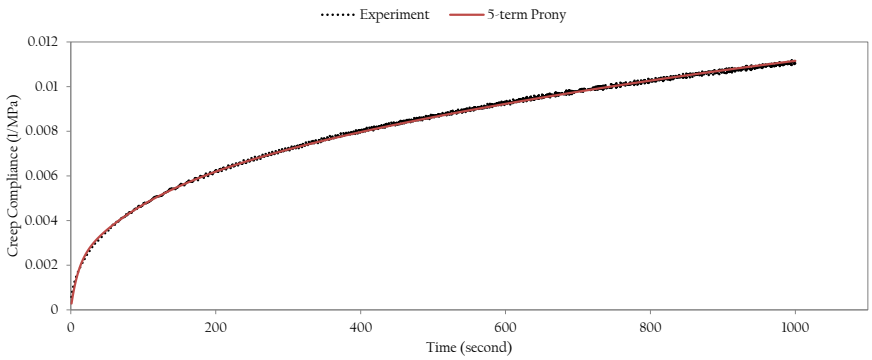

Figure D.3 Prony series fit to experimental data

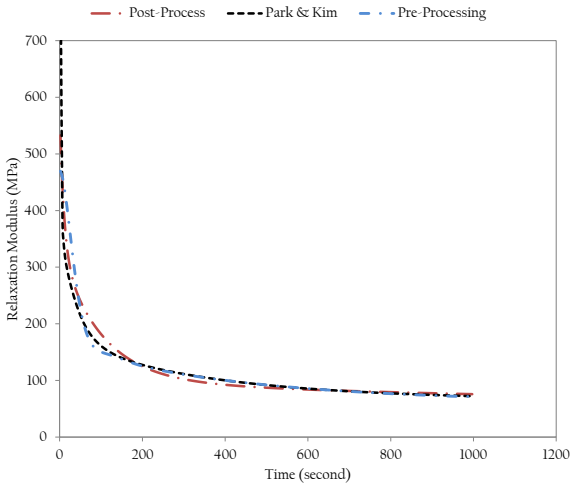

Figure D.4 approximate method versus "Pre" and "Post" processing techniques

D.3 AC 20 @ 15.0 °C

Table D.5 Properties of asphalt mixes

Mix type	Binder	Air void percentage	Temperature
AC 20	60/70	3.5 ± 0.5%	15.0 °C

Table D.6 Prony series coefficients

j	$\boldsymbol{\tau_j}$ **sec**	$\boldsymbol{D_j}$ **1/MPa**
1	10	0.0007642
2	10	0.0010430
3	100	0.0030748
4	1000	0.0042922
5	10000	0.0044600
$D_g = 0.0000383\ (1/MPa)$		

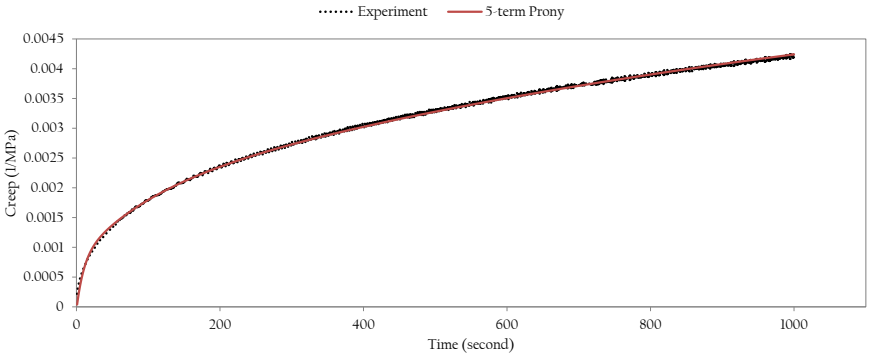

Figure D.5 Prony series fit to experimental data

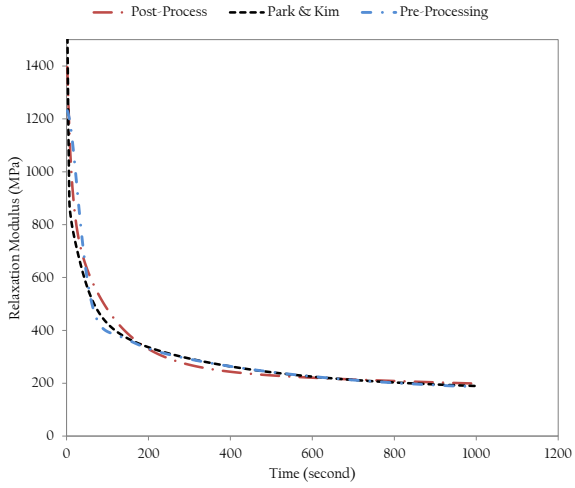

Figure D.6 approximate method versus "Pre" and "Post" processing techniques